IN THE UNITED STATES DISTRICT COURT

FOR THE DISTRICT OF DELAWARE

ZYMOGENETICS, INC., a Washington Corporation, Plaintiff, v. BRISTOL-MYERS SQUIBB CO., a Delaware Corporation, and DOES 1 through 100, Defendants.	C.A. No. 06-500-SLR **PUBLIC VERSION**

DECLARATION OF AMY SUN IN SUPPORT OF ZYMOGENETICS, INC.'S REPLY TO MOTION FOR SUMMARY JUDGMENT OF INFRINGEMENT

Philip A. Rovner (#3215)
POTTER ANDERSON & CORROON LLP
Hercules Plaza
P. O. Box 951
Wilmington, DE 19899
(302) 984-6000
provner@potteranderson.com

Attorneys for Plaintiff
ZymoGenetics, Inc.

OF COUNSEL:

Paul J. André
Lisa Kobialka
KING & SPALDING LLP
1000 Bridge Parkway
Suite 1000
Redwood City, CA 94065
(650) 590-0700

Dated: August 25, 2008
Public Version: September 2, 2008

I, AMY SUN, declare:

1. I am an attorney with the law firm of King & Spalding LLP, counsel of record for Plaintiff ZymoGenetics, Inc ("ZymoGenetics"). I have personal knowledge of the facts set forth in this declaration and can testify competently to those facts.

2. Attached hereto as Exhibit 1 is a true and correct copy of Dall'Acqua et al., "Contribution of Domain Interface Residues to the Stability of Antibody C_H3 Domain Homodimers," Biochemistry 37:9266-973 (1998), bearing Bates numbers ZG054363-70.

3. Attached hereto as Exhibit 2 is a true and correct copy of Hollenbaugh et al., "The human T cell antigen gp39, a member of the TNF gene family, is a ligand for the CD40 receptor: expression of a soluble form of gp39 with B cell co-stimulatory activity," The EMBO Journal, Vol. 11, No. 12, pp. 4313-21 (1992).

4. Attached hereto as Exhibit 3 is a true and correct copy of pages 118-119 from the transcript of the deposition of John Kuriyan, taken on May 9, 2008.

5. Attached hereto as Exhibit 4 is a true and correct copy of the Supplemental Expert Report of Jeffrey V. Ravetch, dated April 24, 2008.

6. Attached hereto as Exhibit 5 is a true and correct copy of the Supplemental Expert Report of John Kuriyan, dated April 23, 2008.

7. Attached hereto as Exhibit 6 is a true and correct copy of pages 85, 94-95, and 266 from the transcript of the deposition of Dr. David Ostrov, taken on May 6, 2008.

8. Attached hereto as Exhibit 7 is a true and correct copy of Bristol-Myers Squibb Company's Objections and Responses to ZymoGenetics' First Set of Interrogatories (Nos. 1-14), dated January 5, 2007.

9. Attached hereto as Exhibit 8 is a true and correct copy of pages 72-73 from the transcript of the deposition of Steven Nadler, taken on September 20, 2007.

10. Attached hereto as Exhibit 9 is a true and correct copy of pages 155, 164-166, and 243-244 from the transcript of the deposition of Dr. Nicholas Gascoigne, taken on April 29, 2008.

11. Attached hereto as Exhibit 10 is a true and correct copy of pages 94-95 from the transcript of the deposition of Dr. Andrzej Sledziewski, taken on August 21, 2007.

12. Attached hereto as Exhibit 11 is a true and correct copy of Linsley et al., "Solution structure of human CTLA-4 and delineation of a CD80/CD86 binding site conserved in CD28," Nature Structural Biology, Vol. 4, No. 7: 527-531 (July 1997), bearing Bates numbers BMS001122376-1122380.

13. Attached hereto as Exhibit 12 is a true and correct copy of Oosterwegel et al., "CTLA-4 and T cell activation," Current Opinion in Immunology, Vol. 11: 294-300 (1999).

14. Attached hereto as Exhibit 13 is a true and correct copy of Ostrov et al., "Structure of Murine CTLA-4 and Its Role in Modulating T Cell Responsiveness," Science, Vol. 290: 816-819 (2000), bearing Bates numbers BMS002569166-2569169.

15. Attached hereto as Exhibit 14 is a true and correct copy of Greene et al., "Covalent Dimerization of CD28/CTLA-4 and Oligomerization of CD80/CD86 Regulate T Cell Costimulatory Interactions," Journal of Biological Chemistry, Vol. 271, No. 43: 26762-26771 (1996).

16. Attached hereto as Exhibit 15 is a true and correct copy of Amgen, Inc.'s Form 8-K for July 15, 2002, available from the Securities and Exchange Commission at http://www.secinfo.com/dsVsn.31R1.htm.

I declare under penalty of perjury under the laws of the State of California and the United States that each of the above statements is true and correct.

Executed on August 25, 2008 in Redwood Shores, California.

Amy Sun

IN THE UNITED STATES DISTRICT COURT
FOR THE DISTRICT OF DELAWARE

CERTIFICATE OF SERVICE

I, Philip A. Rovner, hereby certify that on September 2, 2008, the within document was filed with the Clerk of the Court using CM/ECF which will send notification of such filing(s) to the following; that the document was served on the following counsel as indicated; and that the document is available for viewing and downloading from CM/ECF.

BY HAND DELIVERY AND E-MAIL

Frederick L. Cottrell, III, Esq.
Kelly E. Farnan, Esq.
Richard Layton & Finger, P.A.
One Rodney Square
P. O. Box 551
Wilmington, DE 19899
cottrell@rlf.com
farnan@rlf.com

I hereby certify that on September 2, 2008 I have sent by E-mail the foregoing document to the following non-registered participant:

Christopher P. Borello, Esq.
Colleen Tracy, Esq.
Fitzpatrick Cella Harper & Scinto
30 Rockefeller Plaza
New York, NY 10112
cborello@fchs.com
ctracy@fchs.com

/s/ Philip A. Rovner
Philip A. Rovner (#3215)
Potter Anderson & Corroon LLP
Hercules Plaza
P. O. Box 951
Wilmington, DE 19899
(302) 984-6000
provner@potteranderson.com

748348

EXHIBIT 1

Contribution of Domain Interface Residues to the Stability of Antibody C_H3 Domain Homodimers

William Dall'Acqua,[‡] Alexander L. Simon,[‡,§] Michael G. Mulkerrin,[‖] and Paul Carter*[,‡]

Departments of Molecular Oncology and Medicinal & Analytical Chemistry, Genentech Inc., 1 DNA Way, South San Francisco, California 94080

Received February 3, 1998; Revised Manuscript Received April 22, 1998

ABSTRACT: Dimers of C_H3 domains from human IgG_1 were used to study the effect of mutations constructed at a domain−domain interface upon domain dissociation and unfolding, "complex stability". Alanine replacement mutants were constructed on one side of the interface for each of the sixteen interdomain contact residues by using a single-chain C_H3 dimer in which the carboxyl terminus of one domain was joined to the amino terminus of the second domain via a $(G_4S)_4$ linker. Single-chain variants were expressed in *Escherichia coli* grown in a fermentor and recovered in yields of 6−90 mg L^{-1} by immobilized metal affinity chromatography. Guanidine hydrochloride-induced denaturation was used to follow domain dissociation and unfolding. Surprisingly, the linker did not perturb the complex stability for either the wild type or two destabilizing mutants. The C_H3 domain dissociation and unfolding energetics are dominated by six contact residues where corresponding alanine mutations each destabilize the complex by >2.0 kcal mol^{-1}. Five of these residues (T366, L368, F405, Y407, and K409) form a patch at the center of the interface and are located on the two internal antiparallel β-strands. These energetically key residues are surrounded by 10 residues on the two external β-strands whose contribution to complex stability is small (three have a $\Delta\Delta G$ of 1.1−1.3 kcal mol^{-1}) or very small (seven have a $\Delta\Delta G$ of ≤0.7 kcal mol^{-1}). Thus, at the center of the C_H3 structural interface there is a small "functional interface" of residues that make significant contributions to complex stability.

Understanding protein−protein recognition is of fundamental significance as many biological processes depend on the ability of proteins to form specific and stable complexes. Protein−protein contact surfaces have been defined at atomic resolution by structure determination for a rapidly expanding number of protein complexes (reviewed in refs *1*−*4*). Extensive mutational analyses of such protein complexes have identified the residues that make significant energetic contributions to binding. In some cases, the energetically important residues represent only a small subset of the contact residues (*5*, *6*), whereas for others, a large proportion of the contact residues are functionally important (*7*).

The most detailed mutational analyses of protein−protein interactions to date have involved pairs of different proteins that can exist both free in solution and also in a bound state, such as ligand−receptor complexes (*5*, *6*) and antibody−antigen complexes (*7*), "noncompulsory complexes". In contrast, there is a paucity of data for the exceedingly common biological motif of "compulsory complexes" (*8*) in which free monomers are not readily detected. This likely reflects problems of interpreting the effects of mutations made simultaneously on both sides of an interface and the technical difficulty in making replacements on only one surface. For example, coexpression of mutant and wild-type chains typically leads to the formation of parental homodimers as well as the desired heterodimer, thereby confounding subsequent analysis of the mutational effects. Appending one of the chains with a charge tag (*9*, *10*) or each chain with either an epitope or polyhistidine tag (*11*) permits purification of the heterodimer away from the two parental homodimers. Nevertheless, subunit dissociation and exchange may lead to formation of parental homodimers that interfere with interpretation of mutational analysis.

An additional difficulty in functional analysis of domain interfaces of compulsory complexes is that mutations may affect unfolding of domains as well as their dissociation. Close coupling of these processes may confound partitioning of mutational effects between them. "Complex stability" here encompasses effects on both domain dissociation and unfolding of a compulsory complex.

We have extended the study of protein−protein recognition to investigate the effect of mutations constructed on one contact surface of a compulsory complex, the homodimer of the C_H3 domain (hdC_H3) from human IgG_1. The C_H3 homodimer was converted to a single-chain format (scC_H3) analogous to that originally described for single-chain Fv (scFv) fragments (*12*, *13*) by installing a peptide linker for connecting the carboxyl terminus of one domain to the amino terminus of the second domain. The linker was found not to significantly modify the stability of wild-type C_H3 or for two of the most destabilizing C_H3 mutants. This allowed us to adopt the scC_H3 format in analyzing the effects of

* Corresponding author. Telephone: (650) 225-1932. Fax: (650) 225-1716. E-mail: pjc@gene.com.
‡ Department of Molecular Oncology.
§ Present address: Cancer Biology, MSOB 309, Mail Code 5404, Stanford University, Stanford, CA 94305.
‖ Department of Medicinal & Analytical Chemistry.

S0006-2960(98)00270-0 CCC: $15.00 © 1998 American Chemical Society
Published on Web 06/06/1998

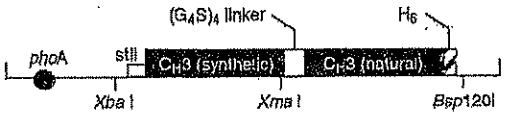

FIGURE 1: Schematic representation of an operon for the expression of scC_H3 in *E. coli* using the phagemid vector pRA4. A synthetic C_H3 gene (*19*) is connected to a natural C_H3 gene (*75*) via a linker encoding the sequence $(G_4S)_4$. The second C_H3 gene is followed by a sequence encoding six histidine residues (H_6) that allows purification by IMAC. The operon is under the transcriptional control of the *E. coli* alkaline phosphatase (*phoA*) promoter (*76*) which can be induced by phosphate starvation. Secretion is directed by the heat stable enterotoxin signal sequence [stII, (*77*)].

mutations installed on only one side of the domain interface upon domain dissociation and unfolding.

The C_H3 interface involves 16 residues located on four antiparallel β-strands that make intermolecular contacts and are buried 1090 Å^2 from each surface (*14*, *15*). These 16 residues were individually replaced with alanine on one side of the interface. Alanine replacements were chosen to minimize unfavorable steric contacts and to avoid imposing new charge interactions or hydrogen bonds from the substituted side chains while minimizing the risk of altering the main chain conformation (*16*−*18*). The contribution of individual residues to complex stability was assessed by comparing guanidine hydrochloride (GuHCl[1])-induced unfolding of wild-type and alanine mutant scC_H3 by far-ultraviolet circular dichroism (far-UV CD) spectroscopy.

MATERIALS AND METHODS

Reagents. Restriction enzymes, Vent DNA polymerase, and other DNA-modifying enzymes were purchased from New England Biolabs, Inc. (Beverly, MA), whereas Sequenase version 2.0 and Muta-Gene kits were obtained from United States Biochemicals (Cleveland, OH) and Bio-Rad (Hercules, CA), respectively. [^{35}S]dATPαS was obtained from Amersham Life Science Inc. (Arlington Heights, IL), and ultrapure guanidine hydrochloride (GuHCl) was purchased from Gibco-BRL. HiTrap nickel nitrilotriacetic acid (Ni^{2+}-NTA) and Superdex 75 columns were obtained from Pharmacia (Uppsala, Sweden). Oligonucleotides were synthesized on an Applied Biosystems (Foster City, CA) model 394 DNA synthesizer.

Single-Chain C_H3 Construction. Phagemid pRA2 contains a dicistronic operon in which C_H3 expressed from a synthetic gene is cosecreted with a second copy of C_H3 expressed from the natural gene as a fusion with M13 gene III (*19*). Phagemid pRA2 was modified to create pRA4 for scC_H3 expression by connecting two C_H3 domains via a $(G_4S)_4$ linker (Figure 1). In addition, the second C_H3 gene was mutagenized to replace M13 gene III with a sequence encoding six histidines to facilitate purification by immobilized metal affinity chromatography (IMAC; *20*). Briefly, the natural C_H3 gene (100 ng) was subjected to a two-step PCR mutagenesis using 50 pmol of the primer 5′-CAAACGAAGGGCCCTTATTAGTGATGGTGATGGTGA-TGTTTACCCGGAGACAGGGAGAGG-3′ (*Bsp*120I site underlined) with successively 50 pmol of the primer 5′-GGCGGAGGTGGTTCTGGCGGTGGCGGATCGGGGCAGCCCCGAGAACCACAGGTGTACACCCTGCCCCCATCTCGGGAAG-3′ and 50 pmol of the primer 5′-AAAAAGGGTATCTAGAGGTTGAGGTGATTTTTCCCTGTCTCCCGGGAAAGGTGGAGGCGGTTCAGGTGGAGGCGGTTCAGGCGGAGGTGGTT-3′ (underlined sites for *Xba*I and *Xma*I, respectively), each dNTP at 200 μM, 100 mM Tris-HCl (pH 8.3), 500 mM KCl, 1.5 mM $MgCl_2$, 0.01% (w/v) gelatin, and 3 units of Vent DNA polymerase. The sample was incubated at 94 °C for 5 min followed by 30 rounds of thermocycling (94 °C for 1 min, 50 °C for 1 min, and 72 °C for 1 min) using a GeneAmp PCR System 9600 (Perkin-Elmer, Norwalk, CT). The amplified DNA was digested with *Xba*I and *Bsp*120I and cloned into pRA2 (*19*) restricted with the same enzymes to create phagemid pRA3. The scC_H3 expression phagemid, pRA4, was constructed by subcloning the synthetic C_H3 gene as an *Xba*I−*Xma*I fragment into similarly cleaved pRA3. The sequence was verified by dideoxynucleotide sequencing (*21*) using Sequenase version 2.0.

Site-Directed Mutagenesis. Mutants were prepared by site-directed mutagenesis using the method of Kunkel (*22*) in conjunction with a Muta-Gene kit. The oligonucleotides for mutagenesis were designed to replace the chosen wild-type codons in the synthetic C_H3 gene with the alanine codon, GCT. Mutations were constructed using phagemid pRA2 (*19*) modified to contain either synthetic or natural C_H3 and verified by dideoxynucleotide sequencing.

Expression and Purification of C_H3 Variants. Phagemids for the expression of hdC_H3 and scC_H3 variants were transformed into *Escherichia coli* 33B6 (*23*). The C_H3 variants were secreted from corresponding *E. coli* cells cultured for approximately 48 h at 30 °C in an aerated 10 L fermentor (*24*). The cell density at harvest was in the range of 100−150 OD_{550}. The hdC_H3 and scC_H3 variants were purified as described previously (*19*) or below, respectively.

A periplasmic fraction was prepared (*19*) from 100 g of fermentation paste for each scC_H3 variant and dialyzed extensively against 50 mM Tris-HCl (pH 8.0). The dialysate was adjusted to 25 mM imidazole and applied to a 5 mL Ni^{2+}-NTA affinity column. The resin was washed with 20 column volumes of 50 mM Tris-HCl (pH 8.0), and the scC_H3 variants were eluted with a linear gradient of 0 to 500 mM imidazole in 50 mM Tris-HCl (pH 7.5). The purified scC_H3 variants were dialyzed against 50 mM sodium phosphate buffer (pH 7.4) or 10 mM Tris-HCl (pH 8.0) and 10 mM NaCl. The scC_H3 variants were analyzed by size exclusion chromatography on a Superdex 75 column in phosphate-buffered saline.

The purified hdC_H3 and scC_H3 variants were concentrated using Centriprep-10 concentrators (Amicon, Beverley, MA), flash-frozen in liquid nitrogen, and stored at −70 °C. The protein yields were estimated from the absorbance at 280 nm using the extinction coefficients (ϵ_{280}) for the wild-type hdC_H3 and scC_H3 determined by amino acid hydrolysis to be 32 204 and 38 107 cm^{-1} M^{-1}, respectively.

Far-UV CD Spectroscopy. Data were obtained as described by Zhukovsky et al. (*25*) on an AVIV (Lakewood, NJ) 60DS spectropolarimeter. Briefly, spectra for scC_H3 and hdC_H3 variants (25−80 μM) were recorded at 20.0 ± 0.1

[1] Abbreviations: Flk-1, fetal liver kinase 1; GuHCl, guanidine hydrochloride; HEL, hen egg white lysozyme; hdC_H3, homodimer C_H3; IMAC, immobilized metal affinity chromatography; KDR, kinase insert domain-containing receptor; NTA, nitrilotriacetic acid; scC_H3, single-chain C_H3; UV CD, ultraviolet circular dichroism; VEGF, vascular endothelial growth factor; θ_{obs}, ellipticity.

°C in 10 mM Tris-HCl (pH 8.0) and 10 mM NaCl. Data were collected over the wavelength range of 250−200 nm in 0.25 nm intervals in a thermostated circular cuvette with a 0.1 cm path length. The final spectra represent the mean of five far-UV CD scans with an integration time of 2 s per data point. Results are reported as mean residue weight ellipticity (θ_{MRW}, in deg cm^2 dmol^{-1}) calculated using the appropriate mean residue weights for each hdC_H3 and scC_H3 variant.

Equilibrium Denaturation Assays. Guanidine hydrochloride-induced unfolding of hdC_H3 and scC_H3 variants was followed by far-UV CD spectroscopy at a wavelength of 225 nm. The C_H3 variants (25−30 samples at ~1 mg mL^{-1}) were prepared with varying concentrations of GuHCl (0−8 M) in 50 mM sodium phosphate (pH 7.4) and equilibrated for 24 h at 20.0 ± 0.1 °C prior to data collection. Ellipticity θ_{obs} was measured at a wavelength of 225 nm in circular cuvettes with a 0.1 cm path length. A total of 120 data points were taken in a 2 min trace, and the mean was calculated. The final concentrations of GuHCl in each sample were determined by measurement of the refractive index (*26*).

The ellipticity data were fitted by a nonlinear least-squares method to both two-state (*27*) and three-state (*28*) models of unfolding using KaleidaGraph, version 3.0.8 (Synergy Software, PCS Inc., Reading, PA), taking into account the slopes of the pre- and post-transitional baselines. Virtually identical estimates were obtained using the linear extrapolation method (*29*), as already noted (*25*) (data not shown). Denaturation parameters that were estimated include ΔG_0, the free energy of unfolding in the absence of denaturant, and $D_{50\%}$, the denaturant concentration at which the apparent free energy change of unfolding, ΔG_U, is zero. In addition, estimates were made for m, the slope of ΔG_U versus the denaturant concentration D. The errors associated with $D_{50\%}$ values are commonly less significant than those associated with ΔG_0 values which are extrapolated to 0 M GuHCl (*30*, *31*). Consequently, the difference in the free energy of domain dissociation and unfolding between the wild type and the mutant, $\Delta\Delta G$, is more accurately determined in the transition region, using the following equation:

$$\Delta\Delta G = \langle m \rangle (D_{50\%\,wt} - D_{50\%\,mut}) \qquad (1)$$

where $\langle m \rangle$ is the mean value of m for all of the variants (*25*, *32*). A one-way analysis of variance (ANOVA) was consistent with m being independent of variant except for the F405A/F405′A[2] mutant in hdC_H3 and scC_H3 formats. The F405A/F405′A mutant was therefore excluded in the calculation of $\langle m \rangle$ (*25*).

Mass Spectrometry. C_H3 variants in 50 mM sodium phosphate buffer (pH 7.4) were mass analyzed with a packed capillary liquid chromatography system coupled directly to a PE-Sciex API 3 triple-quadrupole mass spectrometer as described (*33*).

[2] Mutations in C_H3 domains are denoted by the amino acid residue and number [Eu numbering scheme of Kabat et al. (*78*)], followed by the replacement amino acid. Mutations constructed in a pair of C_H3 domains are separated by a slash with a prime sign used to indicate the residue on the second domain. For example, F405A and F405A/F405′A represent replacements of the phenylalanine at position 405 with alanine on one or both domains, respectively.

Table 1: Expression, Purification, and Mass Analysis of C_H3 Variants

C_H3 variant	yield (mg L^{-1})	observed mass (Da)	expected mass (Da)[a]
homodimers			
wild-type	310	12 106 ± 2	12 107
F405A/F405′A	20	12 032 ± 1	12 031
Y407A/Y407′A	35	12 015 ± 1	12 015
single chains			
wild-type	18	26 281 ± 1	26 281
Q347A	61	26 222 ± 2	26 224
Y349A	36	26 190 ± 1	26 189
T350A	81	26 252 ± 1	26 251
L351A	41	26 239 ± 1	26 239
T366A	75	26 249 ± 2	26 251
L368A	90	26 239 ± 1	26 239
K370A	72	26 224 ± 1	26 224
K392A	9	26 222 ± 2	26 224
T394A	41	26 249 ± 2	26 251
P395A	52	26 252 ± 3	26 255
V397A	65	26 252 ± 1	26 253
L398A	6	26 240 ± 2	26 239
D399A	10	26 237 ± 1	26 237
F405A	14	26 204 ± 1	26 205
F405A/F405′A	8	26 129 ± 1	26 129
Y407A	37	26 189 ± 2	26 189
Y407A/Y407′A	57	26 097 ± 3	26 097
K409A	8	26 223 ± 2	26 224

[a] By high-resolution mass spectrometry.

RESULTS

Design of scC_H3 and Mutational Analysis Strategy. A single-chain form of C_H3 was designed by utilizing a flexible linker to span from K453 at the carboxyl terminus of C_H3 to G341 at the amino terminus of the partner C_H3 domain. Unfortunately, this distance could not be accurately estimated since the 10 carboxyl-terminal residues, S444−K453, are not defined in the original 2.8 Å X-ray crystallographic structure of human IgG$_1$ Fc (*14*) or in a more recent higher-resolution (2.0 Å) structure (M. Ultsch and A. M. de Vos, personal communication). L443, the carboxyl-terminal structurally defined residue, is approximately 37 Å from residue G341 of the partner C_H3 domain. scC_H3 domains were constructed with a long linker, $(G_4S)_4$, in an attempt to accommodate the uncertainty in the distance to be spanned. The second copy of C_H3 was followed by a sequence encoding six histidines to permit purification by IMAC (Figure 1).

The 16 domain interface residues were individually replaced with alanine on one side of the interface, the amino-terminal C_H3 domain of scC_H3. Mutants with replacements on both sides of the interface, namely, F405A/F405′A and Y407A/Y407′A, together with the wild type were constructed in both hdC_H3 and scC_H3 formats to assess the effect of the linker upon complex stability.

Expression and Purification of hdC_H3 and scC_H3 Variants. All C_H3 variants were secreted from *E. coli* grown to high cell density in a fermentor. The scC_H3 variants were purified by IMAC and eluted as a single peak at ~150 mM imidazole (not shown), whereas the hdC_H3 variants were recovered by chromatography using ion exchange and ABx resins as described previously (*19*). Sufficient protein was recovered for all C_H3 variants to support further analysis, although the recovered yield varied from 35−310 to 6−90 mg L^{-1} for hdC_H3 and scC_H3 variants, respectively (Table 1). The molecular masses of all C_H3 variants determined by high-

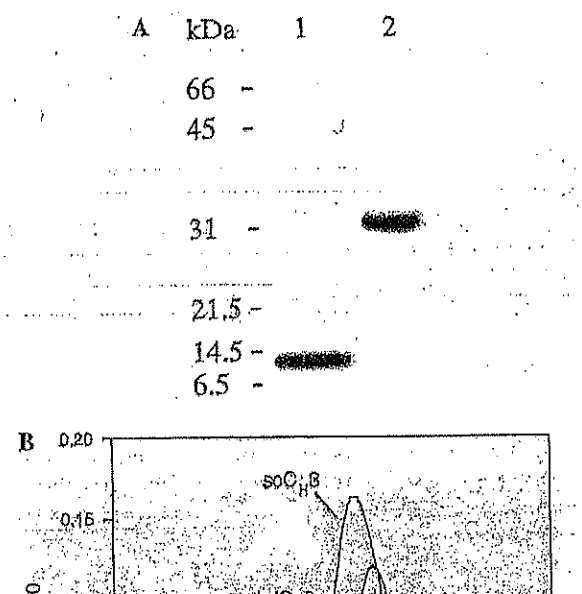

FIGURE 2: Purification of wild-type hdC_H3 and scC_H3 variants. (A) SDS–PAGE analysis using 4 to 20% acrylamide (Novex, San Diego, CA) after staining with Coomassie Blue; lane 1, purified wild-type scC_H3; and lane 2, purified wild-type hdC_H3. (B) Size exclusion chromatography of wild-type hdC_H3 and scC_H3 variants. The molecular mass standards elute as follows: bovine chymotrypsinogen A, 25 kDa, 12.0 min; chicken ovalbumin, 44 kDa, 9.9 min; and bovine serum albumin, 67 kDa, 9.4 min.

resolution electrospray mass spectrometry are consistent with those expected (Table 1).

Wild-type scC_H3 and hdC_H3 each migrate as a single major band when analyzed by SDS–PAGE with apparent molecular masses of 31 and 12 kDa, respectively (Figure 2A). Wild-type scC_H3 has an electrophoretic mobility lower than expected from its molecular mass (27 kDa), which may reflect the presence of the hexahistidine tag. Similar results were obtained with all other scC_H3 and hdC_H3 variants (not shown). Size exclusion chromatographs of wild-type (Figure 2B) and mutant scC_H3 (not shown) are consistent with the presence of the anticipated ~25 kDa monomer with no evidence for dimers or higher-order polymers.

Far-UV CD Spectroscopy and Equilibrium Denaturation Assays for C_H3 Variants. The wild-type scC_H3 fragment gave rise to a far-UV CD spectrum that is indistinguishable from that of the corresponding hdC_H3 (Figure 3), including a minimum at a wavelength of 225 nm characteristic of β-sheet structures (*34*). This wavelength was chosen for following the GuHCl-induced unfolding and dissociation of C_H3 variants. Unfolding and dissociation is fully reversible as judged by the complete recovery of original ellipticity upon dilution of the denatured samples as described (*25*, *35*). In contrast, thermal unfolding of hdC_H3 is not fully reversible and aggregation occurs at elevated temperatures (*19*).

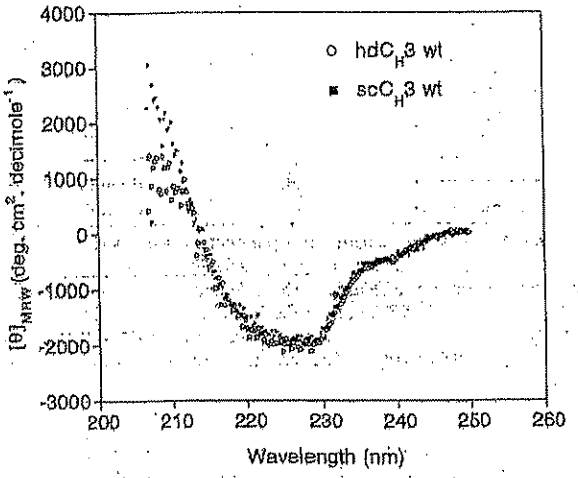

FIGURE 3: Far-UV CD spectra of wild-type scC_H3 and hdC_H3 variants recorded at 20.0 ± 0.1 °C in 10 mM Tris-HCl (pH 8.0) and 10 mM NaCl.

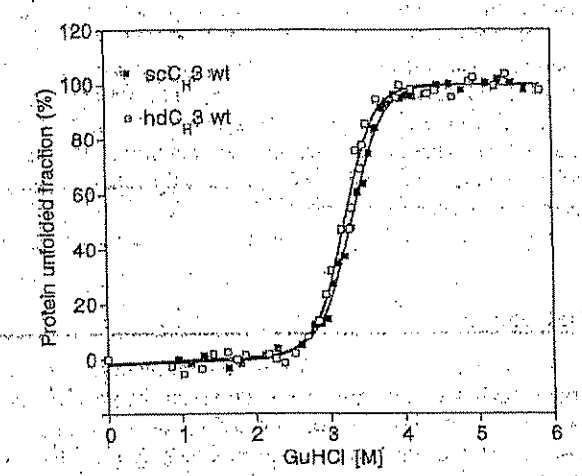

FIGURE 4: Equilibration denaturation profiles of wild-type scC_H3 and hdC_H3 recorded in 50 mM sodium phosphate (pH 7.4) at 20.0 ± 0.1 °C in the presence of varying amounts of GuHCl. Data were fitted using a nonlinear least-squares method to a two-state model (*27*).

GuHCl-induced denaturation data were analyzed by the nonlinear least-squares method of Santoro and Bolen (*27*) to estimate ΔG_0. All data were found to fit better to two-state than to three-state models as judged by lower χ^2 values (not shown). In addition, the transitions observed were continuous, an indication of rapid equilibration between two states (*27*) consistent with close coupling between dissociation of C_H3 domains and their unfolding.

Validation of the Use of the Linker. Wild-type C_H3 in single-chain and homodimer formats show identical stability profiles (Figure 4) and fitted parameters (Table 2) following GuHCl-induced denaturation, indicating that the linker does not significantly modify complex stability. Variants F405A/F405'A and Y407A/Y407'A containing destabilizing mutations on both sides of the C_H3 interface also gave very similar denaturation profiles and parameters in hdC_H3 and scC_H3 formats (Table 2). Taken together, these data support the use of the scC_H3 format in analyzing the effect of alanine scanning mutations constructed on one side of the C_H3 domain interface.

Table 2: Equilibrium Denaturation Parameters for hdC_H3 and scC_H3 Variants[a]

C_H3 variant	format	ΔG_0[b] (kcal mol^{-1})	$D_{50\%}$[c] (M)	m[d] (kcal mol^{-2} L)	$\Delta\Delta G$[e] (kcal mol^{-1})
wild-type	hd	9.1 ± 0.4	3.19 ± 0.14	2.92 ± 0.24	(0)
wild-type	sc	9.1 ± 0.3	3.25 ± 0.08	2.80 ± 0.06	(0)
F405A/F405′A	hd	1.1 ± 0.2	1.20 ± 0.02	0.92 ± 0.22	6.4
F405A/F405′A	sc	1.2 ± 0.3	1.05 ± 0.17	1.15 ± 0.07	6.1
Y407A/Y407′A	hd	4.9 ± 0.4	1.66 ± 0.08	2.81 ± 0.06	4.0
Y407A/Y407′A	sc	4.3 ± 0.4	1.74 ± 0.15	2.52 ± 0.11	4.0

[a] Estimates of the denaturation parameters were performed in duplicate or triplicate. Errors shown are twice the standard deviation of the measurements. [b] ΔG_0, free energy of unfolding in the absence of the denaturant estimated by nonlinear least-squares fitting of the raw data to a two-state model for unfolding. [c] $D_{50\%}$, denaturant concentration at which the apparent free energy of unfolding $\Delta G_u = 0$ kcal mol^{-1}. [d] m, slope of ΔG_u vs D. [e] $\Delta\Delta G$, difference in the free energy of unfolding between wild-type scC_H3 and hdC_H3 and variants in the same format. $\Delta\Delta G$ values were calculated from eq 1 using 2.65 kcal mol^{-1} (SD of 0.18 kcal mol^{-1}), the mean value of m for all proteins, excluding hdC_H3 F405A/F405′A and scC_H3 F405A/F405′A. The standard deviation for $\Delta\Delta G$ values is 0.1−0.15 kcal mol^{-1} except for that for hdC_H3 F405A/F405′A (0.25 kcal mol^{-1}).

Alanine Scanning Mutagenesis of the C_H3 Domain Interface. The largest reductions in complex stability ($\Delta\Delta G >$ 2.0 kcal mol^{-1}) occurred on alanine substitution of residues T366, L368, P395, F405, Y407, and K409. Significant destabilizing effects ($\Delta\Delta G = 1.0-1.3$ kcal mol^{-1}) were also seen on substitution of residues Q347, L351, and K370. Alanine replacements of the seven other interface residues (Y349, T350, K392, T394, V397, L398, and D399) had small or insignificant effects upon complex stability ($\Delta\Delta G \leq 0.7$ kcal mol^{-1}). These data from alanine scanning mutagenesis indicate that residues in the two internal antiparallel β-strands contribute significantly more to complex stability than residues in the two external antiparallel β-strands (Figure 5).

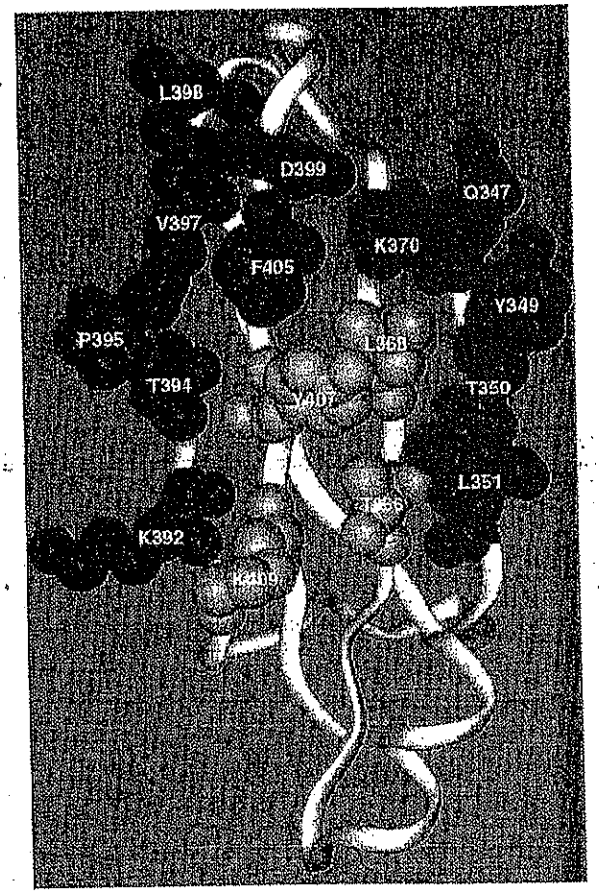

FIGURE 5: Space-filling model of the surface of C_H3 in contact in the C_H3-C_H3 complex based upon the human IgG_1 structure of Deisenhofer (*14*). Residues are color-coded according to the loss of free energy of stabilization upon alanine substitution: red, ≥2.5 kcal mol^{-1}; yellow, 2.0−2.4 kcal mol^{-1}; and blue, <1.5 kcal mol^{-1}.

DISCUSSION

Single-Chain Strategy. A mutational analysis of the human IgG_1 C_H3 domain was undertaken to quantify the contribution of interdomain contact residues to domain dissociation and unfolding of this compulsory complex. A scC_H3 dimer was constructed by joining the carboxyl terminus of one domain to the amino terminus of the second domain via a 20-residue linker. This permitted mutations to be constructed on one side of the interface, thereby avoiding the complication of attempting to interpret mutations constructed simultaneously on both sides of the interface.

The linker was anticipated to stabilize the C_H3 dimer by virtue of increasing the local concentration of monomers. Such stabilization has been previously demonstrated for analogous linkers in a scFv fragment (*36*) and a single-chain version of the homodimeric bacteriophage P22 Arc repressor (*37*). Surprisingly, the linker did not significantly affect the free energy change upon domain dissociation and unfolding for wild-type C_H3 and two destabilized mutants, F405A/F405′A and Y407A/Y407′A (Table 2). The $(G_4S)_4$ linker may be sufficiently long and flexible that the increased stability anticipated from a high local concentration of monomers (*37*) is lost. Alternatively, the concentration of C_H3 variants (1 mg mL^{-1}) used for denaturation experiments may be too high to observe the effects due to the covalent linkage. Wild-type C_H3 in homodimeric and single-chain formats exhibits indistinguishable CD spectra (Figure 3), indicating no gross perturbation of the secondary structure (*38*) or of the β-sheets packing (*39*, *40*). Taken together, these data suggest that scC_H3 is a good substitute for heterodimeric C_H3 for analyzing the effect of mutations on only one side of the domain interface.

No free monomer has been detected in C_H3 (pFc′) preparations at concentrations as low as 10^{-10} M (*41*). This is consistent with C_H3 dimers having a dissociation constant (K_D) of $<10^{-10}$ M (*42*) corresponding to a free energy change upon dissociation of >13 kcal mol^{-1} calculated using the well-known relationship

$$\Delta G = RT \ln K_D \qquad (2)$$

where R is the gas constant and T the absolute temperature (293 K). In contrast, the free energy change upon hdC_H3 dissociation and unfolding was estimated to be 9.1 kcal mol^{-1} (Table 2). These data are consistent with the C_H3 domains being stabilized by their association.

A concern with the interdomain linker is that it might promote C_H3 dimerization or multimerization as shown with single-chain Fv fragments, particularly with linkers of 10 or fewer residues (*43*−*45*). The scC_H3 constructed with a 20-residue linker is monomeric as judged by size exclusion chromatography, with no evidence for multimerization (Figure 2B). In contrast, size exclusion chromatography of scC_H3 constructed with a shorter linker, $(G_4S)_3$, is consistent with a monomer−dimer equilibrium (data not shown).

Interpretation of the Denaturation Parameters. Stabilization of C_H3 dimers is largely mediated by six of the 16 residues tested: T366, L368, P395, F405, Y407, and K409 (Figure 5). Residues T366 and Y407 form a hydrogen bond and represent the principal intermolecular and intramolecular contact with each other. Alanine substitution of Y407 and T366 reduces the complex stability by 2.3 and 2.1 kcal mol^{-1}, respectively. This loss in stability is consistent with the 1.0−2.5 kcal mol^{-1} reduction in free energy seen on replacing hydrogen-bonding residues in other proteins where both donor and acceptor residues are uncharged (*46*−*49*). Unfortunately, the exact strength of hydrogen bonds cannot be accurately determined from such single-mutation data since other interactions (van der Waals and hydrophobic) that may contribute to stabilization of the interface are concomitantly perturbed (*32*, *50*, *51*). Furthermore, the introduction of cavity-creating mutations might be followed by compensatory structural rearrangements (*52*−*54*) or solvent reorganization (*55*). A more accurate estimation of strength of the hydrogen bond between residues T366 and Y407′ awaits the construction of additional mutations and structural analysis of the corresponding mutant proteins.

Residue K409 forms a hydrogen bond with residue D399 on the partner C_H3 domain (*14*, *15*). Truncation of the K409 side chain to alanine significantly decreases complex stability ($\Delta\Delta G$ = 2.4 kcal mol^{-1}), whereas pruning the D399 side chain results in only a small reduction in stability ($\Delta\Delta G$ = 0.7 kcal mol^{-1}) (Table 3). There are numerous possible explanations for the asymmetry of these mutational effects at residues K409 and D399, including the possibility that these residues are not the major energetic contacts with each other. For example, the near functional silence of D399 may reflect that the fact that the cost of desolvating this residue is comparable to the energy gained through intermolecular contact with K409. The release of water molecules is not a major contributor to the stabilization of some protein−protein complexes (*56*, *57*). Alternatively, the larger effect observed for substitution of residue K409 than for D399, its hydrogen bond partner, can be explained by an effect of K409 on folding of the corresponding domain.

Residues L368 and F405 form intermolecular and intramolecular contacts through van der Waals interactions only. The large decrease in stability upon substitution of these residues with alanine likely reflects the contribution of the hydrophobic effect and of van der Waals contacts as well as probable solvent and protein structure rearrangements. The strength of the van der Waals contacts has been estimated to be approximately 0.5 kcal mol^{-1} (*49*, *55*).

Table 3: Equilibrium Denaturation Parameters for scC_H3 Alanine Variants[a]

C_H3 variant	ΔG_0 (kcal mol^{-1})	$D_{50\%}$ (M)	m (kcal mol^{-2} L)	$\Delta\Delta G^b$ (kcal mol^{-1})
Q347A	8.4 ± 0.4	2.86 ± 0.06	2.93 ± 0.20	1.1
Y349A	8.5 ± 0.2	3.00 ± 0.01	2.83 ± 0.06	0.7
T350A	8.8 ± 0.1	3.21 ± 0.01	2.76 ± 0.06	0.1
L351A	7.0 ± 0.4	2.76 ± 0.02	2.52 ± 0.18	1.3
T366A	6.3 ± 0.2	2.38 ± 0.02	2.65 ± 0.11	2.3
L368A	6.1 ± 0.3	2.40 ± 0.04	2.52 ± 0.20	2.2
K370A	6.9 ± 0.3	2.83 ± 0.08	2.45 ± 0.12	1.1
K392A	8.5 ± 0.3	3.11 ± 0.19	2.75 ± 0.04	0.4
T394A	8.1 ± 0.1	3.02 ± 0.01	2.67 ± 0.04	0.6
P395A	5.3 ± 0.4	2.08 ± 0.03	2.62 ± 0.11	3.2
V397A	7.7 ± 0.3	3.02 ± 0.01	2.57 ± 0.09	0.6
L398A	8.2 ± 0.3	3.23 ± 0.04	2.55 ± 0.08	0.1
D399A	8.2 ± 0.3	2.99 ± 0.02	2.72 ± 0.06	0.7
F405A	5.8 ± 0.1	2.32 ± 0.03	2.50 ± 0.07	2.5
Y407A	6.6 ± 0.4	2.49 ± 0.02	2.65 ± 0.16	2.1
K409A	5.2 ± 0.1	2.37 ± 0.11	2.21 ± 0.04	2.4

[a] Details as described in Table 2. [b] The standard deviation for $\Delta\Delta G$ values was 0.1−0.15 kcal mol^{-1} except for that for K392A (0.25 kcal mol^{-1}).

The most destabilizing mutation ($\Delta\Delta G$ = 3.2 kcal mol^{-1}), P395A, is located in a peripheral β-strand. Replacement of this proline residue likely perturbs the local backbone conformation, thereby indirectly affecting intermolecular interactions involving neighboring residues. Cis to trans isomerization of the peptide bond at P395 is not a plausible hypothesis for explaining the effects of the P395A replacement since this residue in wild-type C_H3 is in the trans rather than in the cis conformation (M. Ultsch and A. M. de Vos, personal communication). Substitution of proline residues in proteins with smaller amino acids is believed to be destabilizing through local conformational effects (*58*−*60*) or through stabilization of the unfolded state (*61*). A proline to serine substitution in nucleoside diphosphate kinase compromised the ability of the isolated subunits to associate into a hexamer (*60*). This effect was attributed to a change in the flexibility of the proline-containing loop constituting the domain−domain interface.

The m parameter reflects the difference between the solvent-exposed nonpolar surface area of the denatured and native states of proteins and/or the cooperativity of protein unfolding (*29*, *62*). Thus, the significant change in m for the F405A/F405′A double mutant may reflect the presence of equilibrium intermediates during unfolding or changes in the solvation properties of the denatured state.

Additivity of Mutational Effects. The reduction in stability for the double mutant, Y407A/Y407′A scC_H3 ($\Delta\Delta G$ = 4.0 kcal mol^{-1}), approximately equals the sum of stability reductions of the constituent single mutants Y407A and Y407′A ($\Delta\Delta G$ = 2.1 kcal mol^{-1}). This functional additivity (*63*) is consistent with Y407A and Y407′A having only local effects that are independent of each other. Residues Y407 and Y407′ are ~5 Å apart at the interface and do not form any intermolecular contacts (*14*). In contrast, the double mutant F405A/F405′A scC_H3 is destabilized by 1.1 kcal mol^{-1} more than predicted by adding the $\Delta\Delta G$ terms for the component single mutants. Thus, residues F405 and F405′ are energetically coupled although separated by >12 Å. Nonadditivity of distant mutations has been observed in several other systems, including barnase−barstar (*64*), sta-

phylococcal nuclease (*65*), human hemoglobin (*66*), and an antibody−anti-idiotype (*49*). Several possible explanations for long distance nonadditivity have been proposed (*67*), including solvent rearrangements, as described at the domain interface for a complex between a mutant antibody and chicken lysozyme (*55*, *68*).

Relationship between Structural and Functional Interface. A priori, the binding interaction between two proteins might be mediated primarily by a few strong interactions involving a small subset of interface residues or through a larger number of contact residues each making small contributions. In the case of the scC_H3 compulsory complex, six of the 16 interface residues account for the majority of the energy of stabilization. The residues most critical for scC_H3 stabilization are located on the two interior β-strands, forming a patch at the center of the interface (Figure 5). P395 notwithstanding, residues at the periphery make very little net contribution to the free energy of scC_H3 stabilization. Thus, scC_H3 is stabilized by an "energetic interface" between C_H3 domains located at the heart of a larger "structural interface".

Small energetic interfaces have been observed previously for the noncompulsory complexes between human growth hormone and its receptor (*5*, *69*) and for vascular endothelial growth factor (VEGF) and its KDR and Flk-1 receptors (*6*). A few strong interactions at the center of an interface also dominate the energetics of binding of the complex between hen egg white lysozyme and the monoclonal antibody D1.3 (*7*). In contrast, the majority of the contact residues play a significant role in binding (> 1.5 kcal mol^{-1}) for an antibody−anti-idiotype complex (*7*).

Nature of the Functional Interface. Mutational analysis of the compulsory complex of scC_H3 indicates that residues making major contributions to domain stability and/or association have side chains that are hydrophobic (F405 and L368), polar (T366 and Y407), or charged (K409). Similarly, both polar and nonpolar residues play an important energetic role in association of the noncompulsory complexes of chicken lysozyme with a cognate monoclonal antibody (*7*) and of VEGF with its KDR receptor (*6*). In contrast, the energetics of human growth hormone associating with its receptor relies primarily upon hydrophobic residues (*5*). Thus, there is much variation in the chemical nature of the energetic interface residues among compulsory and noncompulsory complexes studied to date.

The free energy of the C_H3-C_H3 complex stabilization appears to arise from only half of the antiparallel β-strand constituting the interface. Several different models of β-sheet packing have been described, including aligned (*70*), three-layer (*71*), and intercalated (*15*). Whether the main features of the energetic map we describe here are to be generalized for those different kinds of β-sheets-involving interfaces is still to be determined. Since the interior of many monomeric proteins is formed by β-sheet packing, the quantitative information we gained from this study is also highly relevant to the issue of protein stabilization.

Summary. We have shown that approximately one-third of the contact side chains at the human IgG1 C_H3 domain interface can account for the majority of contributions to domain folding and association. These residues cluster near the center of the structural interface. This study will help us to progress from purely anatomical descriptions of protein−protein interfaces such as their sizes, the identity of contact residues, the amount of buried surface areas, the number of hydrogen bonds, and van der Waals interactions (*72*−*74*) to a detailed understanding of how these structural features contribute to the affinity and specificity of the binding reactions. To our knowledge, this is the first extensive mutational analysis of the domain interface of a compulsory protein complex.

ACKNOWLEDGMENT

We thank Bart de Vos and Mark Ultsch for sharing unpublished X-ray crystallographic coordinates of a human IgG_1 Fc, Mark Vasser, Parkash Jhurani, Peter Ng, and Kristina Azizian for synthetic oligonucleotides, Brad Snedecor and Han Chen for *E. coli* fermentations, Jim Bourell for mass spectrometry of the proteins, Allan Padua for amino acid hydrolysis analysis, and Bob Kelley for helpful discussions and review of the manuscript.

REFERENCES

1. Davies, D. R., Padlan, E., and Sheriff, S. (1990) *Annu. Rev. Biochem. 59*, 439−473.
2. Mariuzza, R. A., and Poljak, R. J. (1993) *Curr. Opin. Immunol. 5*, 50−55.
3. Webster, D. M., Henry, A. H., and Rees, A. R. (1994) *Curr. Opin. Struct. Biol. 4*, 123−129.
4. Braden, B. C., and Poljak, R. J. (1995) *FASEB J. 9*, 9−16.
5. Clackson, T., and Wells, J. A. (1995) *Science 267*, 383−386.
6. Muller, Y. A., Li, B., Christinger, H. W., Wells, J. A., Cunningham, B. C., and de Vos, A. M. (1997) *Proc. Natl. Acad. Sci. U.S.A. 94*, 7192−7197.
7. Dall'Acqua, W., Goldman, E. R., Eisenstein, E., and Mariuzza, R. A. (1996) *Biochemistry 35*, 9667−9676.
8. Goodsell, D. S., and Olson, A. J. (1993) *Trends Biochem. Sci. 18*, 65−68.
9. Deonarain, M. P., Scrutton, N. S., and Perham, R. N. (1992) *Biochemistry 31*, 1491−1497.
10. Deonarain, M. P., Scrutton, N. S., and Perham, R. N. (1992) *Biochemistry 31*, 1498−1504.
11. Elsevier, J. P., Wells, L., Quimby, B. B., and Fridovich-Keil, J. L. (1996) *Proc. Natl. Acad. Sci. U.S.A. 93*, 7166−7171.
12. Bird, R. E., Hardman, K. D., Jacobson, J. W., Johnson, S., Kaufman, B. M., Lee, S. M., Lee, T., Pope, S. H., Riordan, G. S., and Whitlow, M. (1988) *Science 242*, 423−426.
13. Huston, J. S., Levinson, D., Mudgett-Hunter, M., Tai, M. S., Novotny, J., Margolies, M. N., Ridge, R. J., Bruccoleri, R. E., Haber, E., and Crea, R. (1988) *Proc. Natl. Acad. Sci. U.S.A. 85*, 5879−5883.
14. Deisenhofer, J. (1981) *Biochemistry 20*, 2361−2370.
15. Miller, S. (1990) *J. Mol. Biol. 216*, 965−973.
16. Carter, P., and Wells, J. A. (1988) *Nature 332*, 564−568.
17. Duncan, A. R., and Winter, G. (1988) *Nature 332*, 563−564.
18. Cunningham, B. C., and Wells, J. A. (1989) *Science 244*, 1081−1085.
19. Atwell, S., Ridgway, J. B. B., Wells, J. A., and Carter, P. (1997) *J. Mol. Biol. 270*, 26−35.
20. Hochuli, E. (1988) *J. Chromatogr. 444*, 293−302.
21. Sanger, F., Nicklen, S., and Coulson, A. R. (1977) *Proc. Natl. Acad. Sci. U.S.A. 74*, 5463−5467.
22. Kunkel, T. A., Roberts, J. D., and Zakour, R. A. (1987) *Methods Enzymol. 154*, 367−382.
23. Rodrigues, M. L., Presta, L. G., Kotts, C. E., Wirth, C., Mordenti, J., Osaka, G., Wong, W. L. T., Nuijens, A., Blackburn, B., and Carter, P. (1995) *Cancer Res. 55*, 63−70.
24. Carter, P., Kelley, R. F., Rodrigues, M. L., Snedecor, B., Covarrubias, M., Velligan, M. D., Wong, W. L. T., Rowland, A. M., Kotts, C. E., Carver, M. E., Yang, M., Bourell, J. H., Shephard, H. M., and Henner, D. (1992) *Bio/Technology 10*, 163−168.
25. Zhukovsky, E. A., Mulkerrin, M. G., and Presta, L. G. (1994) *Biochemistry 33*, 9856−9864.

26. Nozaki, Y. (1972) *Methods Enzymol. 26*, 43−50.
27. Santoro, M. M., and Bolen, D. W. (1988) *Biochemistry 27*, 8063−8068.
28. Barrick, D., and Baldwin, R. L. (1993) *Biochemistry 32*, 3790−3796.
29. Greene, R. F., and Pace, C. N. (1974) *J. Biol. Chem. 249*, 5388−5393.
30. Kellis, J. T., Jr., Nyberg, K., and Fersht, A. R. (1989) *Biochemistry 28*, 4914−4922.
31. Horovitz, A., Matthews, J. M., and Fersht, A. R. (1992) *J. Mol. Biol. 227*, 560−568.
32. Serrano, L., Horovitz, A., Avron, B., Bycroft, M., and Fersht, A. R. (1990) *Biochemistry 29*, 9343−9352.
33. Bourell, J. H., Clauser, K. P., Kelley, R., Carter, P., and Stults, J. T. (1994) *Anal. Chem. 66*, 2088−2095.
34. Venyaminov, S. Y., and Yang, J. S. (1996) in *Circular Dichroism and the Conformational Analysis of Biomolecules*, pp 69−107, Plenum Press, New York.
35. Missiakas, D., Betton, J. M., Minard, P., and Yon, J. M. (1990) *Biochemistry 29*, 8683−8689.
36. Glockshuber, R., Malia, M., Pfitzinger, I., and Pluckthun, A. A. (1990) *Biochemistry 29*, 1362−1367.
37. Robinson, C. R., and Sauer, R. T. (1996) *Biochemistry 35*, 13878−13884.
38. Provencher, S. W., and Glockner, J. (1981) *Biochemistry 20*, 33−37.
39. Manning, M. C., and Woody, R. W. (1987) *Biopolymers 26*, 1731−1752.
40. Manning, M. C., Illangasekare, M., and Woody, R. W. (1988) *Biophys. Chem. 31*, 77−86.
41. Ellerson, J. R., Yasmeen, D., Painter, R. H., and Dorrington, K. J. (1976) *J. Immunol. 116*, 510−517.
42. Schiffer, M., Chang, C. H., Naik, V. M., and Stevens, F. J. (1988) *J. Mol. Biol. 203*, 799−802.
43. Holliger, P., Prospero, T., and Winter, G. (1993) *Proc. Natl. Acad. Sci. U.S.A. 90*, 6444−6448.
44. Whitlow, M., Filpula, D., Rollence, M. L., Feng, S. L., and Wood, J. F. (1994) *Protein Eng. 7*, 1017−1026.
45. Desplancq, D., King, D. J., Lawson, A. D. G., and Mountain, A. (1994) *Protein Eng. 7*, 1027−1033.
46. Fersht, A. R., Shi, J., Knill-Jones, J., Lowe, D. M., Wilkinson, A. J., Blow, D. M., Brick, P., Carter, P., Waye, M. M. Y., and Winter, G. (1985) *Nature 314*, 235−238.
47. Street, I. P., Armstrong, C. R., and Withers, S. G. (1986) *Biochemistry 25*, 6021−6027.
48. Shirley, B. A., Stanssens, P., Hahn, U., and Pace, C. N. (1992) *Biochemistry 31*, 725−732.
49. Goldman, E. R., Dall'Acqua, W., Braden, B. C., and Mariuzza, R. A. (1997) *Biochemistry 36*, 49−56.
50. Ackers, G. K., and Smith, F. R. (1985) *Annu. Rev. Biochem. 54*, 597−629.
51. Fersht, A. R. (1988) *Biochemistry 27*, 1577−1580.
52. Eriksson, A. E., Baase, W. A., Zhang, X. J., Heinz, D. W., Blaber, M., Baldwin, E. P., and Matthews, B. W. (1992) *Science 255*, 178−183.
53. Rashin, A. A., Rashin, B. H., Rashin, A., and Abagyan, R. (1997) *Protein Sci. 6*, 2143−2158.
54. Atwell, S., Ultsch, M., de Vos, A. M., and Wells, J. A. (1997) *Science 278*, 1125−1128.
55. Ysern, X., Fields, B. A., Bhat, T. N., Goldbaum, F. A., Dall'Acqua, W., Schwartz, F. P., Poljak, R. J., and Mariuzza, R. A. (1994) *J. Mol. Biol. 238*, 496−500.
56. Ross, P. D., and Subramanian, S. (1981) *Biochemistry 20*, 3096−3102.
57. Bhat, T. N., Bentley, G. A., Boulot, G., Greene, M. I., Tello, D., Dall'Acqua, W., Souchon, H., Schwartz, F. P., Mariuzza, R. A., and Poljak, R. J. (1994) *Proc. Natl. Acad. Sci. U.S.A. 91*, 1089−1093.
58. Koshy, T. I., Luntz, T. L., Schejter, A., and Margoliash, E. (1990) *Proc. Natl. Acad. Sci. U.S.A. 87*, 8697−8701.
59. Schejter, A., Luntz, T. L., Koshy, T. I., and Margoliash, E. (1992) *Biochemistry 31*, 8336−8343.
60. Lascu, I., Deville-Bonne, D., Glaser, P., and Veron, M. (1993) *J. Biol. Chem. 268*, 20268−20275.
61. Alber, T. (1989) *Annu. Rev. Biochem. 58*, 765−798.
62. Shortle, D., and Meeker, A. K. (1986) *Proteins: Struct., Funct., Genet. 1*, 81−89.
63. Wells, J. A. (1991) *Methods Enzymol. 202*, 390−414.
64. Schreiber, G., and Fersht, A. R. (1995) *J. Mol. Biol. 248*, 478−486.
65. Green, S. M., and Shortle, D. (1993) *Biochemistry 32*, 10131−10139.
66. Speros, P. C., LiCata, V. J., Yontani, T., and Ackers, G. K. (1991) *Biochemistry 30*, 7254−7262.
67. LiCata, V. J., and Ackers, G. K. (1995) *Biochemistry 34*, 3133−3139.
68. Fields, B. A., Goldbaum, F. A., Dall'Acqua, W., Malchiodi, E. L., Cauerhff, A., Schwartz, F. P., Ysern, X., Poljak, R. J., and Mariuzza, R. A. (1996) *Biochemistry 35*, 15494−15503.
69. Cunningham, B. C., and Wells, J. A. (1993) *J. Mol. Biol. 234*, 554−563.
70. Chothia, C., and Janin, J. (1981) *Proc. Natl. Acad. Sci. U.S.A. 78*, 4146−4150.
71. Chothia, C., Novotny, J., Bruccoleri, R., and Karplus, M. (1985) *J. Mol. Biol. 186*, 651−663.
72. Janin, J., and Chothia, C. (1990) *J. Biol. Chem. 265*, 16027−16030.
73. Wilson, L. A., and Stanfield, R. L. (1993) *Curr. Opin. Struct. Biol. 3*, 113−118.
74. Davies, D. R., and Cohen, G. H. (1996) *Proc. Natl. Acad. Sci. U.S.A. 93*, 7−12.
75. Ellison, J. W., Berson, B. J., and Hood, L. E. (1982) *Nucleic Acids Res. 10*, 4071−4079.
76. Chang, C. N., Kuang, W. J., and Chen, E. Y. (1986) *Gene 44*, 121−125.
77. Picken, R. N., Mazaitis, A. J., Maas, W. K., Rey, M., and Heyneker, H. (1983) *Infect. Immun. 42*, 269−275.
78. Kabat, E. A., Wu, T. T., Perry, H. M., Gottesman, K. S., and Foeller, C. (1991) *Sequences of Proteins of Immunological Interest*, 5th ed., Vol. 1, pp 688−696, National Institutes of Health, Bethesda, MD.

BI980270I

EXHIBIT 2

The EMBO Journal vol.11 no.12 pp.4313–4321, 1992

The human T cell antigen gp39, a member of the TNF gene family, is a ligand for the CD40 receptor: expression of a soluble form of gp39 with B cell co-stimulatory activity

Diane Hollenbaugh, Laura S.Grosmaire, Christopher D.Kullas, N.Jan Chalupny, Sten Braesch-Andersen[1], Randolph J.Noelle[2], Ivan Stamenkovic[1], Jeffrey A.Ledbetter and Alejandro Aruffo

Bristol-Myers Squibb Pharmaceutical Research Institute, Seattle, WA 98121, [1]Department of Pathology, Massachusetts General Hospital and Harvard Medical School, Boston MA 02114 and [2]Department of Microbiology, Dartmouth Medical School, Lebanon, NH 03745, USA

Communicated by D.Kolakofsky

Signals delivered to B cells via CD40 can synergize with those provided by other B cell surface receptors to induce B cell proliferation and antibody class switching as well as modulate cytokine production and cell adhesion. Recently, it has been shown that the ligand for CD40 is a cell surface protein of ~39 kDa expressed by activated T cells, gp39. Here we report on the isolation and characterization of a cDNA clone encoding human gp39, a type II membrane protein with homology to TNF, and the construction and characterization of a soluble recombinant form of gp39. COS cell transfectants expressing gp39 synergized with either anti-CD20 mAb or PMA to drive strong B cell proliferation and alone were able to drive B cells to proliferate weakly. In all cases the B cell proliferation induced by gp39-expressing COS cells was reduced to background levels by the addition of soluble CD40. Unlike gp39-expressing COS cells, recombinant soluble gp39 was not mitogenic alone and required co-stimulation to drive B cell proliferation. These results suggest that B cells require a second signal besides gp39–CD40 to drive proliferation and that soluble gp39 alone in a non-membrane bound form is able to provide co-stimulatory signals to B cells.

Key words: Bp50/CD20/fusion protein/IgE/type II membrane protein

Introduction

CD40 is a ~50 kDa glycoprotein expressed on the surface of B cells, follicular dendritic cells, normal basal epithelium and some carcinoma and melanoma derived cell lines (Paulie *et al.*, 1985, 1989; Clark and Ledbetter, 1986; Ledbetter *et al.*, 1987; Young *et al.*, 1989). Isolation of a human cDNA encoding CD40 showed that this protein is a type I membrane protein that is significantly related to the members of the nerve growth factor receptor family (Stamenkovic *et al.*, 1989). The role of CD40 in B cell activation is well established. Crosslinking CD40 with anti-CD40 monoclonal antibodies (mAb) induces B cell aggregation via LFA-1 (Gordon *et al.*, 1988; Barrett *et al.*, 1991), increases Ser/Thr (Gordon *et al.*, 1988) and Tyr (Uckun *et al.*, 1991) phosphorylation of a number of intracellular substrates and provides a 'competence' signal that allows B cells to proliferate and undergo class switching when stimulated with the appropriate second signal. For example, anti-CD40 mAb can synergize with PMA (Gordon *et al.*, 1987) or anti-CD20 mAb (Clark and Ledbetter, 1986) to induce B cell proliferation, with IL-4 to induce B cell proliferation (Gordon *et al.*, 1987; Rousset *et al.*, 1991) and IgE secretion (Jabara *et al.*, 1990; Gascan *et al.*, 1991; Rousset *et al.*, 1991; Zhang *et al.*, 1991; Shapira *et al.*, 1992) and with IL-10 and TGF-β to induce IgA secretion by $sIgD^+$ B cells (DeFrance *et al.*, 1992). There is also evidence that CD40-mediated signals are involved in modulating cytokine production by activated B cells (Cairns *et al.*, 1988; Clark and Shu, 1990). Crosslinking of anti-CD40 mAb alone is not sufficient to induce B cell proliferation as demonstrated by the observation that anti-CD40 mAb immobilized on plastic in conjunction with IL-4 are unable to induce vigorous B cell proliferation (Banchereau *et al.*, 1991). However, anti-CD40 mAb immobilized on murine L cells transfected with an Fc receptor, CD32, are able to induce B cell proliferation in the presence of IL-4 (Banchereau *et al.*, 1991), suggesting that a signal provided by the fibroblasts synergizes with the CD40 signal and IL-4 to drive B cell proliferation.

We and others have used soluble forms of the extracellular domain of human CD40, CD40–Ig, to show that the CD40 ligand gp39 is a glycoprotein of ~39 kDa expressed on the surface of activated $CD4^+$ murine T cells (Armitage *et al.*, 1992; Noelle *et al.*, 1992). Interaction with gp39 induces B cells to enter the cell cycle and become responsive to the growth and differentiation effects of lymphokines (Armitage *et al.*, 1992; Noelle *et al.*, 1992). Both CD40–Ig and a hamster mAb specific to murine gp39, MR1, are able to block B cell proliferation induced by activated T cells (PM^{Act}), but not by lipopolysaccharide (LPS) (Noelle *et al.*, 1992). In addition, the polyclonal differentiation of B cells to produce Ig elicited by T cells in conjunction with IL-4 and IL-5 can be blocked by both CD40–Ig and MR1 (Noelle *et al.*, 1992). Recently, a cDNA encoding murine gp39 has been isolated and shown to be functionally active when expressed as a membrane protein on transfected cells (Armitage *et al.*, 1992). This cDNA encodes a 260 amino acid polypeptide with the typical features of a type II membrane protein and CV1/EBNA cells expressing murine gp39 were shown to induce murine and human B cell proliferation without additional co-stimulus.

Here we report the isolation and characterization of a human cDNA encoding gp39, discuss the homology of gp39 with tumor necrosis factor (TNF) and describe the preparation of a functional, soluble and recombinant form of gp39. Using the soluble recombinant gp39 we show that human gp39 is unable to induce the proliferation of B cells in the

© Oxford University Press

absence of a co-stimulus but is able to synergize with known B cell co-stimuli.

Results

Isolation and characterization of a cDNA encoding human gp39

A cDNA encoding the human gp39 was amplified from a cDNA library prepared from mRNA isolated from PHA activated human peripheral blood T cells by PCR using synthetic oligonucleotides based on the murine gp39 sequence (Armitage *et al.*, 1992). The PCR product was subcloned into the expression vector CDM8 (Seed, 1987). COS cells transfected with the CDM8–gp39 plasmid produced a cell surface protein that bound to CD40–Ig (data not shown) (Noelle *et al.*, 1992). A complete human gp39 gene was isolated by colony hybridization from the same cDNA library that was used for the PCR amplification of gp39 using the subcloned PCR product as a probe. A number of positive clones were isolated and analyzed by restriction enzyme digestion. DNA corresponding to those clones containing the largest inserts, 1.8–1.5 kb, were transfected into COS cells and their ability to direct the expression of a CD40–Ig binding protein examined. One such clone that was positive by these criteria was analyzed further and is referred to hereafter as human gp39. Immunoprecipitation of cDNA-encoded human gp39 protein from transfected COS cells using CD40–Ig showed a single band corresponding to a molecular mass of ~32–33 kDa (Figure 1). The COS cell derived protein is smaller than expected based on previous studies of murine gp39. However, we have observed in many instances that the apparent molecular masses of a number of different T cell surface proteins obtained from COS cell transfectants are smaller than those obtained from T cells (Aruffo and Seed, 1987; Aruffo *et al.*, 1991). We believe that these differences in size are the result of incomplete glycosylation of the proteins by COS cells.

The isolated human gp39 clone is ~1.8 kb, encoding a polypeptide of 261 amino acids (aa) with a predicted molecular mass of ~29 kDa. The absence of a secretory signal peptide suggests that the first 22 amino-terminal residues are intracellular. This is followed by 24 predominantly hydrophobic residues consistent with a transmembrane domain and 215 aa constituting the putative carboxy-terminal extracellular (EC) domain. One N-linked glycosylation site (Asn-X-Ser/Thr) exists in the EC and one in the cytoplasmic domain (nucleotide sequences corresponding to coding sequence and the predicted aa sequence are shown in Figure 2A). The expected orientation of the protein, with an extracellular carboxy-terminus, classifies it as a type II membrane protein and the difference between the predicted and observed molecular mass suggests that it undergoes post-translational modifications, most probably the addition of carbohydrate groups. Murine (Armitage *et al.*, 1992) and human gp39 are highly homologous. Within the coding region they share ~83% identity at the nucleotide level and ~73% identity at the aa level (Figure 2B; data not shown). The predicted amino acid sequence of human gp39 was compared with those in the National Biomedical Research Foundation (NBRF) database using the FASTP algorithm and found to have significant homology with TNFα (Gray *et al.*, 1984) and TNFβ (Pennica *et al.*, 1984; Wang *et al.*, 1985) (Figure 2B).

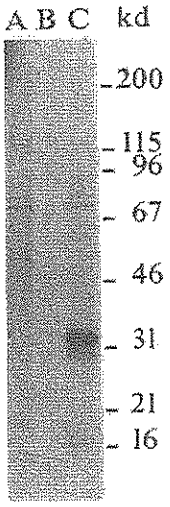

Fig. 1. Precipitation of gp39 from COS cells using CD40–Ig. Radiolabeled proteins from surface iodinated COS cells transfected with vector alone (mock, lane A) or gp39 (lanes B–C) were precipitated with CD40–Ig (lanes A and C) or Leu8–Ig (lane B) and analyzed by SDS–PAGE under reducing conditions as described in Materials and methods. The electrophoretic mobility of molecular mass standards of the indicated mass in kDa are shown to the right.

Preparation and characterization of the soluble recombinant gp39 as a chimeric fusion protein

Previously, recombinant soluble forms of type I cell surface proteins have been generated as fusion proteins in which the EC domain (amino-terminal domain) of the membrane proteins have been joined to a tag polypeptide, such as an immunoglobulin heavy chain constant region (e.g. CD40–Ig and Leu8–Ig fusions used in this study) (for a review see Hollenbaugh *et al.*, 1992). In these cases, the Ig region replaces the transmembrane and cytoplasmic domains of the surface proteins and is used as a 'handle' for manipulating the soluble recombinant surface proteins with reagents developed for use with antibodies. Because type II membrane proteins are oriented with a carboxy-terminal EC domain, an alternate fusion was designed such that the tag polypeptide is amino-terminal to the EC portion of the protein, again replacing the transmembrane and cytoplasmic domains of the surface protein. This tag polypeptide should also contain an amino-terminal secretory signal sequence to allow export of the fusion protein. We chose the murine CD8 EC domain (Nakauchi *et al.*, 1985) as our tag polypeptide to construct our fusion proteins of type II membrane proteins for four reasons: (i) the use of a complete extracellular protein domain as the tag polypeptide minimizes the chances that the tag polypeptide will affect the tertiary structure of the surface protein to which it is fused while maximizing the likelihood that the fusion protein will be expressed and exported; (ii) a previously studied CD8–Ig chimera demonstrated that CD8 fusion proteins are produced and exported by COS cells in high yield; (iii) a large number of mAb directed to CD8 are available and can be used to manipulate the recombinant CD8 fusion proteins; and (iv) the interaction between murine CD8 and human MHC I is not detectable. To generate the CD8–gp39 fusion gene, $_{s}$gp39, a cDNA fragment encoding the EC domain of murine CD8, was fused with a cDNA fragment encoding the EC domain of gp39, as described in Materials and methods (Figure 3A). The $_{s}$gp39

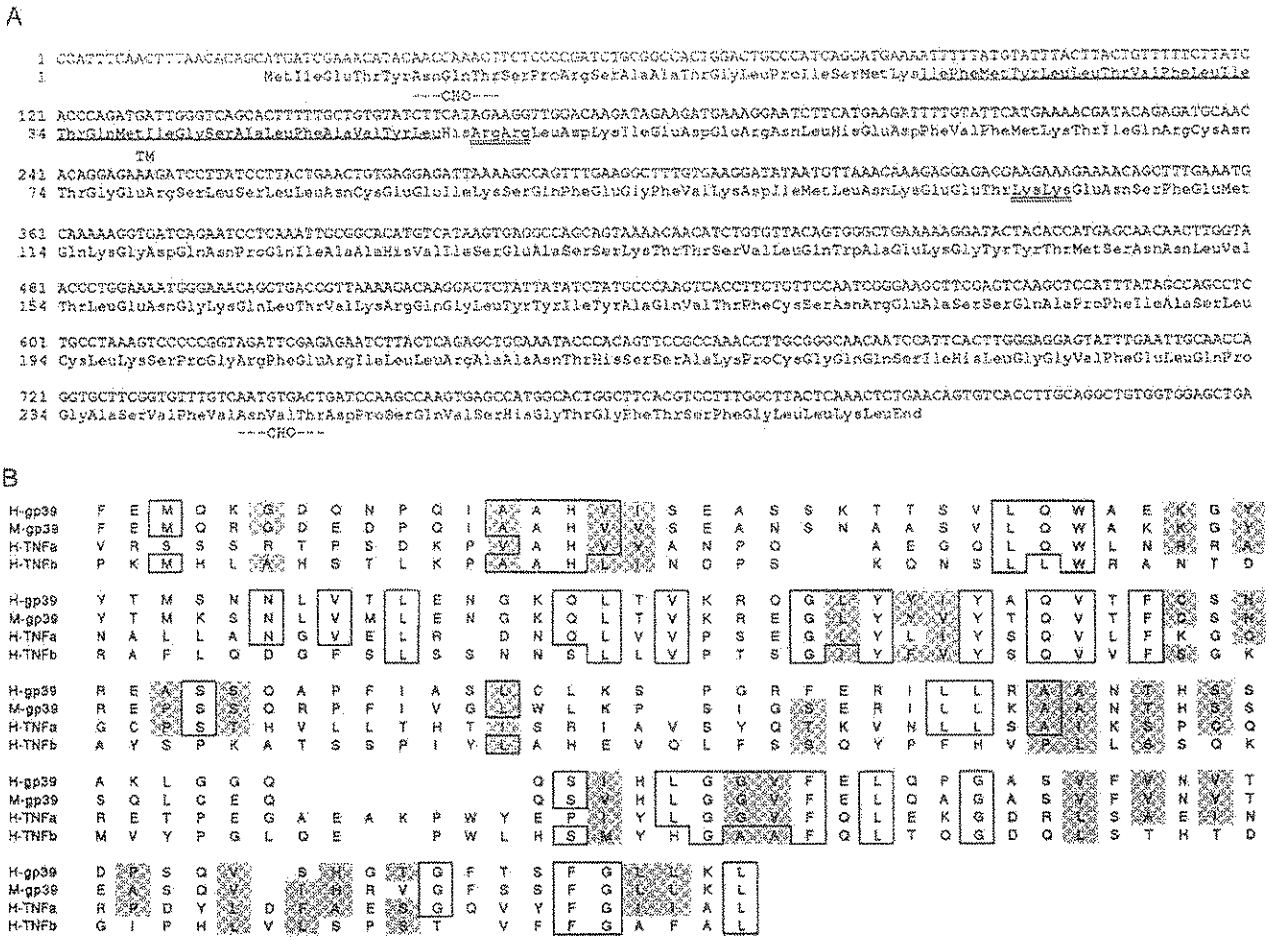

Fig. 2. Nucleotide and predicted amino acid sequence of human gp39 and homology to murine gp39, TNFα and TNFβ. (**A**) The nucleotide sequence and translated ORF are numbered at left. Sites of potential N-linked glycosylation are marked (CHO), the predicted transmembrane domain (TM) is underlined and the two Arg residues and the two Lys residues discussed in the text are double underlined. Nucleotide and amino acid numbering is given to the left. The nucleotide sequence is available from EMBL/GenBank/DDBJ under accession number Z15017. (**B**) Alignment of the predicted amino acid sequence of human gp39 (H-gp39), murine gp39 (M-gp39), human TNFα (H-TNFα), and human TNFβ (H-TNFβ). Amino acids shared by at least three proteins are shown boxed; similar amino acids shared by at least three of the proteins are shown shaded.

protein was prepared by transient expression in COS cells and recovered from COS cell supernatants with anti-CD8 mAb or with a soluble recombinant CD40−Ig chimera, which we used in our earlier murine gp39 studies (Figure 3B). The $_s$gp39 protein has a molecular mass of ~50 kDa (Figure 3B) when analyzed by SDS−PAGE under reducing conditions. Preliminary results indicate that $_s$gp39 forms dimers and trimers in solution (data not shown).

As a control, a chimeric gene encoding a soluble recombinant form of the B cell antigen CD72 (Von Heogen *et al.*, 1990), another type II membrane protein, was constructed (Figure 3A). The $_s$CD72 protein was also produced by transient expression in COS cells and recovered from COS cell supernatants with anti-CD8 mAb or with three anti-CD72 mAb tested, but not with the CD40−Ig fusion protein (Figure 3C; data not shown).

To characterize further the interaction between CD40 and the soluble recombinant gp39, COS cells were transfected with a cDNA encoding the full length CD40 protein (Stamenkovic *et al.*, 1989) and their ability to bind to $_s$gp39, $_s$CD72 and anti-CD40 mAb examined by fluorescence microscopy. Both the $_s$gp39 and the anti-CD40 mAb bound to the transfectants while $_s$CD72 did not (Figure 4; data not shown). In addition, COS cells were transfected with a cDNA encoding the full length gp39 and their ability to bind to CD40−Ig (Noelle *et al.*, 1992) or an irrelevant Ig fusion protein, Leu8−Ig (Aruffo *et al.*, 1992), was examined. CD40−Ig, but not Leu8−Ig, bound to gp39-expressing COS cells (Figure 4; data not shown).

In parallel experiments, $_s$gp39 and $_s$CD72 were immobilized in the wells of a 96-well microtiter dish via an anti-CD8 mAb and their binding was examined in relation to increasing concentrations of CD40−Ig or a control immunoglobulin fusion protein, Leu8−Ig. The binding of CD40−Ig to immobilized $_s$gp39 was saturable, while CD40−Ig did not bind to $_s$CD72 and Leu8−Ig did not bind to $_s$gp39 (Figure 5). Similarly, CD40−Ig and Leu8−Ig were immobilized via anti-human Fc antibodies and the binding of $_s$gp39 or $_s$CD72 from increasing dilutions of COS cell supernatants was measured. Immobilized CD40−Ig bound $_s$gp39 but not $_s$CD72 and Leu8−Ig did not bind $_s$gp39 (data not shown).

Human gp39 requires a co-stimulus to induce B cell proliferation

To examine the role of gp39−CD40 interactions in B cell activation, COS cells transfected with either the cDNA

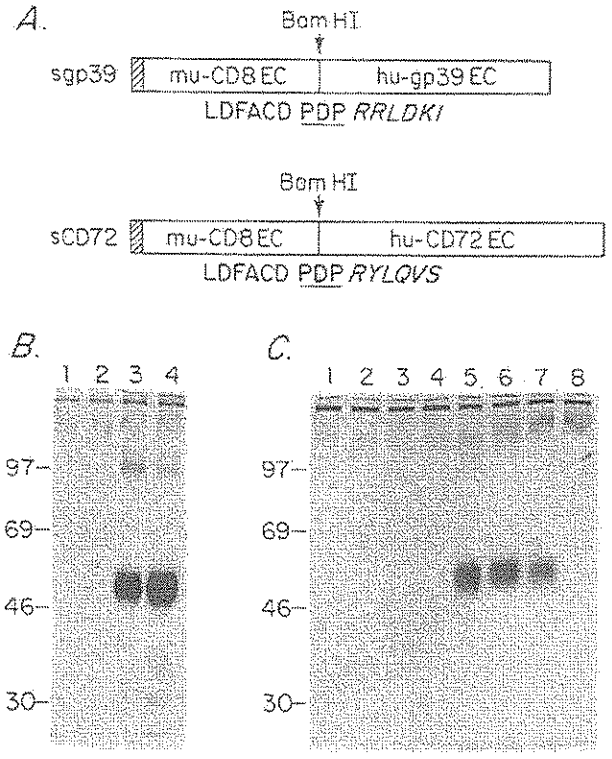

Fig. 3. Soluble recombinant human gp39 and CD72, $_s$gp39 and $_s$CD72. **(A)** The cDNA fragment encoding the extracellular domain of murine CD8 is designated, mu-CD8 EC. The murine CD8 amino terminal secretory signal sequence is shown stippled. The cDNA fragments encoding the extracellular domain of human gp39 or CD72 are designated hu-gp39 EC and hu-CD72 EC, respectively. The amino acid sequences predicted at the site of fusion of the extracellular domain of murine CD8 and human gp39 (italic) or CD72 (italic) are shown below the individual diagrams. Residues introduced at the junction of the two cDNA fragments are shown underlined. The unique *Bam*HI restriction enzyme recognition site at the junction of the two genes is shown. **(B)** Radiolabeled proteins from the supernatants of metabolically-labeled mock (lanes 1 and 2) or CD8–gp39 (lanes 3 and 4) transfected COS cells were immunoprecipitated based on their interaction with the anti-murine CD8 mAb 53-6 (lanes 1 and 3) or the CD40–Ig (lanes 2 and 4) and analyzed by SDS–PAGE under reducing conditions as described in Materials and methods. The electrophoretic mobility of molecular mass standards of the indicated mass in kDa are shown to the left. **(C)** Radiolabeled proteins from the supernatants of metabolically labeled mock (lanes 1–4) and CD8–CD72 (lanes 5–8) transfected COS cells were recovered based on their reactivity with the anti-murine mAb 53-6 (lanes 1 and 5), the anti-CD72 mAb J3101 (lanes 2 and 6), the anti-CD72 mAb BU41 (lanes 3 and 7) and CD40–Ig (lanes 4 and 8) and analyzed by SDS–PAGE under reducing conditions as described in Materials and methods. The electrophoretic mobility of molecular mass standards of the indicated mass in kDa are shown to the left.

encoding gp39 or vector alone (mock) were tested for their ability to stimulate B cell proliferation. Peripheral blood B cells proliferated only weakly when incubated with gp39-expressing COS cells alone (Figure 6). However, upon exposure to gp39-expressing COS cells in conjunction with either the IF5 mAb (Clark *et al.*, 1985) directed against the B cell surface protein CD20 or PMA, vigorous B cell proliferation was observed. In both cases, the gp39-driven B cell proliferation could be reduced to background levels with the soluble CD40–Ig fusion protein (Figure 6). B cells proliferated weakly when incubated with mock-transfected COS cells in the presence of either the anti-CD20 mAb or PMA and this proliferation was unaffected by the presence of CD40–Ig (Figure 6). The weak B cell proliferation observed with gp39-expressing COS cells in the absence of a co-stimulatory signal suggests that in this case COS cells also provide co-stimulatory signals that synergize with CD40 signals to drive B cell proliferation.

Human peripheral blood B cells were incubated with a soluble recombinant gp39, $_s$gp39 or a control fusion protein, $_s$CD72, in the absence or presence of anti-CD20 mAb or PMA. B cells responded with weak proliferation in the presence of $_s$gp39 alone. However, $_s$gp39 induced vigorous B cell proliferation when either anti-CD20 mAb or PMA was present (Figure 7). B cell proliferation was not observed with $_s$CD72, anti-CD20 mAb or PMA alone or with $_s$CD72 in conjunction with anti-CD20 mAb or PMA (Figure 7).

In parallel experiments, dense human tonsillar B cells were prepared and their ability to proliferate in response to $_s$gp39 and $_s$CD72 was examined (Figure 8; data not shown). As seen with peripheral blood B cells, tonsillar B cells proliferated weakly in response to $_s$gp39, but showed strong proliferation when incubated with $_s$gp39 in the presence of the anti-CD20 mAb 1F5 or PMA. No significant proliferation over background levels was observed when the cells were incubated with $_s$CD72 alone or in the presence of the 1F5 mAb or PMA. To examine the specificity of the $_s$gp39-driven activation response, the ability of CD40–Ig to block the $_s$gp39 and 1F5 or $_s$gp39 and PMA driven B cell proliferation was examined. CD40–Ig was able to reduce the $_s$gp39 driven B cell activation under the conditions used (~20 μg/ml gave ~50% inhibition, Figure 8A) while the control fusion protein Leu8–Ig had no effect (Figure 8B).

Discussion

The ability of the B cell surface receptor CD40 to transduce signals has been established using monoclonal antibodies (Clark and Ledbetter, 1986; Gordon *et al.*, 1987). To study further the role of CD40, we have isolated and characterized a cDNA encoding the ligand from a human source. In addition, we have developed a means of generating a soluble form of the protein so that isolated co-stimulatory signals may be studied in the absence of stimuli contributed by the heterologous cells expressing the full length protein.

Isolation of a cDNA clone encoding human gp39 showed that the predicted polypeptide is a type II membrane protein, closely related to its murine homolog and more distantly related to TNFα (Gray *et al.*, 1984) and TNFβ (Pennica *et al.*, 1984; Wang *et al.*, 1985). TNFα and TNFβ are pleiotropic cytokines that exist predominantly as secreted proteins (for a review see Vassalli, 1992), although membrane bound forms have been reported (Kriegler *et al.*, 1988). Presently, there is no evidence for the existence of a soluble form of gp39. However, human gp39, like murine gp39 (Armitage *et al.*, 1992), contains two Arg residues at the junction of the extracellular and transmembrane domains, which may be a site of proteolytic cleavage to give rise to soluble gp39 (Thomas *et al.*, 1988). Alternatively, cleavage could take place at the two Lys residues located at the start of the region of gp39, which is homologous to TNF. The three dimensional structures of TNFα (Eck and Sprang, 1989; Jones *et al.*, 1989) and TNFβ (Eck *et al.*, 1992) have been reported. Soluble TNFα and TNFβ are trimers composed of monomers with a distinctive anti-parallel β-sheet tertiary structure with a 'jelly-roll' topology. Structural

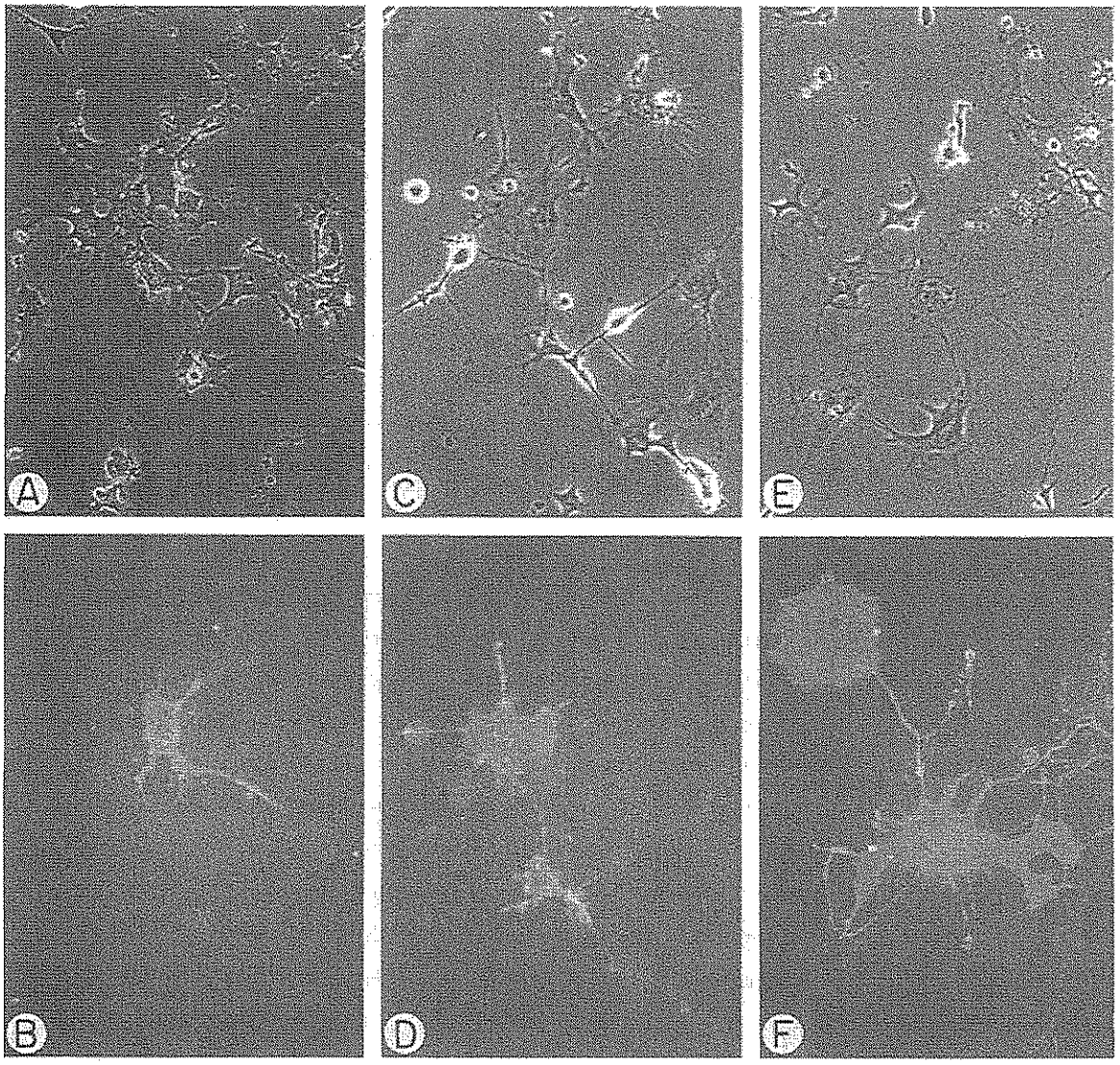

Fig. 4. Binding of $_s$gp39 or CD40-Ig to transfected COS cells. COS cells transfected with either a gp39 (**A** and **B**) or a CD40 (**C**–**F**) cDNA expression plasmid were examined for their ability to bind either soluble recombinant CD40 (A and B), or soluble recombinant gp39 (C and D) or the anti-CD40 mAb G28-5 (E and F) as described in Materials and methods. Phase (A, C and E) and fluorescence (B, D and F) images of representative fields are shown (magnification, 200×).

alignment studies suggest that the amino acid sequence of gp39 is compatible with a TNF-like fold and the formation of a trimeric quarternary structure (J.Bajorath, personal communication). The proposed relationship between gp39 and TNF is also strengthened by the observation that the gp39 receptor, CD40, is significantly homologous to the members of the TNF receptor superfamily (Stamenkovic *et al.*, 1989) and that similar to gp39, the membrane bound form of TNFα is a type II glycoprotein (Kriegler *et al.*, 1988).

It has been reported that purified murine splenic B cells and human tonsillar B cells proliferate when incubated with CV1/EBNA cells expressing murine gp39 in the absence of co-stimulus (Armitage *et al.*, 1992). Based on these data it had been thought that gp39 is directly mitogenic for B cells. To determine whether gp39 binding to CD40 is able to stimulate B cells to proliferate in the absence of other co-stimulatory signals, the effect of gp39 expressed in fibroblast cells on the proliferation of B cells was compared with that of soluble gp39. The gp39 was active in both forms, however, interesting differences between gp39-expressing COS cells and $_s$gp39 were seen. COS cells expressing human gp39 were able to induce weak B cell proliferation in the absence of co-stimuli and could synergize with either anti-CD20 mAb or PMA to induce vigorous B cell proliferation. In all cases, the B cell proliferation could be reduced to background levels with soluble recombinant gp39 receptor, CD40–Ig. Meanwhile $_s$gp39 was only able to induce B cells, isolated from either peripheral blood or tonsils, to proliferate in conjunction with either anti-CD20 mAb or PMA and as observed with gp39-expressing COS cells, $_s$gp39-driven B cell activation could be inhibited with CD40–Ig, but not with an irrelevant Ig fusion protein. These data indicate that gp39 requires a co-stimulatory signal to drive B cell proliferation most effectively and that there is no strict requirement for cell surface expression of gp39 for activity. In addition, the ability of gp39 expressed on the surface of COS cells to stimulate weak B cell proliferation

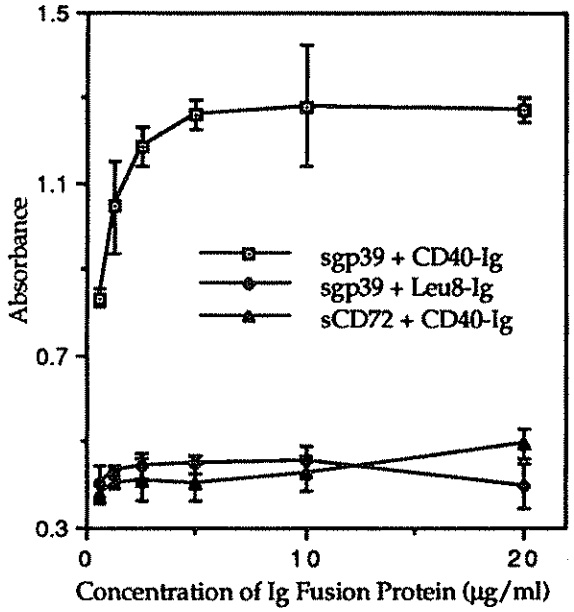

Fig. 5. Characterization of the $_s$gp39–CD40–Ig interaction. The ability of increasing concentrations of CD40–Ig (0.6–20 μg/ml) and the control immunoglobulin fusion protein, Leu8–Ig (0.6–20 μg/ml), to bind to immobilized $_s$gp39 was examined by ELISA as described in Materials and methods. The ability of increasing concentrations of CD40–Ig to bind to the immobilized control fusion protein $_s$CD72 was also examined in the same way. In both cases the $_s$gp39 and $_s$CD72 were immobilized on plastic that had been previously coated with the anti-murine CD8 mAb 53-6 as described in Materials and methods.

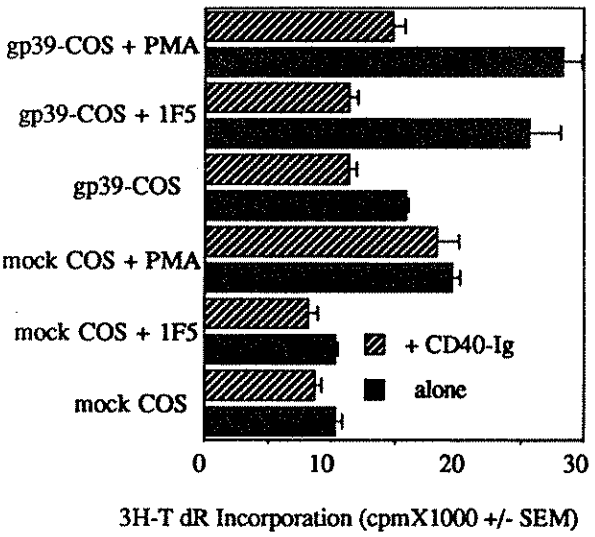

Fig. 6. Activation of human B cells by surface bound gp39. The ability of gp39-expressing COS cells (gp39-COS) or mock transfected COS cells (mock COS) to stimulate the proliferation of human peripheral blood B cells alone or in the presence of the anti-CD20 mAb 1F5 (+ 1F5) or PMA (+ PMA) in the absence (solid bars, alone) or presence of CD40–Ig (hatched bars, + CD40–Ig) was examined as described in Materials and methods and evaluated by [^{3}H]thymidine incorporation.

supports the idea that COS cells may also provide co-stimulatory signals, as yet undefined, which can weakly synergize with those provided by gp39. These observations parallel those in which L cell transfectants expressing the

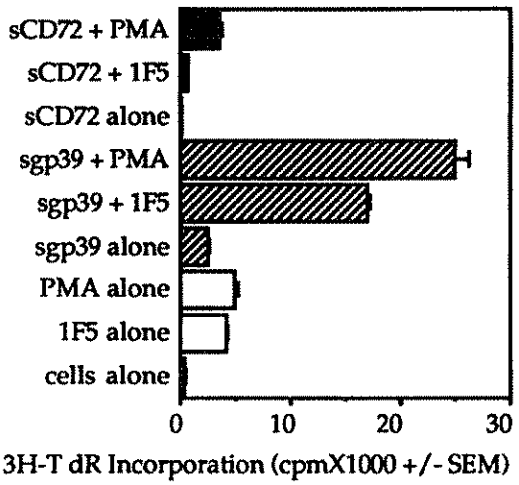

Fig. 7. Activation of human peripheral blood B cells by $_s$gp39. The ability of soluble recombinant gp39 ($_s$gp39, hatched bars) or control soluble recombinant fusion protein ($_s$CD72, solid bars) to stimulate the proliferation of human peripheral blood B cells alone or in conjunction with the anti-CD20 mAb 1F5 (+ 1F5) or PMA (+ PMA) was examined as described in the Materials and methods, evaluated by [^{3}H]thymidine incorporation and compared to that of B cells incubated for an equivalent amount of time in the absence of exogenous stimuli (cells alone, open bars) or in the presence of either 1F5 alone or PMA alone (open bars).

Fc receptor CD32 presenting anti-CD40 mAb in conjunction with IL-4 were found to induce B cells to proliferate more efficiently than did anti-CD40 mAb immobilized on plastic in conjunction with IL-4 (Banchereau *et al.*, 1991). Thus the findings suggest that fibroblasts are capable of providing stimulatory signals that synergize with those provided by anti-CD40 mAb resulting in efficient B cell proliferation.

The development of factor-dependent, long-term B cell cultures has important implications for the study of B cell growth and differentiation, and the development of antigen-specific B cell lines (Tisch *et al.*, 1988). Experiments with anti-CD40 mAb showed that CD40 signals can synergize with other co-stimulatory signals such as those delivered by anti-CD20 mAb to drive B cell proliferation, and that treatment of B cells with anti-CD40 mAb induces a state of B cell 'alertness' that allows them to respond more readily to subsequent activation signals. These observations led to the development of long-term B cell cultures using the L cell/CD32/anti-CD40 mAb system described above. The ability of $_s$gp39 to stimulate B cell proliferation in conjunction with anti-CD20 mAb or PMA suggests that it might replace the anti-CD40 presenting L cells in an *in vitro* system for long-term B cell growth. Further work is needed to investigate whether $_s$gp39 will function as a novel recombinant B cell growth factor that can be used in conjunction with IL-4 or other growth factors in a simple *in vitro* system for the long-term propagation of B cell cultures. It is interesting to note that the CD40–Ig and the $_s$gp39 fusion proteins described here can be used to either inhibit or stimulate the CD40 response in B cells and thus are useful research tools with which to study B cell–T cell interactions and might have a clinical application by permitting either up regulation or down regulation of B cell responses.

Recently, a large number of cDNA clones encoding type II

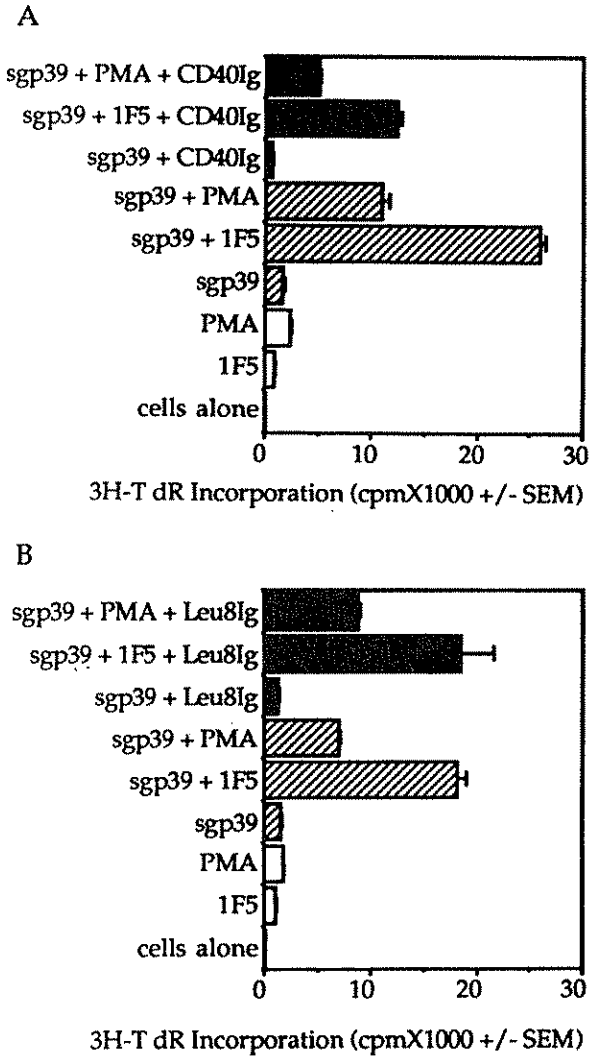

Fig. 8. Activation of dense human tonsillar B cells by $_s$gp39. The ability of soluble recombinant gp39 ($_s$gp39, hatched and solid bars) to stimulate the proliferation of dense tonsillar B cells alone or in conjunction with the anti-CD20 mAb 1F5 (+1F5) or PMA (+ PMA) was examined as described in the Materials and methods, evaluated by [^{3}H]thymidine incorporation and compared to that of B cells incubated alone (cells alone, open bars) or in the presence of either 1F5 alone or PMA alone (open bars). The ability of CD40-Ig (solid bars) to block the $_s$gp39-driven B cell activation was examined at a concentration of 20 μg/ml (**A**) and compared with an equal concentration of an irrelevant immunoglobulin fusion protein, Leu8-Ig (solid bars, **B**).

membrane proteins have been isolated. These proteins include amongst others the B cell antigen CD72 (Von Hoegen *et al.*, 1990), which has been reported to interact with the T cell protein CD5 (Van de Velde *et al.*, 1991) and the T cell antigen CD26, a dipeptidyl peptidase (Marguet *et al.*, 1992). Methodologies designed to prepare and purify recombinant soluble forms of these proteins will have a significant impact in facilitating studies on their structure and function. Although recombinant forms of type II membrane proteins have been prepared in the past by replacing the cytoplasmic domain of the type II protein with a cleavable signal peptide (Lemay *et al.*, 1989), these methods have not been used widely since they do not provide for facile purification and manipulation of the recombinant protein unless antibodies directed against it are readily available. Here an alternative method for the preparation of recombinant soluble forms of type II membrane proteins is described in which the extracellular domain of a type I membrane protein serves as a tag polypeptide replacing the transmembrane and cytoplasmic domain of the type II membrane protein. The resulting chimeric protein is secreted into the supernatant of appropriately transfected cells, from which it can be purified and manipulated with antibodies directed to the tag polypeptide. The extensive immunoprecipitation and cell binding studies presented herein for the chimeric soluble forms of gp39 and CD72 suggest that this type of fusion protein is structurally and functionally sound and thus provide a valuable tool with which to study the function of type II membrane proteins *in vitro* and possibly *in vivo*.

Materials and methods

Isolation and characterization of a human cDNA encoding gp39

The previously described CD40-Ig was modified by the introduction of three mutations in the immunoglobulin domain to reduce the binding to Fc receptors (W.Brady and P.Linsley, personal communication). The modified CD40-Ig was purified from COS cell supernatants as previously described by Aruffo *et al.* (1990). Human gp39 cDNA was amplified by PCR from a library prepared from mRNA isolated from PHA-activated human peripheral blood T-cells (Camerini *et al.*, 1989). The oligonucleotide primers were designed based on the sequence of the murine gp39 (Armitage *et al.*, 1992) and included sites for the restriction enzymes *Xba*I and *Hin*dIII to be used in subcloning the PCR product. The oligonucleotides used were: 5′-GCG AAG CTT TCA GTC AGC ATG ATA GAA ACA-3′ and 5′-CGC TCT AGA TGT TCA GAG TTT GAG TAA GCC-3′. Amplification was performed with *Taq* polymerase and the reaction buffer recommended by the manufacturer (Perkin-Elmer Cetus) using 30 cycles of the following temperature program: 2 min at 95°C, 2 min at 55°C and 3 min at 72°C. The PCR product was digested with *Hin*dIII and *Xba*I, and was found to contain an internal *Hin*dIII restriction site. The *Hin*dIII-*Xba*I fragment was subcloned into the CDM8 vector. The complete gene product was constructed by subcloning the *Hin*dIII-*Hin*dIII fragment into the vector containing the *Hin*dIII-*Xba*I fragment. The resulting construct was transfected into COS cells using DEAE-dextran as previously described by Aruffo *et al.* (1990). Transfectants were stained with CD40-Ig (25 μg/ml in DMEM) followed by FITC-conjugated goat anti-human IgG Fc antibody (1:50 dilution in DMEM; TAGO, Burlingame, CA) and visualized by immunofluorescence microscopy. The complete human gp39 was obtained by colony hybridization as described (Sambrook *et al.*, 1989). The subcloned *Hin*dIII-*Hin*dIII fragment of the PCR product was used to generate a ^{32}P-labeled probe by random primed polymerization. Plasmid DNA from three individual clones was transfected into COS cells and cells were stained with CD40-Ig. One clone, clone 19, was positive by this criteria and used in the remainder of the study. The sequence was determined by dideoxy sequencing using Sequenase™ (United States Biochemical Co, Cleveland, OH).

Plasmid containing gp39 or vector alone (mock) was transfected into COS cells by the DEAE-dextran method. 48 h post-transfection, cells were detached with EDTA, radiolabeled with ^{125}I using Iodo-beads (Pierce Chemical Co., Rockford, IL) and lysed with 1% NP-40 with aprotinin as protease inhibitor. Lysates were incubated with 10 μg of CD40-Ig or Leu8-Ig at 4°C overnight in the presence of Protein A-Sepharose beads (Pierce Chemical Co.). Beads were washed several times in lysis buffer and precipitated proteins eluted by boiling in loading buffer in the presence of 2% β-mercaptoethanol. Samples were subjected to SDS-8%PAGE, the gel was dried and exposed for autoradiography at −80°C overnight.

Construction, characterization and preparation of a soluble gp39 chimera

The extracellular domain of the human gp39 was amplified from the cDNA library prepared from mRNA from PHA activated human peripheral blood lymphocytes. The oligonucleotide primers were designed based on sequence information obtained from the PCR product described above and were designed to place a *Bam*HI site at the 5′ end of the gene such that the reading frame would be preserved when the chimeric gene was constructed. The oligonucleotides used were 5′-CGA AGC TTG GAT CCG AGG AGG TTG GAC AAG ATA GAA GAT-3′ and 5′-CGC TCT AGA TGT TCA GAG TTT GAG TAA GCC-3′. The PCR was performed using the *Pfu* polymerase

with the buffer supplied by the manufacturer (Stratagene, La Jolla, CA) with the following temperature program: 5 min at 95°C, 2 min at 72°C and 2 min at 55°C; 40 cycles of amplification consisting of 1 min at 95°C, 2 min at 55°C, 3 min at 72°C and 10 min at 72°C. The PCR product was digested with *Bam*HI and *Xba*I, and subcloned in a vector containing the gene encoding the murine CD8 (Lyt2a) extracellular domain with a *Bam*HI restriction site generated by PCR (N.J.Chalupny, unpublished data). Similarly, the gene encoding the extracellular domain of human CD72 was generated by PCR to contain a *Bam*HI restriction site and subcloned in the CD8-containing vector in the same manner using the oligonucleotides 5′-CGA AGC TTG GAT CCG CGC TAT CTG CAG GTG TCT CAG CAG-3′ and 5′-CGC TCT AGA CTC GAG GTC CTA ATC TGG AAA CCT GAA AGC-3′ and *Taq* polymerase (Perkin–Elmer Cetus).

The ability of COS cells to express and export $_s$gp39 and $_s$CD72 was tested. First, COS cells were transfected using DEAE-dextran. One day after transfection, cells were trypsinized and replated. One day later, cells were fixed with 2% formaldehyde in PBS (20 min at room temperature) and permeabilized with 2% formaldehyde in PBS containing 0.1% Triton X-100 (20 min at room temperature). Cells transfected with $_s$gp39 were stained with CD40–Ig (25 μg/ml in DMEM for 30 min at room temperature) followed by FITC-conjugated goat anti-human Fc antibody (TAGO, Burlingame, CA) diluted 1:500 in DMEM. Cells transfected with $_s$CD72 were stained with the anti-CD72 antibody BU40 (The Binding Site, Birmingham, UK) followed by FITC-conjugated goat anti-mouse Fc antibody (TAGO, Burlingame, CA) diluted 1:500 in DMEM.

COS cells transfected with the $_s$gp39 or $_s$CD72 constructs or vector alone (mock) were grown overnight in Cys- and Met-free DMEM to which [^{35}S]L-methionine and [^{35}S]L-cysteine had been added (Tran^{35}S-label, ICN, Costa Mesa, CA, 27 μCi/ml). Supernatants were harvested and centrifuged at 1000 r.p.m. for 10 min. Fusion proteins were recovered from the supernatant using CD40–Ig, 53-6 (anti-murine CD8) plus goat anti-rat Fc, BU40, BU41 (The Binding Site, Birmingham, UK) plus goat anti-mouse IgM Fc or J3.101 (AMAC Inc., Westbrook, ME). Goat antibodies were purchased from Organon Teknika Co., West Chester, PA. For each sample, 1 ml of supernatant, 75 μl Protein A–Sepharose (Repligen, Cambridge, MA) and the precipitating agent(s) were mixed and incubated at 4°C for 2 h. The Sepharose was washed extensively with PBS containing 0.1% NP-40 and resuspended in loading buffer containing 5% β-mercaptoethanol. Proteins were subjected to SDS–PAGE in an 8% polyacrylamide gel. The gel was fixed, dried and exposed to film. COS cell supernatants containing $_s$gp39 or $_s$CD72 were generated by transfection of COS cells. One day after transfection, cell medium was changed to DMEM containing 2% FBS. Supernatants were harvested 8 days after transfection.

Binding assays

The binding of gp39 and CD40 to the soluble forms of their respective ligands was tested by staining of transfected COS cells. COS cells were transfected with CD40, gp39 or vector alone (mock) using DEAE-dextran. One day after transfection, cells were trypsinized and replated. Cells were stained on the following day. Cells expressing gp39 or mock transfected cells were stained with CD40–Ig (25 μg/ml) followed by FITC-conjugated goat anti-human Fc. Cells expressing CD40 were stained by incubation with COS cell supernatants containing $_s$gp39 followed by mAb 53-6 (anti-murine CD8, 2.5 μg/ml) then FITC-conjugated goat anti-rat Fc (Organon Teknika Co., West Chester, PA, 1.5 μg/ml). As controls, COS cells expressing CD40 were stained with FITC-conjugated G28-5 (anti-CD40) or using COS cell supernatants containing $_s$CD72. All incubations were done at room temperature in PBS containing 1 mM $CaCl_2$, 1 mM $MgCl_2$ and 2% FBS and the same buffer was used for all washes. Following staining, cells were fixed with 1% paraformaldehyde in PBS.

The binding of $_s$gp39 to CD40–Ig was investigated by ELISA. Wells of a 96-well plate (Immunolon-2, Dynatech) were coated with 53-6 antibody (anti-murine CD8, 10 μg/ml, 100 μl/well and 50 mM sodium bicarbonate, pH 9.6 for 1 h at room temperature). Wells were washed with phosphate buffered saline containing 0.05% Tween-20 (TPBS) and blocked with 1 × specimen diluent concentrate (Genetic Systems, Seattle, WA, 225 μl/well for 2 h at room temperature). Wells were washed with TPBS. Supernatants from COS cells expressing either $_s$gp39 or $_s$CD72 were added (150 μl/well) and plates were incubated at 4°C overnight. Wells were washed (TPBS) and fusion proteins CD40–Ig or Leu8–Ig were added (serially diluted in PBS containing 1 mM $CaCl_2$ and 1 mM $MgCl_2$, 20–0.6 μg/ml, 100 μl/well for 1 h at room temperature). Wells were washed in TPBS and peroxidase-conjugated goat F(ab′)2 anti-human IgG was added to each well (TAGO, Burlingame, CA, 1:5000 dilution in 1 × specimen diluent, 100 μl/well for 1 h at room temperature). Wells were washed in TPBS and chromogenic substrate was added (Genetic Systems chromagen diluted 1:100 in EIA Buffered Substrate, Genetic Systems, 100 μl/well). The reaction was stopped after 10 min with the addition of Stop Buffer (Genetic Systems, 100 μl/well) and the absorbance was measured on an ELISA reader at dual wavelengths, 450 and 630 nm. Additionally, the ELISA was performed by immobilization of CD40–Ig on plates coated with goat anti-human Fc. Binding of $_s$gp39 from increasing dilutions of COS cell supernatants was detected using 53-6 mAb followed by FITC conjugated goat anti-rat Fc. Fluorescence was measured on a microplate reader.

B cell proliferation assays

PBMC were isolated by centrifugation through lymphocyte separation medium (Litton Bionetics, Kensington, MD). Human B lymphocytes were enriched from PBMC by passage of cells over nylon columns (Wako Chemicals USA, Inc., Richmond, VA) and harvesting of adherent cells. These cells were then treated with leu–leu methyl ester (Sigma, St Louis, MO) to deplete monocytes and NK cells. The resulting cell population was analyzed by flow cytometry on an EPICS C (Coulter Electronics, Hialeah, FL) and consisted of 50% human peripheral B cells.

Tonsillar B cells were prepared from intact tonsils by mincing to give a tonsillar cell suspension. The cells were then centrifuged through Lymphocyte Separation Medium, washed twice and fractionated on a discontinuous Percoll (Sigma, St Louis, MO) gradient. Cells with a density >50% were collected, washed twice and used in proliferation assays.

COS cells transfected with the gp39 construct or vector alone (mock-COS) were harvested from tissue culture plates with EDTA, washed twice with PBS, suspended at 5×10^6 cells/ml and irradiated with 5000 rads from a ^{137}Cs source. COS cells were used at a ratio of 1:4 (1×10^4 COS cells: 4×10^4 B cells) in proliferation assays.

Measurement of proliferation was performed by culturing cells in quadruplicate samples in flat-bottomed 96-well microtiter plates at 5×10^4 cells/well in complete RPMI medium containing 10% FCS. Reagents used were 1F5 (anti-CD20, 1 μg/ml), PMA (10 ng/ml, LC Services Woburn, MA), G28-5 (anti-CD40, 1 μg/ml), CD40–Ig (5 μg/ml in assays of peripheral blood B cells, 20 μg/ml in assays of tonsillar B cells) and supernatants of COS cells expressing $_s$gp39 or $_s$CD72 (diluted 1:4). Cell proliferation was measured by uptake of [^{3}H]thymidine (6.7 Ci/mmol; New England Nuclear, Boston, MA) after 5 days of culture and an overnight pulse. Cells were harvested onto glass fibre filters and radioactivity was measured in a liquid scintillation counter.

Acknowledgements

We thank Gena Whitney for her help in screening the PHA-activated T cell cDNA library, Peter Linsley and Shiu-lok Hu for critical review of the manuscript, Omar Haffar and Peter Linsley for helpful discussions on the preparation of soluble type II membrane proteins, Jürgen Bajorath for helpful discussions on the homology between gp39 and TNF, Brian Seed for the gift of the PHA-activated T cell cDNA library and Mary West for help in preparing this manuscript. This work was supported in part by grants from the NIH (GM43257, S.B.-A and I.S. AI26296, R.J.N.) and the Bristol-Myers Squibb Pharmaceutical Research Institute.

References

Armitage,R.J. *et al.* (1992) *Nature*, **357**, 80–82.
Aruffo,A. and Seed,B. (1987) *EMBO J.*, **11**, 3313–3316.
Aruffo,A., Stamenkovic,I., Melnick,M., Underhill,C.B. and Seed,B. (1990) *Cell*, **61**, 1303–1313.
Aruffo,A., Melnick,M.B., Linsley,P.S. and Seed,B. (1991) *J. Exp. Med.*, **174**, 949–952.
Aruffo,A., Dietsch,M.T., Wan,H., Hellström,K.E. and Hellström,I. (1992) *Proc. Natl. Acad. Sci. USA*, **89**, 2292–2296.
Banchereau,J., de Paoli,P., Vallé,A., Garcia,E. and Rousset,F. (1991) *Science*, **251**, 70–72.
Barrett,T.B., Shu,G. and Clark,E.A. (1991) *J. Immunol.*, **146**, 1722–1729.
Cairns,J., Flores-Romo,L., Millsum,M.J., Guy,G.R., Gillis,S., Ledbetter,J.A. and Gordon,J. (1988) *Eur. J. Immunol.*, **18**, 349–353.
Camerini,D., James,S.P., Stamenkovic,I. and Seed,B. (1989) *Nature*, **342**, 78–82.
Clark,E.A. and Ledbetter,J.A. (1986) *Proc. Natl. Acad. Sci. USA*, **83**, 4494–4498.
Clark,E.A. and Shu,G. (1990) *J. Immunol.*, **145**, 1400–1406.
Clark,E.A., Shu,G. and Ledbetter,J.A. (1985) *Proc. Natl. Acad. Sci. USA*, **82**, 1766–1770.
DeFrance,T., Vanbervliet,B., Brière,F., Durand,I., Rousset,F. and Banchereau,J. (1992) *J. Exp. Med.*, **175**, 671–682.
Eck,M.J. and Sprang,S.R. (1989) *J. Biol. Chem.*, **264**, 17595–17605.

Eck,M.J., Ultsch,M., Rinderknecht,E., de Vos,A.M. and Sprange,S.R. (1992) *J. Biol. Chem.*, **267**, 2119–2122.
Gascan,H., Gauchat,J.F., Aversa,G., Van Vlasselaer,P. and De Vries,J.E. (1991) *J. Immunol.*, **147**, 8–13.
Gordon,J., Millsum,M.J., Guy,G.R. and Ledbetter,J.A. (1987) *Eur. J. Immunol.*, **17**, 1535–1538.
Gordon,J., Millsum,M.J., Guy,G.R. and Ledbetter,J.A. (1988) *J. Immunol.*, **140**, 1425–1430.
Gray,P.W. *et al.* (1984) *Nature*, **312**, 721–724.
Hollenbaugh,D., Chalupny,N.J. and Aruffo,A. (1992) *Curr. Opin. Immunol.*, **4**, 216–219.
Jabara,H.H., Fu,S.M., Geha,R.S. and Vercelli,D. (1990) *J. Exp. Med.*, **172**, 1861–1864.
Jones,E.Y., Stuart,D.I. and Walker,N.P.C. (1989) *Nature*, **338**, 225–228.
Kriegler,M., Perez,C., DeFay,K., Albert,I. and Lu,S.D. (1988) *Cell*, **53**, 45–53.
Lemay,G., Waksman,G., Roques,B.P., Crine,P. and Boileau,G. (1989) *J. Biol. Chem.*, **264**, 15620–15623.
Ledbetter,J.A., Shu,G., Gallagher,M. and Clark,E.A. (1987) *J. Immunol.*, **138**, 788–794.
Marguet,D., Bernard,A.M., Vivier,I., Darmoul,D., Naquet,P. and Pierres,M. (1992) *J. Biol. Chem.*, **267**, 2200–2208.
Nakauchi,H., Nolan,G.P., Hsu,C., Huang,H.S., Kavathas,P. and Herzenberg,L.A. (1985) *Proc. Natl. Acad. Sci. USA*, **82**, 5126–5130.
Noelle,R.J., Roy,M., Shepherd,D.M., Stamenkovic,I., Ledbetter,J.A. and Aruffo,A. (1992) *Proc. Natl. Acad. Sci. USA*, **89**, 6550–6554.
Paulie,S., Ehlin-Henriksson,B., Mellstedt,H., Koho,H., Ben-Aissa,H. and Perlmann,P. (1985) *Cancer Immunol. Immunother.*, **20**, 23–28.
Paulie,S., Rosen,A., Ehlin-Henriksson,B., Braesch-Andersen,S., Jakobsen,E., Koho,H. and Perlmann,P. (1989) *J. Immunol.*, **142**, 590–595.
Pennica,D., Nedwin,G.E., Hayflick,J.S., Seeburg,P.H., Derynck,R., Palladino,M.A., Kohr,W.J., Aggarwal,B.B. and Goeddel,D.V. (1984) *Nature*, **312**, 724–729.
Rousset,F., Garcia,E. and Banchereau,J. (1991) *J. Exp. Med.*, **173**, 705–710.
Sambrook,J., Fritsch,E.F. and Maniatis,T. (1989) *Molecular Cloning: A Laboratory Manual*. Cold Spring Harbor Laboratory Press, Cold Spring Harbor, NY.
Shapira,S.K., Vercelli,D., Jabara,H.H. Fu,S.M. and Geha,R.S. (1992) *J. Exp. Med.*, **175**, 289–292.
Stamenkovic,I., Clark,E.A. and Seed,B. (1989) *EMBO J.*, **8**, 1403–1410.
Seed,B. (1987) *Nature*, **329**, 840–842.
Tisch,R., Watanabe,M. and Hozumi,N. (1988) *Immunol. Today*, **9**, 145–150.
Thomas,G., Thorne,B.A. and Hruby,D.E. (1988) *Annu. Rev. Physiol.*, **50**, 323–332.
Uckun,F.M., Schieven,G.L., Dibirdik,I., Chandan-Langlie,M., Tuel-Ahlgren,L. and Ledbetter,J.A. (1991) *J. Biol. Chem.*, **266**, 17478–17485.
Van de Velde,H., Von Hoegen,I., Lou,W., Parnes,J.R. and Thielemans,K. (1991) *Nature*, **351**, 662–665.
Vassalli,P. (1992) *Annu. Rev. Immunol.*, **10**, 411–452.
Von Hoegen,I., Nakayama,E. and Parnes,J.R. (1990) *J. Immunol.*, **144**, 4870–4877.
Wang,A.M., Creasey,A.A., Ladner,M.B., Lin,L.S., Strickler,J., Van Arsdell,J.N., Yamamoto,R. and Mark,D.F. (1985) *Science*, **228**, 149–154.
Young,L.S., Dawson,C.W., Brown,K.W. and Rickinson,A.D. (1989) *Int. J. Cancer*, **43**, 786–794.
Zhang,K., Clark,E.A. and Saxon,A. (1991) *J. Immunol.*, **146**, 1836–1842.

Received on July 23, 1992

Note added in proof

While this manuscript was in press, sequence similarity between the murine ligand of CD40 and TNF-a and TNF-b was described [*Nature*, **358**, 26 (1992)].

EXHIBIT 3

THIS EXHIBIT HAS BEEN REDACTED IN ITS ENTIRETY

EXHIBIT 4

THIS EXHIBIT HAS BEEN REDACTED IN ITS ENTIRETY

EXHIBIT 5

THIS EXHIBIT HAS BEEN REDACTED IN ITS ENTIRETY

EXHIBIT 6

THIS EXHIBIT HAS BEEN REDACTED IN ITS ENTIRETY

EXHIBIT 7

THIS EXHIBIT HAS BEEN REDACTED IN ITS ENTIRETY

EXHIBIT 8

THIS EXHIBIT HAS BEEN REDACTED IN ITS ENTIRETY

EXHIBIT 9

THIS EXHIBIT HAS BEEN REDACTED IN ITS ENTIRETY

EXHIBIT 10

THIS EXHIBIT HAS BEEN REDACTED IN ITS ENTIRETY

EXHIBIT 11

Solution structure of human CTLA-4 and delineation of a CD80/CD86 binding site conserved in CD28

The structure of human CTLA-4 reveals that residues Met 99, Tyr 100 and Tyr 104 of the $M_{99}YPPPY_{104}$ motif are adjacent to a patch of charged surface residues on the A'GFCC' face of the protein. Mutation of these residues, which are conserved in the CTLA-4/CD28 family, significantly reduces binding to CD80 and/or CD86, implicating this patch as a ligand binding site.

Cytotoxic T Lymphocyte–Associated Protein-4 (CTLA-4 or CD152) and CD28 are homologous T-lymphocyte receptors which bind common ligands (CD80 and CD86), but have distinct functions during an immune response[1]. CD28 engagement stimulates production of interleukin-2 and other T-cell cytokines which are essential for effective T-cell proliferation[1]. CTLA-4, on the other hand, negatively regulates T-cell activation[2–5], and mice deficient for this molecule exhibit a severe lymphoproliferative disorder and early lethality[6–7]. CTLA-4 binds CD80 and CD86 with >500-fold higher avidity than does CD28[8]. Covalent dimerization of CTLA-4 is required for its high binding avidity, but each monomeric subunit contains a binding site for CD80 and CD86[9]. A soluble immunoglobulin (Ig) fusion protein of CTLA-4 (CTLA4Ig) blocks T cell co-stimulation through CD28[10], and is immunosuppressive in *in vivo* models of autoimmune diseases and organ graft rejection[11].

We have determined the solution structure of CTLA-4ex, an extracellular fragment of human CTLA-4 by multidimensional, heteronuclear NMR spectroscopy (Fig. 1, Table 1). Although CTLA-4 occurs as a disulphide-linked dimer *in vivo*, we found no evidence for association of monomeric subunits of CTLA-4ex into dimers under the conditions of the NMR experiments. A rotational correlation time of 8.2 ± 0.2 ns was estimated from the ratio of ^1H_N T_1 and T_2 relaxation times, consistent with previous biochemical studies suggesting that, in the absence of the disulphide, CTLA-4 was monomeric in solution[8]. The structure of CTLA-4ex is most similar to immuno-globulin superfamily variable–domains (IgSVF). In CTLA-4ex, the two β-sheets of the V-fold comprise the ABED and A'GFCC' strands,

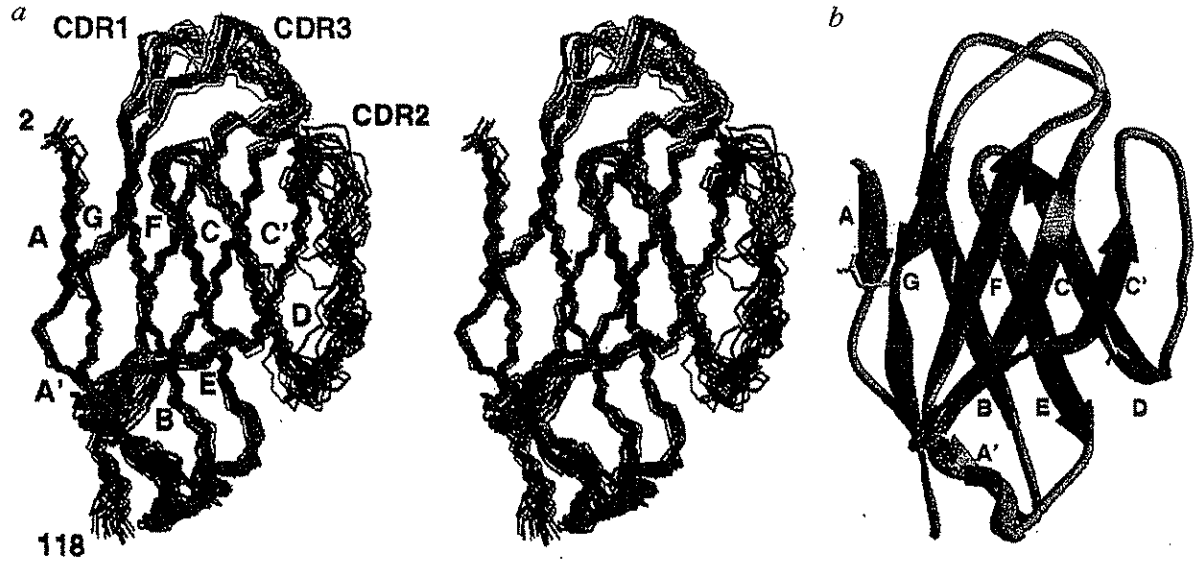

Fig. 1 Structure of CTLA-4ex. ***a***, The 20 structures representing the NMR ensemble. The structures were superimposed for the best fit of the backbone (N, Cα, C') atoms of the residues 2–54, and 68–118 to the average structure. The first two N-terminal residues and the last 13 C-terminal residues are ill-defined structurally and are not shown. The structures are coloured as in (*b*). ***b***, Ribbon diagram[27] depicting the secondary structure: β-strands A (residues Thr 4–Pro 6), A' (Val 9–Ala 11), B (Ile 17–Tyr 23), C (Val 32–Ala 40), C' (Gln 43–Ala 50), D (Ile 67–Ser 73), E (Gln 76–Gln 82), F (Gly 90–Glu 97) and G (Gly 108–Gly 110,Gly 112–Tyr 116) form two β-pleated sheets — strands ADEB are blue and A'GFCC' are red — that adopt a β-sandwich conformation. Strands C and C' are joined by a type 1 β-turn (Ala 40–Gln 43); Strands D and E by a type II' β-turn; and strands E and F by one 3_{10}-helical turn (Ala 86–Asp 88). Also highlighted are the CDR1 (green) and CDR3 (magenta) analogous loops, the disulphide bonds (yellow), and Asn 111 (orange). The second glycosylation site, Asn 78, is hidden in this orientation behind strand E.

respectively, which are connected by two disulphide bonds, the canonical Ig-disulphide (Cys 21–94) and an additional non-Ig disulphide bond (Cys 48–68). CTLA-4ex contains two N-linked glycosylation sites (Asn 78 and Asn 111). After partial deglycosylation, both of these residues carry the glycans, mannose-β1→4-N-acetylglucosamine-β1→4-(α1→6-fucose) N-acetylglucosamine.

The Asn 78 glycan interacts extensively with the side chains of residues on the DEB face of CTLA-4ex. Numerous nuclear Overhauser effects (NOEs) were observed between the N-acetylglucosamine (GlcNac) and fucose protons, and protein residues in three different strands: Ile 16, Ser 18, and Val 20 (strand B); Thr 71 (strand D); and Thr 80 (strand E). These intimate protein–carbohydrate interactions are reminiscent of CD2[12], where an N-linked glycan also shows NOEs with residues in several β-strands. In CD2, the carbohydrate counterbalances a high local concentration of positively charged residues[12], but the DEB surface of CTLA-4ex does not contain such a basic patch. The Asn 78 glycosylation is completly conserved in CTLA-4, but not CD28, homologues (Fig. 2*a*). Mutation of Asn 78 in CTLA4Ig leads to protein aggregation, which is accompanied by a reduction in binding activity (Table 2), suggesting that glycosylation at Asn 78 is important for structural integrity and/or solubility of CTLA-4.

Table 1 Structural Statistics of CTLA-4ex

R.m.s.d.[1]	
residues 2–118 (N, Cα, C)[1]	0.83 Å
residues 2–54, 68–118 (N, Cα, C')[1]	0.69 Å
residues 2–118 (non-hydrogens)	1.26 Å
residues 2–54, 68–118 (non-hydrogens)	1.07 Å
residues 2–118 and ordered sugar residues (non-hydrogens) [2]	1.31 Å
Deviations from experimental restraints[3]	
r.m.s.d. of NOE restraints (Å)	0.055 ± 0.003
largest NOE violation[4] (Å)	0.49
# NOE violations > 0.4 Å	3.2 ± 1.2
# NOE violations > 0.3 Å	9.7 ± 2.1
r.m.s.d. of Φ and χ_1 torsion restraints (°)	0.27 ± 0.14
largest torsion angle violation[4] (°)	2.4
Deviations from idealized covalent geometry	
r.m.s.d. of bond lengths (Å)	0.010 ± 9e-4
r.m.s.d. of bond angles (°)	1.34 ± 0.04
r.m.s.d. of improper angles (°)	1.60 ± 1.08
Energies[5]	
E(NOE)	144 ± 16
E(cdih)	16.1 ± 17.2
E(L-J)	-379 ± 76

[1]The r.m.s.d. listed is the average root-mean-squared distance deviation obtained after superposition of each individual structure on the average structure.
[2]Four sugars were included in the calculation: the two GlcNac and fucose residues attached at Asn 78, and the N-linked GlcNac attached at Asn 111.
[3]All deviations are represented as the average ± 1 standard deviation and are calculated for the ensemble of 20 CTLA-4ex structures.
[4]The largest individual NOE or torsion angle restraint violation in any of the 20 refined structures is listed.
[5]Energies are calculated with X-PLOR using the parallhdg_new.pro and param3_mod.cho parameter sets, and are reported in units of kcal mol^{-1}. E(NOE) and E(cdih) were calculated with a square-well quadratic potential with force constants of 50 kcal mol^{-1} Å^{-2} and 200 kcal mol^{-1} rad^{-2}, respectively. E(L-J), the Leonard-Jones van der Waals energy calculated with the X-PLOR empirical energy function, was not used during structure refinement. In addition, a quartic van der Waals repulsion function was included. The force constant on the NOE restraints and torsion angle restraints were set to 50 kcal mol^{-1} Å^{-2} and 50 kcal mol^{-1} rad^{-2} respectively.

In contrast, limited interactions were detected between the protein residues and the Asn 111 glycan. NOEs were only observed be-tween the N-linked GlcNac H1, H2 and N-acetyl methyl group, and protein residues Ile 93 and Ile 109. Thus, this GlcNac is the only conformationally well-defined sugar residue attached to Asn 111. The Asn 111 glycan is accomodated by the β-bulge in the G strand. The Asn111Asp mutation of CTLA4Ig did not detectably affect binding activity to CD80 and CD86 (Table 2), indicating that the glycan is not essential for binding or maintaining protein solubility. This result is surprising in light of the rigorous conservation of the Asn 111 glycosylation site in all CTLA-4 and CD28 homologues (Fig. 2*a*).

CTLA-4 is a disulphide-linked homodimer. In binding studies with CD80 and CD86, the CTLA-4 dimer was found to have a much slower off rate relative to monomeric CTLA-4, reflecting the higher avidity of the dimer (there are two binding sites per dimer)[8]. The spacing of six residues between the end of Ig fold (Val 117) and the cysteine involved in homodimerization (Cys 123) could provide sufficient rotational freedom for the two subunits of a CTLA-4 dimer to adopt many possible orientations. Although we have no direct physical evidence for or against a preferred orientation of the monomeric subunits in the disulphide-linked dimer, indirect evidence argues against certain orientations. The possible modes of dimerization are limited by the N-linked glycans. Dimerization of subunits along the G strands would be sterically restricted by the Asn 111 glycan. Dimerization involving the ABED face would be also be sterically restricted by glycan at Asn 78. In antibodies and CD8, dimerization is mediated through the A'GFCC' face[13]. Several structural features would argue against this mode of dimerization in CTLA-4. First, residues in the CDR1- and CDR3-analogous loops interact, which results in a reduction of curvature of the F and G strands, and excludes a number of the stabilizing dimerization contacts found in antibodies. Second, of the two β-bulges involved in Fv-like dimerization[13], only the G strand β-bulge is present in CTLA-4ex; the β-bulge immediately N-terminal to the C' strand is absent. Third, the A'GFCC' face in CTLA-4ex is not distinctly hydrophobic, but contains several charged residues (Fig. 2). Finally, residue Ile 109 in CTLA-4ex, which corresponds to a residue involved in dimerization of Fv fragments, interacts with the Asn 111 glycan. These structural features suggest that the A'GFCC' face of CTLA-4ex has evolved to serve a different function than that of the corresponding face in antibodies. One potential dimerization interface of the subunits could involve parts of the A'B and G strands that are conserved in CTLA-4 but not in CD28. This region is located between the two N-linked glycans and forms a coherent surface. However, if there is a preferred orientation of the subunits in the dimer, the interactions between these subunits must be weak, since CTLA-4ex is monomeric in solution.

The hexapeptide MYPPPY motif in the F–G loop (CDR3-analogous region) is conserved in CTLA-4 and CD28, and is essential for ligand binding. Mutation of any of these residues in CTLA-4 or CD28 leads to reduced binding of CD80 and/or CD86[14–17] (Table 2). In CTLA-4ex, this motif forms a loop that is conformationally restrained due to the presence of three consecutive prolines, the last of which, Pro 103, is in the *cis* conformation (see Methods). The loop is stabilized by a

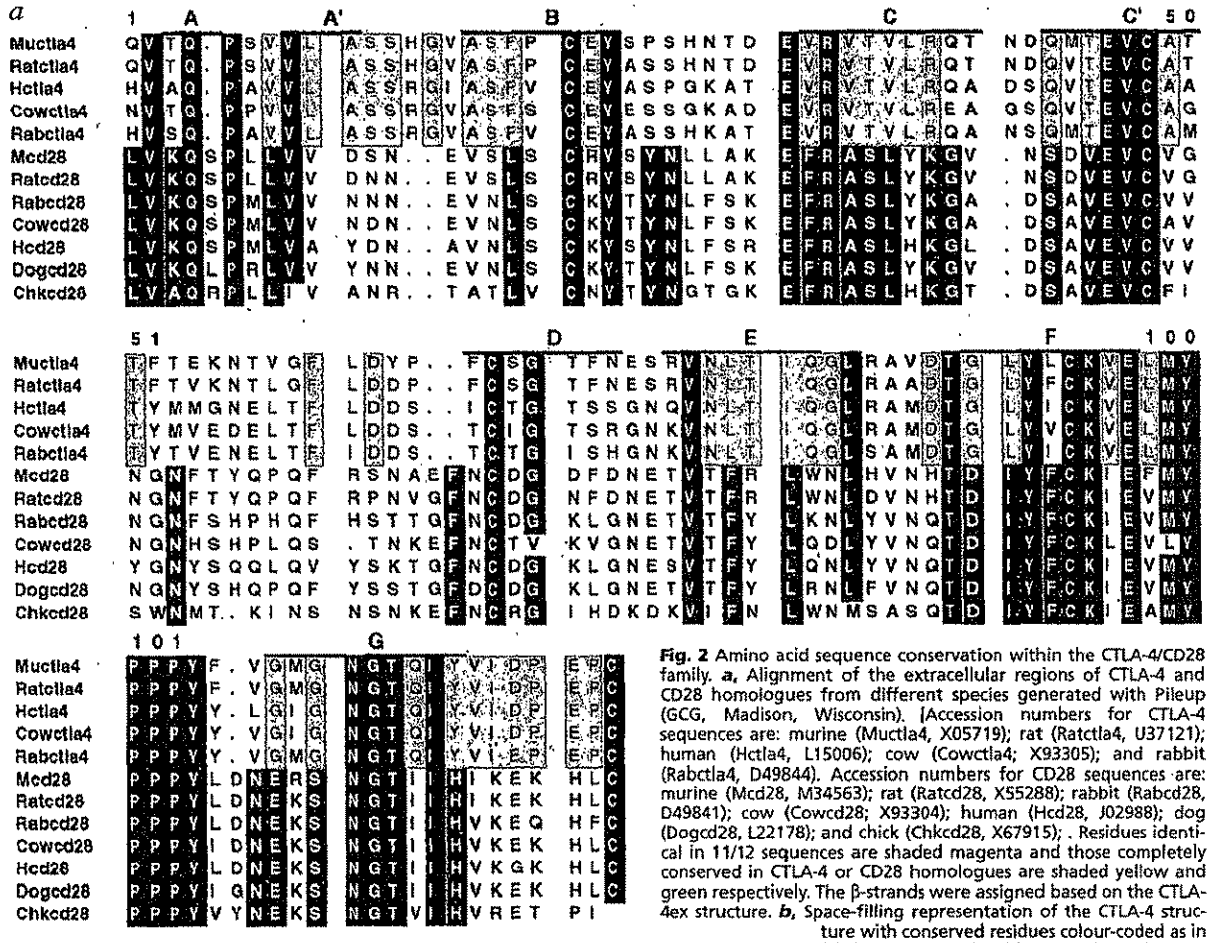

Fig. 2 Amino acid sequence conservation within the CTLA-4/CD28 family. ***a***, Alignment of the extracellular regions of CTLA-4 and CD28 homologues from different species generated with Pileup (GCG, Madison, Wisconsin). [Accession numbers for CTLA-4 sequences are: murine (Muctla4, X05719); rat (Ratctla4, U37121); human (Hctla4, L15006); cow (Cowctla4; X93305); and rabbit (Rabctla4, D49844). Accession numbers for CD28 sequences are: murine (Mcd28, M34563); rat (Ratcd28, X55288); rabbit (Rabcd28, D49841); cow (Cowcd28; X93304); human (Hcd28, J02988); dog (Dogcd28, L22178); and chick (Chkcd28, X67915); . Residues identical in 11/12 sequences are shaded magenta and those completely conserved in CTLA-4 or CD28 homologues are shaded yellow and green respectively. The β-strands were assigned based on the CTLA-4ex structure. ***b***, Space-filling representation of the CTLA-4 structure with conserved residues colour-coded as in (*a*). Non-conserved residues are shown in gray. The left image represents a depiction of the A'GFCC' face; this was rotated ~180° around the vertical axis to obtain the right image, which is a depiction of the BED face. Glycosylated asparagines are shaded blue. A number of highly conserved surface residues have been labelled.

hydrogen bond between the Pro 101 O and the Tyr 104 H_N. The conformation of the MYPPPY loop places Met 99, Tyr 100, and Tyr 104 on the A'GFCC' β-sheet surface. In contrast, both Leu 98 and Leu 106 point in the opposite direction and pack closely against Tyr 23 and Ser 25 of the CDR1-analogous loop. The conformation of the MYPPPY loop extends the A'GFCC' face by making the β-sheet surface flatter than usually found in IgSF V-domains, and in combination with the absence of Fv-like dimerization, provides a large accessible surface suitable for mediating binding interactions.

The binding of common ligands by CTLA-4 and CD28 suggests that their binding sites should overlap and include conserved residues. Sequence conservation within the CTLA-4/CD28 family was determined by an amino acid sequence alignment of the extracellular regions (Fig. 2*a*). While sequence conservation was scattered throughout the primary structure, many of the conserved residues clustered spatially (Fig. 2*b*). When conserved residues were mapped on the CTLA-4ex structure, the BED face showed

little sequence conservation (Fig. 2*b*), especially in the vicinity of the non-Ig disulphide bond (Cys 48–68) and the glycosylation site at Asn 78 . Thus, while the non-Ig disulphide bond is completely conserved in the CTLA-4/CD28 family, the intervening residues show the least conservation within the family. The lack of sequence conservation in this region suggested that the BED face is not involved in ligand binding. Consistent with this, simultaneous mutation of several adjacent residues on the BED face of CD28 did not affect ligand binding (Table 2).

In contrast, the A'GFCC' face, extended by the MYPPPY loop, contains a patch of residues conserved in both CTLA-4 and CD28 (Fig. 2*b*). Included in this patch are residues comprising the hydrophobic MYPPPY loop in close proximity to a number of charged residues (Glu 31, Arg 33, Glu 46, Lys 95 and Glu 97). This juxtaposition of conserved hydrophobic and charged residues makes this an attractive candidate ligand binding site of CTLA-4ex. This hypothesis is substantiated by site-specific mutagenesis experiments. Mutations of most of the residues in the conserved surface patch on the A'GFCC' face abolish binding to CD80 and/or CD86 (Table 2). Several of these mutations, such as Arg33Ser and Glu46Ser, affected CTLA-4 binding to CD86 more than to CD80. Another example of this is the conservative Tyr100Phe mutation of CTLA4Ig, which abolishes CTLA4Ig binding to CD86 without affecting binding to CD80[18]. Thus, an overlapping but non-identical set of residues on the A'GFCC' face of CTLA-4 determine binding to CD80 and CD86.

In the absence of three-dimensional structures of the CTLA-4 mutant proteins, we cannot rule out completely the possibility that their reduced CD80/CD86 binding is caused by alterations in their backbone conformations. However, several lines of evidence suggest that the mutant proteins adopt the native fold, and that the reduced CD80/CD86 binding is due to altered interactions with the side chains of the CTLA-4 mutants. First, all mutations listed in Table 2 result in proteins that are bound by a panel of monoclonal antibodies that bind native CTLA-4. Second, certain mutations selectively affect either CD80 or CD86 binding, suggesting that the effects of the mutations are due to specific interactions. In addition to the CTLA-4 mutants described above, Tyr100Phe and Tyr104Phe mutations in CD28 also selectively perturbed binding to CD86[17]. Furthermore, at high concentrations, several Ala mutants of the MYPPPY motif retained binding activity to CD80 (but not CD86)[14–15]. Finally, the mutants occupy surface positions in CTLA-4 structure, and thus are not expected to significantly perturb the structure.

Table 2 Effects of mutations of CTLA-4 on CD80 and CD86 ligand binding

Location of mutation	Mutation	CD80	CD86
	Wild type	+	+
Glycosylation site	N78D	-#	-#
Glycosylation site	N111D	+	+
A'GFCC' face	E31S	-	-
A'GFCC' face	R33S	-/+	-
A'GFCC' face	T35S	+	+
A'GFCC' face	L37S	+	+
A'GFCC' face	E46S	+/-	-
A'GFCC' face	T51S	+	+
A'GFCC' face	K95S	-	-

Listed are the effects of mutations of residues of CTLA-4 on CD80 and CD86 ligand binding. Mutations which substantially reduced binding to either CD80 or CD86 (that is, binding reduced by >80%, compared to wild type CTLA4Ig) are depicted as - ; mutations which had little effect on binding (that is, binding reduced by <20%) are depicted as +. #, This mutation led to significant aggregation of CTLA-4.
Other CTLA-4 (¥) or CD28 (§) mutations that were shown previously to affect binding to CD80 or CD86 include: KE(95,97)AA[¥15]; M99A[¥14]; Y100A[¥14]; P101A[¥14]; P102A[¥14]; P103A[¥14,16]; Y104A[¥§14,16]; MYPPPY(99-104)SGGG[§16–17]; YP(100,102)LG[§16]; PP(101,103)GL[§16]; YY(100,104)FF[§17]; YLD(104-106)LAS[§16]. Other mutations that were shown previously to have no affect on binding include: K14A[¥15]; EY(22-23)AF[¥15]; YSQ(54-56)FTY[§16]; SQQ(55-57)ATS[§16]; KLG(71-73)DFD[§16].

The identification of a CTLA-4ex ligand binding site sheds new light on one of the key biological properties of the CTLA-4 receptor, its high avidity for CD80 and CD86 ligands. Homologue mutagenesis studies showed that the binding avidity of CD28 was increased by replacement of segments from the G strand and B–C loop (CDR-1 analogous region) with the corresponding regions from CTLA-4[14]. Neither of these sequences is well conserved between CTLA-4 and CD28 (Fig. 2*a*); the G strand, in particular, is distinctly different in both length and charge between the two molecules. The CTLA-4ex structure shows that the G strand and B–C loop are spatially adjacent to the conserved ligand binding site. Residues in the N-terminal portion of the G strand extend to one side of the conserved surface patch in CTLA-4ex, whereas the C-terminal section of the B-C loop extends to the other. Thus, the structure suggests that non-conserved residues peripheral to a conserved central binding site modulate the binding characteristics of the CTLA-4/CD28 receptor family, and may contribute to the different biological properties of these receptors.

Methods

Sample Preparation. CTLA4Ig, a soluble fusion protein of the immunoglobulin Cγ1 chain with the extracellular domain of human CTLA-4[10], was expressed by a Chinese hamster ovary (CHO) cell line and was purified from the culture medium by Protein-A chromatography[10]. Dimeric CTLA-4t dimer was prepared as described[9]. CTLA-4ex monomer was obtained by reduction of the interchain disulphide in CTLA-4t by 1 mM DTT followed by iodoacetamide modification of the free sulphydryl and ion-exchange chromatography on a Resource-Q (Pharmacia) column. The two N-linked carbohydrates on each monomer were nominally converted to a tetrasaccharide core (complete deglycosylation of CTLA-4ex results in protein aggregates at concentrations under which the NMR experiments were performed.) by treatment with *Arthobacter. ureafaciens* sialidase, *Streptococcus pneumoniae* β-galactosidase, jack bean β-N-acetylhexosaminidase and jack bean α-mannosidase (Oxford Glycosystems) in 100 mM NaAc, 2 mM ZnCl2, pH 5. The sample was then dialyzed into 25 mM deuterated Tris-maleate, 0.1 mM EDTA, 0.1 mM NaN_3, 7% D_2O, pH 7.03, and concentrated to 0.7 mM. After trimming the carbohydrate with the cocktail of enzymes, we estimated that ~30 heterogeneity existed in the carbohydrate. We were unable to detect this heterogeneity in the NMR as resonances from the terminal mannoses were overlapped. All of this heterogeneity appears to be the result of an additional mannose attached to the remaining tetrasaccharide core at either N111 and/or N78 (as determined by mass spectroscopy, gel filtration, and carbohydrate analysis; unpublished results). The resulting partially deglycosylated CTLA-4ex was as active as fully glycosylated CTLA-4ex by ELISA CD80 binding inhibition assay. For multidimensional NMR experiments, CHO cell-produced CTLA4Ig was labelled with ^{15}N and ^{13}C by growth in Select-Amine media (Gibco) containing all $^{15}N/^{13}C$ labeled amino acids (CIL) except for cysteine (^{15}N labelled) and tryptophan (unlabelled). CTLA-4ex contains no tryptophan. Amino acids were added at concentrations equivalent to alpha-MEM media (Gibco); the media also contained ^{13}C labelled glucose (2 g l^{-1}) and ^{13}C labelled pyruvate (110 mg l^{-1}). Cells were innoculated into cell factories (NUNC) and allowed to grow for 1 week, at which point the media was harvested and the CTLA4Ig was processed as described above. Approximately 7 mg of $^{15}N/^{13}C$-labeled, partially deglycosylated CTLA-4 was obtained from 3 l of culture. This sample was very stable, lasting over 9

BMS 001122379

months at 30 °C and able to undergo multiple exchanges from H_2O to D_2O.

Structure determination. NMR experiments were collected at 30 °C on a Varian UnityPlus 600 spectrometer, using a single, 0.7 mM, ^{13}C-^{15}N labelled sample of CTLA-4ex. Sequential resonance assignments were made through analysis of the following three dimensional experiments: HNCO, HNCA, HN(CO)CA, HNCACB, CBCA(CO)NH, HBHA(CO)NH, CC-TOCSY(CO)NH, ^{15}N-separated TOCSY, and HCCH-TOCSY[19]. Interproton distance restraints were derived primarily from the cross-peak intensities of the 3D ^{15}N-separated and 3D ^{13}C-separated NOESY spectra[19] acquired with a mixing time of 80 ms. In addition, a 4D $^{13}C/^{13}C$-separated NOESY spectrum[19] (mixing time = 60 ms) was used to resolve assignment ambiguities, particular for NOEs arising from methyl resonances. Restraint bounds were generated by setting the lower bound equal to the sum of the van der Waal's radii (1.8 Å) and by setting the upper bound equal to 1.3 times the calculated target distance. Φ angle restraints were derived from $^3J_{HN,H\alpha}$ values obtained by analysis of a gradient-enhanced (GE) version of the HSQC-J-modulated [^{15}N,^1H]-COSY experiment[20]. Observed J values were corrected for the effect of relaxation due to $T_{1sel}(^1H\alpha)$[21]. Restraint ranges for Φ were set to -120° +/- 40° (for $^3J_{HN,H\alpha} \geq 8.0$ Hz) and -60° +/- 40° (for $^3J_{HN,H\alpha} < 5.6$ Hz and when the short range NOE data could unambiguously discern between +60° and -60°). Stereospecific valine γ-methyl assignments and restraints on χ_1 for isoleucine, valine and threonine were based on the values of $J_{N\gamma}$ and $J_{C'\gamma}$ obtained from the 2D {^{15}N} and {^{13}C} spin-echo difference, constant-time HSQC experiments[22–23] and relative intraresidue NOE intensities. The chemical shifts of $^{13}C\beta$ and $^{13}C\gamma$ resonances of Pro 103, 34.6 and 24.6 p.p.m. respectively, indicate that Pro 103 is in the *cis* conformation. The conformation of the loop is well-determined, despite the fact that no resonance assignments were obtained for either Pro 101 or Pro 102. Strong NOEs are observed between the ε-methyl of Met 99 and the aromatic protons of Tyr 104. Additional NOEs are observed between the back bone and side chain protons of Leu 98–Tyr 100 and Tyr 104–Leu 106.

Structures were generated using a combined distance geometry/restrained dynamic simulated annealing approach in X-PLOR 3.1[24–25], which had been modified to include conformational database refinement[26]. Final structure calculations were based on 938 interproton distance restraints [372 intraresidue restraints, 188 sequential restraints, 57 medium-range restraints ($2 \leq |i-j| \leq 4$), and 277 long-range restraints ($|i-j| > 4$), 23 carbohydrate–protein distance restraints, and 21 intracarbohydrate restraints]. These were supplemented with 63 torsion angle restraints [41 Φ and 22 χ_1], 62 restraints for 31 hydrogen bonds associated with slowly exchanging backbone amide protons, and two disulphide bond restraints. In addition, because the relative intensities of intrasugar NOEs indicated these sugars were predominantly in their lowest energy chair conformations, the sugars were forced into these conformations with torsion angle restraints, and the corresponding intrasugar NOE restraints were excluded. The final structures were analyzed for best fit to the experimental NMR restraints and the overall energy. As the energy did not vary significantly among the structures, the twenty structures with the lowest residual experimental restraint violations were chosen to represent the ensemble of solution conformations for CTLA-4ex. Coordinates have deposited in the Brookhaven Protein Data Bank (accession code: 1AH1).

Mutagenesis. Site directed mutagenesis of CTLA4Ig was performed using PCR forward mutagenic primers as previously described[14]. All mutations were verified by DNA sequencing and mutant proteins were expressed in COS cells[14]. The structural integrity of each mutant was confirmed by testing its ability to bind a panel of anti-CTLA-4 monoclonal antibodies; all molecules bound monoclonal antibodies similar to wild type CTLA4Ig. Binding of graded concentrations of each protein to immobilized CD80Ig and CD86Ig proteins was measured and compared to wild type CTLA4Ig[14]. The activities relative to wild type CTLA4Ig for binding of each new mutant to CD80Ig and CD86Ig, respectively, were: wt, 100% and 100%; N78D, ~20%, ~20%; N111D, ~100%, ~100%; E31S, <1% and <1%; R33S, 28% and <1%; T35S, 100% and 100%; L37S, 100% and 100%; E46S, 61% and 14%; T51S, 100% and 100%; and K95S, 14% and 16%.

William J. Metzler[1], Jürgen Bajorath[3], William Fenderson[2], Shyh-Yu Shaw[2], Keith L. Constantine[1], Joseph Naemura[4], Gina Leytze[4], Robert J. Peach[4], Thomas B. Lavoie[2], Luciano Mueller[1] and Peter S. Linsley[4]

[1]Departments of Macromolecular NMR, [2]Peptide and Protein Research, Bristol-Myers Squibb Pharmaceutical Research Institute, PO Box 4000, Princeton, New Jersey 08543-4000, USA. [3]Departments of Inflammation, and [4]Immunomodulation, Bristol-Myers Squibb Pharmaceutical Research Institute, 3005 First Avenue, Seattle, Washington 98121, USA.

Correspondence should be addressed to W.J.M. *email: metzler@laplaya.bms.com*

Acknowledgements
We thank the Bristol-Myers Squibb Bioprocess Research Group for production of CTLA4Ig, B.T. Farmer for assistance with NMR techniques, M. Friedrichs for computational support, T. Skinner for technical assistance, M. Hail and B. Warrack for mass spectral analysis, Y. Wu for determination of carbohydrate composition, and S. Sheriff, G.R. Matsueda and H. Einspahr and especialy G.R. Matueda for insights and discussions.

Received 25 February; accepted 16 May 1997.

1. June, C. H., Bluestone, J.A., Nadler, L.M. & Thompson, C.B. *Immunol. Today* **15**, 321–332 (1994).
2. Walunas, T.L. et al. *Immunity* **1**, 405–413 (1994).
3. Krummel, M.F. & Allison, J.P. *J. Exp. Med.* **182**, 459–465 (1995).
4. Kearney, E.R. et al. *J. Immunol.* **155**, 1032–1036 (1995).
5. Leach, D. R., Krummel, M. F. & Allison, J. P. *Science* **271**, 1734–1736 (1996).
6. P. Waterhouse, et al., *Science* **270**, 985–988 (1995).
7. Tivol, E. A. et al. *Immunity* **3**, 541–547 (1995).
8. Greene, J. L. et al., *J. Biol. Chem.* **271**, 26762–26771 (1996).
9. Linsley, P.S. et al. *J. Biol. Chem.* **270**, 15417–15424 (1995).
10. Linsley, P.S., Brady, W., Urnes, M., Grosmaire, L. S., Damle, N. K. & Ledbetter, J. A. *J. Exp. Med.* **174**, 561–570 (1991).
11. Finck, B.K., Linsley, P.S. & Wofsy, D. *Science* **265**, 1225–1227 (1994).
12. Wyss, D.F., et al. *Science* **269**, 1273–1278 (1995).
13. Chothia, C., Novotny, J., Bruccoleri, R., & Karplus, M. *J. Mol. Biol.* **186**, 651–663 (1985).
14. Peach, R.J., et al. *J. Exp. Med.* **180**, 2049–2058 (1994).
15. Morton et al., *J. Immunol.* **156**, 1047–1054 (1996).
16. Truneh, et al., *Mol. Immunol.* **33**, 321-334 (1996).
17. Karlin, K., Truneh, A. & Sweet, R. W. *J. Immunol.* **157**, 29–38 (1996).
18. Harris et al., *J. Exp. Med.* **In the press**
19. Clore, G. M. & Gronenborn, A. M. *Meth. Enzymol.* **239**, 349–363 (1994).
20. Billiter, M., Neri, D., Otting, G., Qian, Y., & Wuthrich, K. *J. Biomol. NMR* **2**, 257–274.
21. Kuboniwa, H., Grzesiek, S., Delaglio, F., Bax, A. *J. Biomol. NMR* **4**, 871–878 (1994).
22. Bax, A., Max, D. & Zax, D. *J. Amer. Chem. Soc.* **114**, 6923–6925 (1992).
23. Vuister, G. W., Wang, A. C. & Bax, A. *J. Am. Chem. Soc.* **115**, 5334–5335 (1993).
24. AT Brunger, XPLOR Version 3.1: A system for X-ray Crystallography and NMR (Yale Univ. Press, New Haven, CT) 1993.
25. Nilges, M., Clore, G.M. & Gronenborn, A.M. *FEBS Lett.* **229**, 317–324 (1988).
26. Kuszewski, J., Gronenborn, A.M. & Clore, G.M. *Prot. Sci.* **5**, 1067–1077 (1996).
27. M Carson, Ribbons 2.0. *J. Appl. Cryst.* **24**, 958–961 (1991).

EXHIBIT 12

CTLA-4 and T cell activation

Mariette A Oosterwegel*, Rebecca J Greenwald†, Didier A Mandelbrot‡, Robert B Lorsbach and Arlene H Sharpe§

The past year has seen significant advances in our understanding of the role of cytotoxic T lymphocyte antigen 4 (CTLA-4) in regulating T cell activation and tolerance. Recent studies indicate that CTLA-4 not only counterbalances CD28 signals but also can inhibit T cell responses independently of CD28. Recent work has also revealed a role for CTLA-4 in regulating Th1/Th2 differentiation. Manipulation of CTLA-4 in animal models of autoimmunity has shown that CTLA-4 regulates both the initiation and the progression of autoimmune diseases.

Addresses
Immunology Research Division, Department of Pathology, Brigham and Women's Hospital, 221 Longwood Avenue, Boston, MA 02115, USA
* e-mail: moosterwegel@rics.bwh.harvard.edu
† e-mail: rgreenwald@rics.bwh.harvard.edu
‡ e-mail: damandelbr@bics.bwh.harvard.edu
§ e-mail: asharpe@rics.bwh.harvard.edu

Current Opinion in Immunology 1999, 11:294–300

http://biomednet.com/elecref/0952791501100294

© Elsevier Science Ltd ISSN 0952-7915

Abbreviations

CTLA-4	cytotoxic T lymphocyte antigen 4
ICOS	inducible T cell co-stimulator
IFN-γ	interferon γ
LCMV	lymphocytic choriomeningitis virus
Rag	*recombinase-activating gene*
SEB	staphylococcal enterotoxin B
TGF-β	transforming growth factor β

Introduction

The co-stimulatory pathway that includes B7, CD28 and cytotoxic T lymphocyte antigen 4 (CTLA-4) plays a key role in regulating T cell activation and tolerance and is a promising therapeutic target. The B7 family of proteins, B7-1 (CD80) and B7-2 (CD86), is expressed on antigen presenting cells and T cells and provides the major co-stimulatory signal for augmenting and sustaining a T cell response via interaction with the CD28 receptor on T cells [1,2•]. The B7 molecules also bind to CTLA-4 (CD152), a CD28 homologue. The function of B7 molecules is more than one of co-stimulation, since B7–CTLA-4 interactions provide a critical negative signal for T cell activation [3,4•]. The potent downregulatory role of CTLA-4 on T cell responses has been demonstrated *in vivo* in models of tumor immunity, microbial immunity and autoimmunity [5,6•]. This review focuses on recent advances in our understanding of the function of CTLA-4: the role of CTLA-4 during the maturation, activation and differentiation of T cells will be discussed; studies examining the role of CTLA-4 in autoimmunity and tolerance will be summarized; finally, recent insights into the mechanisms by which CTLA-4 exerts its negative regulatory effects will be discussed.

Receptors and ligands in the B7–CD28/CTLA-4 pathway

The B7–CD28/CTLA-4 pathway consists of two B7 ligands, which have specificity for the same two receptors — CD28 and CTLA-4. These receptors have distinct kinetics of expression and affinities for the B7 ligands (reviewed in [2•]). CD28 is expressed constitutively on T cells whereas CTLA-4 is rapidly upregulated after T cell activation. CTLA-4 has a 10–20-fold higher binding affinity for both B7 molecules, as compared with CD28. B7-1 binds and dissociates more slowly from CD28 and CTLA-4 than B7-2 does. The kinetics of expression of B7-1 and B7-2 also differ. The constitutive expression or rapid upregulation of B7-2 has led to the hypothesis that B7-2 functions primarily in initiating an immune response, thereby playing a critical role in T cell activation and anergy. B7-1, being expressed later, may serve to amplify or regulate an immune response. There do not appear to be additional stimulatory CD28 counter-receptors, as demonstrated by the absence of T cell activation in a mouse strain lacking B7-1, B7-2 and CTLA-4 [7•].

Additional complexity comes from the recent identification of a new CD28 homologue, inducible T cell co-stimulator (ICOS) [8••]. It is not yet clear how ICOS interacts with the B7 CD28/CTLA-4 pathway. The MYPPPY motif (using single-letter code for amino acids), needed for the binding of CD28 and CTLA-4 to B7 ligands, is not conserved in ICOS. In contrast to CD28, co-stimulation via anti-ICOS monoclonal antibodies does not upregulate IL-2 production but induces IL-10 production. Since IL-10 downregulates B7 expression, ICOS co-stimulation may alter B7 expression — favoring a B7–CTLA-4 interaction.

Insights into CTLA-4 function *in vivo*

Studies using anti-CTLA-4 antibodies provided the first indication of a negative regulatory role for CTLA-4 but these studies were controversial. The fatal lymphoproliferative disease with multiorgan tissue destruction that develops in CTLA-4-deficient (CTLA-4$^{-/-}$) mice provided direct evidence for a critical role of CTLA-4 in downregulating T cell activation and maintaining immunologic homeostasis [9,10]. This phenotype also suggested that B7–CTLA-4 interactions have a critical role in regulating autoreactive T cells in the periphery. Recent studies have begun to elucidate the mechanism(s) by which CTLA-4 downregulates T cell activation: CTLA-4 could inhibit T cell responses, firstly, by outcompeting CD28 for binding to B7 ligands, secondly, by antagonizing CD28-mediated signaling and/or, thirdly, by antagonizing TCR-mediated signaling. These mechanisms are not mutually exclusive.

CTLA-4 and T cell activation

Mariette A Oosterwegel*, Rebecca J Greenwald†, Didier A Mandelbrot‡, Robert B Lorsbach and Arlene H Sharpe§

The past year has seen significant advances in our understanding of the role of cytotoxic T lymphocyte antigen 4 (CTLA-4) in regulating T cell activation and tolerance. Recent studies indicate that CTLA-4 not only counterbalances CD28 signals but also can inhibit T cell responses independently of CD28. Recent work has also revealed a role for CTLA-4 in regulating Th1/Th2 differentiation. Manipulation of CTLA-4 in animal models of autoimmunity has shown that CTLA-4 regulates both the initiation and the progression of autoimmune diseases.

Addresses
Immunology Research Division, Department of Pathology, Brigham and Women's Hospital, 221 Longwood Avenue, Boston, MA 02115, USA
* e-mail: moosterwegel@rics.bwh.harvard.edu
† e-mail: rgreenwald@rics.bwh.harvard.edu
‡ e-mail: damandelbr@bics.bwh.harvard.edu
§ e-mail: asharpe@rics.bwh.harvard.edu

Current Opinion in Immunology 1999, 11:294–300

http://biomednet.com/elecref/0952791501100294

© Elsevier Science Ltd ISSN 0952-7915

Abbreviations

CTLA-4	cytotoxic T lymphocyte antigen 4
ICOS	inducible T cell co-stimulator
IFN-γ	interferon γ
LCMV	lymphocytic choriomeningitis virus
Rag	*recombinase-activating gene*
SEB	staphylococcal enterotoxin B
TGF-β	transforming growth factor β

Introduction

The co-stimulatory pathway that includes B7, CD28 and cytotoxic T lymphocyte antigen 4 (CTLA-4) plays a key role in regulating T cell activation and tolerance and is a promising therapeutic target. The B7 family of proteins, B7-1 (CD80) and B7-2 (CD86), is expressed on antigen presenting cells and T cells and provides the major co-stimulatory signal for augmenting and sustaining a T cell response via interaction with the CD28 receptor on T cells [1,2•]. The B7 molecules also bind to CTLA-4 (CD152), a CD28 homologue. The function of B7 molecules is more than one of co-stimulation, since B7–CTLA-4 interactions provide a critical negative signal for T cell activation [3,4•]. The potent downregulatory role of CTLA-4 on T cell responses has been demonstrated *in vivo* in models of tumor immunity, microbial immunity and autoimmunity [5,6•]. This review focuses on recent advances in our understanding of the function of CTLA-4: the role of CTLA-4 during the maturation, activation and differentiation of T cells will be discussed; studies examining the role of CTLA-4 in autoimmunity and tolerance will be summarized; finally, recent insights into the mechanisms by which CTLA-4 exerts its negative regulatory effects will be discussed.

Receptors and ligands in the B7–CD28/CTLA-4 pathway

The B7–CD28/CTLA-4 pathway consists of two B7 ligands, which have specificity for the same two receptors — CD28 and CTLA-4. These receptors have distinct kinetics of expression and affinities for the B7 ligands (reviewed in [2•]). CD28 is expressed constitutively on T cells whereas CTLA-4 is rapidly upregulated after T cell activation. CTLA-4 has a 10–20-fold higher binding affinity for both B7 molecules, as compared with CD28. B7-1 binds and dissociates more slowly from CD28 and CTLA-4 than B7-2 does. The kinetics of expression of B7-1 and B7-2 also differ. The constitutive expression or rapid upregulation of B7-2 has led to the hypothesis that B7-2 functions primarily in initiating an immune response, thereby playing a critical role in T cell activation and anergy. B7-1, being expressed later, may serve to amplify or regulate an immune response. There do not appear to be additional stimulatory CD28 counter-receptors, as demonstrated by the absence of T cell activation in a mouse strain lacking B7-1, B7-2 and CTLA-4 [7•].

Additional complexity comes from the recent identification of a new CD28 homologue, inducible T cell co-stimulator (ICOS) [8••]. It is not yet clear how ICOS interacts with the B7–CD28/CTLA-4 pathway. The MYPPPY motif (using single-letter code for amino acids), needed for the binding of CD28 and CTLA-4 to B7 ligands, is not conserved in ICOS. In contrast to CD28, co-stimulation via anti-ICOS monoclonal antibodies does not upregulate IL-2 production but induces IL-10 production. Since IL-10 downregulates B7 expression, ICOS co-stimulation may alter B7 expression — favoring a B7–CTLA-4 interaction.

Insights into CTLA-4 function *in vivo*

Studies using anti-CTLA-4 antibodies provided the first indication of a negative regulatory role for CTLA-4 but these studies were controversial. The fatal lymphoproliferative disease with multiorgan tissue destruction that develops in CTLA-4-deficient (CTLA-4$^{-/-}$) mice provided direct evidence for a critical role of CTLA-4 in downregulating T cell activation and maintaining immunologic homeostasis [9,10]. This phenotype also suggested that B7–CTLA-4 interactions have a critical role in regulating autoreactive T cells in the periphery. Recent studies have begun to elucidate the mechanism(s) by which CTLA-4 downregulates T cell activation: CTLA-4 could inhibit T cell responses, firstly, by outcompeting CD28 for binding to B7 ligands, secondly, by antagonizing CD28-mediated signaling and/or, thirdly, by antagonizing TCR-mediated signaling. These mechanisms are not mutually exclusive.

Case 1:06-cv-00500-SLR-MPT Document 274-3 Filed 09/02/2008 Page 4 of 44

Support for the first potential mechanism, competition for B7 ligands, is based upon the higher affinity of CTLA-4 for both B7-1 and B7-2. The distinct affinities of CD28 and CTLA-4 for B7 ligands — together with the highly regulated expression of receptors and ligands in this pathway — have led to the proposal of a model in which B7–CD28 and B7–CTLA-4 interactions predominate at distinct stages of an immune response. When B7 ligands are expressed at low levels on resting T cells, B7 molecules may preferentially engage the high-affinity inhibitory receptor — CTLA-4. When B7 ligands are upregulated and expressed at high levels, such as upon encounter with immunogenic antigens or adjuvants, the predominant interactions could be between CD28 and B7 — enhancing T cell proliferation and differentiation. Once CTLA-4 expression is upregulated following T cell activation, the inhibitory B7–CTLA-4 interaction could once again predominate — leading to the termination of T cell activation. As B7 expression declines to low levels later, all available B7 may be engaged by the high affinity CTLA-4 — also favoring downregulation of the T cell response. Indirect evidence for CTLA-4 directly antagonizing CD28 signaling is provided by the finding that both CD28 and CTLA-4 bind phosphatidylinositol-3-kinase [11]. Recent biochemical [12,13••] and functional [14•,15•] studies also provide evidence for the third mechanism — direct inhibition of TCR signaling. Molecular studies have suggested that CTLA-4 modulates the immune response by antagonism of TCR signaling independently of CD28 [12,13••]. Blocking B7–CTLA-4 interactions in CD28$^{-/-}$, 2C TCR-transgenic T cells cultured with allomismatched B7-1-transfected P815 cells leads to enhanced proliferation and cytokine secretion — suggesting that signaling through CTLA-4 can antagonize TCR-mediated signaling and inhibit T cell responses in the absence of CD28 [15•].

Role of CTLA-4 during maturation, activation and differentiation of T cells

The activated phenotype of CTLA-4$^{-/-}$ T cells and early demise of CTLA-4$^{-/-}$ mice have made it difficult to use the CTLA-4$^{-/-}$ mouse as a tool for studying the role of CTLA-4 in naive T cells and for comparing the role of CTLA-4 in the initiation phase, compared with the effector phases, of an immune response. To overcome these problems, we and others have bred CTLA-4$^{-/-}$ mice with mice carrying a transgenic TCR in order to restrict the T cell repertoire and to examine CTLA-4$^{-/-}$ T cell responses in an antigen-specific manner. Several different class-I-restricted TCRs [16•,17•] and class-II-restricted TCRs (AH Sharpe, unpublished data) have been examined. Once the TCR repertoire is limited, CTLA-4$^{-/-}$ mice survive significantly longer; however, they eventually develop activated T lymphocytes — most probably due to endogenous TCR rearrangement. This may be overcome by breeding in a mutation in the *recombinase-activating gene* (*Rag*) to generate a population of CTLA-4$^{-/-}$ T cells that solely expresses the desired transgenic TCR. To eliminate *in vivo* activation of CTLA-4$^{-/-}$ T cells, we also have bred CTLA-4$^{-/-}$ mice with mice lacking B7-1 and B7-2; this completely prevents endogenous T cell activation and lymphoproliferative disease. T cells from the latter strain have the phenotypic and functional characteristics of naïve cells [7•], providing an additional reagent for studying naïve T cells lacking CTLA-4. The TCR-transgenic, CTLA-4$^{-/-}$ strain and the CTLA-4$^{-/-}$ B7-1/B7-2$^{-/-}$ strain have enabled the investigation of the role of CTLA-4 in T cell development, differentiation and proliferation — as discussed below.

Thymic development

The apparent autoimmune phenotype of CTLA-4$^{-/-}$ mice prompted an examination of the role of CTLA-4 in thymic development, since this phenotype could be a manifestation of altered deletion of autoreactive cells in the thymus. Although there is a recent report of inhibitory effects of anti-CTLA-4 antibody on anti-CD3-induced thymic negative selection [18], studies with CTLA-4$^{-/-}$ mice do not support a role for CTLA-4 in thymic development — the phenotype of thymocytes from CTLA-4$^{-/-}$ mice is unchanged from wild-type mice [16•,17•,19]. Both positive selection and negative selection appear to be normal in CTLA-4$^{-/-}$ mice with transgenic TCRs specific for H-Y; and the T cells from this strain behave similarly to wild-type T cells in the periphery [16•]. Normal thymocyte maturation also has been observed in various CTLA-4$^{-/-}$ TCR-transgenic mouse strains: mice with CD8$^+$ cells expressing TCRs specific for lymphocytic choriomeningitis virus (LCMV) [16•]; TCR-transgenic CD8$^+$ cells from the 2C strain [17•]; and TCR-transgene CD4$^+$ cells from DO11.10-strain mice (AH Sharpe, unpublished data). Taken together, these studies suggest that CTLA-4 does not have a critical role in thymic selection.

Proliferation and cell death

Primary stimulation of naïve CD4$^+$ or CD8$^+$ TCR-transgenic T cells *in vitro* with appropriate peptide antigens results in comparable proliferation and IL-2 production in both CTLA-4$^{-/-}$ and wild-type T cells [17•]; AH Sharpe, unpublished data]; however, upon re-stimulation, the CTLA-4$^{-/-}$ TCR-transgenic T cells proliferate more than do wild-type TCR-transgene T cells. These findings are consistent with results of a recent study indicating differential functions of CTLA-4 in naïve, compared with previously activated, CD4$^+$ T cells [20•]. This enhanced proliferation could be due to reduced cell death, to increased expression of survival factors or to altered cell cycle regulation; additional studies are needed to distinguish between these alternatives. In contrast to the experiments using CTLA-4$^{-/-}$ cells, studies using anti-CTLA-4 antibodies have indicated a role for CTLA-4 during the initiation of a T cell response. Antibody-mediated cross-linking of CTLA-4 on resting T cells leads to reduction of IL-2 production and cell cycle arrest as early as 16 hours after CTLA-4 cross-linking [21,22,23•] and can result in apoptosis of activated cells by a Fas-independent mechanism [23•]. This study

does not exclude increased cell death as an effect of CTLA-4 triggering. Anti CTLA-4 cross-linking on human resting T cells decreases IL-2 expression but does not affect expression of the cell survival factor, bcl-x_L [24•]. Further studies are needed to clarify the differences observed using anti-CTLA-4 antibodies compared with CTLA-4$^{-/-}$ T cells.

Th cell differentiation

The differentiation of CD4$^+$ T cells into Th1 or Th2 subsets has profound effects on the outcome of autoimmune diseases, infectious diseases and graft rejection. Analyses of CTLA-4$^{-/-}$ T cells have revealed an important role for CTLA-4 in regulating Th cell differentiation. In the absence of CTLA-4, naïve CD4$^+$ T cells differentiate into Th2 cells — secreting large amounts of IL-4, IL-5 and IL-10. This skewing towards Th2 differentiation is observed when either class II-restricted, DO11.10, TCR-transgenic CTLA-4$^{-/-}$ T cells or T cells derived from CTLA-4$^{-/-}$ B7-1/B7-2$^{-/-}$ mice are stimulated with antigen and wild-type antigen-presenting cells (AH Sharpe, unpublished data). Th2 deviation appears not to be dependent on the strength of the TCR signal, since it was observed over a broad range of antigen concentrations.

In vivo experiments also support a role for CTLA-4 in Th cell differentiation. Skewing toward Th2 development was observed when anti-CTLA-4 antibody was used to inhibit staphylococcal enterotoxin B (SEB)-induced T cell responses [25•]. Stimulation using anti-CD28 antibody administration to CTLA-4$^{-/-}$ B7-1/B7-2$^{-/-}$ mice leads to Th2 skewing whereas this deviation is not observed in wild-type mice given anti CD28 antibody (AH Sharpe, unpublished data). CD4$^+$ CTLA-4$^{-/-}$ T cells secrete high levels of IL-4 and very little IFN-γ whereas CD8$^+$ CTLA-4$^{-/-}$ cells produce high amounts of IFN-γ and no IL-4 [26]. Since Th2 cells are more resistant than Th1 cells to activation-induced cell death [27], the Th2 bias of CD4$^+$ CTLA-4$^{-/-}$ T cells could contribute to the enhanced T cell clonal expansion as observed in CTLA-4$^{-/-}$ mice. Taken together, these studies indicate that CTLA-4 plays a pivotal role in regulating the balance between Th1 and Th2 differentiation. Thus, in the B7–CD28/CTLA-4 pathway, signaling through CD28 and CTLA-4 have opposing effects on Th cell differentiation: CD28–B7 interactions promote Th2 differentiation [28•,29] whereas B7 CTLA-4 interactions limit the extent of Th2 differentiation.

A role for CTLA-4 in regulating transforming growth factor β (TGF-β) production has been described recently [30•] and suggested another means by which CTLA-4 may exert its inhibitory effects. TGF-β downregulates immune responses and TGF β$^{-/-}$ mice have a lymphoproliferative phenotype with similarities to the CTLA-4$^{-/-}$ phenotype. CTLA-4 cross-linking increases TGF-β secretion by CD4$^+$ T cells, suggesting that TGF-β may mediate — if only in part — the inhibitory effects of CTLA-4.

Role of CTLA-4 in CD4$^+$ cells, compared with CD8$^+$ T cells

As its name implies, CTLA-4 was originally cloned from CD8$^+$ CTLs; however, it is expressed on both CD4$^+$ and CD8$^+$ T cells [31]. Recent studies have begun to compare the function of CTLA-4 on CD4$^+$ and CD8$^+$ T cells. Anti-CTLA-4 antibody treatment inhibits IL-2 production and causes cell cycle arrest in both CD4$^+$ [21] and CD8$^+$ [22] cells; yet the phenotype of CTLA-4$^{-/-}$ mice suggests distinct roles for CTLA-4 in Th cells and CTLs. The CD4$^+$: CD8$^+$ ratio is increased in CTLA-4$^{-/-}$ mice. Depletion studies show that the lymphoproliferative phenotype is completely dependent upon CD4$^+$ cells, suggesting that CD8$^+$ T cell activation in CTLA-4$^{-/-}$ mice may be a consequence of CD4$^+$ T cell activation [32••]. The absence of CTLA-4 has no effect on CD8$^+$-cell-mediated LCMV clearance [33]; however, CTLA-4 appears to have a negative regulatory role in the absence of CD28 in CD8$^+$ T cells — as demonstrated by studies using 2C-strain, *Rag*$^{-/-}$ CD28$^{-/-}$ T cells [15•]. Further studies are needed to clarify the role of CTLA-4 on CD8$^+$ T cells.

Role of CTLA-4 in autoimmunity

Recent studies in animal models of autoimmunity indicate that CTLA-4 has an important role in downregulating T cell responses throughout the course of an autoimmune disease [6•]. Anti-CTLA-4 treatment exacerbated experimental allergic encephalomyelitis (EAE) when administered following adoptive transfer of primed T cells. When given at the peak of acute disease, anti-CTLA-4 blunted disease remission and worsened relapses. Anti-CTLA-4 also led to greater incidence and severity of relapses when administered during the first disease remission. Anti-CTLA-4 antibody administration enhanced responses to the inducing epitope and accelerated epitope spreading [34]. In a TCR-transgenic model of diabetes, anti-CTLA-4 antibody accelerated the development of diabetes [35••]. The onset of diabetes was only affected when anti-CTLA-4 antibody was administered before the development of insulitis, suggesting that CTLA-4 plays an important role not only in the termination or modification of an ongoing response but also in initiating an autoimmune response. Additional studies are needed to address whether CTLA-4 alters the threshold for activation of self-reactive T cells.

In light of the role of CTLA-4 in the development of autoimmunity in experimental systems and the putative autoimmune phenotype of the CTLA-4$^{-/-}$ mouse, there has been considerable interest in assessing whether CTLA-4 plays a role in the development of human autoimmunity. Several polymorphisms have been identified within the human CTLA-4 gene and have proven useful in genetic linkage studies: these include an A-to-G transition in exon 1 at position 49; a C/T substitution site at position −318, 5′ to the transcription start site; and a microsatellite $(AT)_n$ repeat in the 3′ untranslated region. Recently, polymorphisms in the CTLA-4 gene have been

genetically linked to several human autoimmune diseases — including insulin-dependent diabetes mellitus, Graves' disease, Hashimoto's thyroiditis and other disorders [36–40]. The crucial unresolved issue regarding these linkages is whether the predisposing gene is actually CTLA-4 or another closely linked gene. This is particularly critical since other genes (e.g. CD28) expressed by T lymphocytes and other immune cells are closely linked to the CTLA-4 locus. Further studies are needed to determine whether these polymorphisms either result in altered expression of the CTLA-4 gene or modify CTLA-4 protein function.

Role of CTLA-4 in tolerance

CTLA-4–B7 interactions influence tolerance induction in several allograft models. The effect of anti-CTLA-4 antibody administration has been examined using a mouse skin transplantation model in which long-term survival of skin grafts is induced by a three-component therapy for the recipient: thymectomy, administration of anti-CD154 (CD40 ligand) antibodies and donor-specific transfusion (DST). Anti-CTLA-4 treatment completely prevented the induction of tolerance in this model. The effect of anti-CTLA-4 antibodies on allograft tolerance [41] has also been studied in a mouse heart transplantation model. In this model CTLA4–Ig, which binds to B7-1 and B7-2, can significantly prolong allograft survival. The administration of anti-CTLA-4 antibody to mice previously tolerized with CTLA-4 Ig plus DST significantly reduced mean survival time of grafts, confirming the critical negative regulatory role of CTLA-4 *in vivo* for alloreactive T cells; however, in this system, the prolonged survival of cardiac grafts despite CTLA-4 blockade suggests that this molecule is not obligatory for induction of tolerance. Taken together, the skin and heart transplantation studies indicate that engagement of CTLA-4 by B7 molecules is important in prolonging graft survival. Thus, future therapies should avoid CTLA-4 blockade and should be directed toward cross-linking CTLA-4 as a way to downregulate the alloresponse.

Recent studies also demonstrate that CTLA-4 can function as a negative regulator of alloresponses independently from CD28. Alegre and co-workers [14•] showed that cardiac graft survival in CD28$^{-/-}$ recipient mice is prolonged. Administration of anti-CTLA-4 antibody reduces graft survival, suggesting that CTLA-4 blockade increases T cell responses even in the absence of CD28. These data suggest that future therapies that independently target both CD28 and CTLA-4 might be desirable. Protocols to optimally downregulate the immune response would need to both block CD28 stimulation and increase signaling through CTLA-4.

Although data are limited, CTLA-4 also may function in maternal tolerance to the developing fetus. CTLA-4 mRNA and protein are expressed in placental fibroblasts at the maternal–fetal interface throughout gestation [42] and both B7-1 and CTLA-4 are expressed in embryonic stem cells. There is preferential transmission of maternal CTLA-4 alleles encoding shorter $(AT)_n$ repeats in the 3′ untranslated region of liveborn, compared with aborted, fetuses [43]. These intriguing findings suggest that reduced CTLA-4 expression, presumably mediated by decreased mRNA stability, may play a role in loss of tolerance at the maternal–fetal interface and recurrent spontaneous abortion.

Signaling through CTLA-4

The signaling pathways by which CTLA-4 exerts its inhibitory effects have been the subject of intense investigation. CTLA-4 has a short cytoplasmic tail that is 100% conserved between species and contains two tyrosine-containing motifs, YVKM and YFIP (reviewed in [3]). The YVKM motif plays a pivotal role in the tightly controlled localization of CTLA-4 as well as in the interaction with key signaling molecules [3,44,45]. The nonphosphorylated YVKM motif can associate with μ-2, one of the subunits of the clathrin-associated adaptor complex AP-2; this complex is responsible for continuous translocation of CTLA-4 to and from the cell surface. Phosphorylation of CTLA-4 releases AP-2 and results in increased cell surface expression [3,46••]. In a phosphorylated state, CTLA-4 can interact with the p85 subunit of phosphatidylinositol-3-kinase at the YVKM motif [46••,47,48] and/or form a complex with the tyrosine phosphatase SHP-2 [13••,18,46••,48,49]. It has been suggested that this CTLA-4–SHP-2 interaction could negatively regulate TCR signaling by dephosphorylating key signaling proteins [49]. Although SHP-2 can be coprecipitated with CTLA-4 under certain circumstances, the functional consequences of this interaction are not yet certain. Studies performed in T cell lines with dominant negative SHP-2 mutants support a positive role for SHP-2 in TCR signaling [50]. One report has demonstrated the binding of SHP-1, a tyrosine phosphatase with homology to SHP-2, to a CTLA-4-derived phosphopeptide [48]. Although SHP-1 has been implicated in negative signaling, no functional differences of CTLA-4 cross-linking were observed in the SHP-1-deficient strain [51]. There have been no reports of proteins binding the YFIP motif.

Several tyrosine kinases are capable of phosphorylating CTLA-4 during T cell activation. Lck and Fyn (kinases of the Src-family) [45,46••] and Lyk/Rlk (a member from the Btk/Tec-family) [52] have been shown to associate with and phosphorylate CTLA-4 on both tyrosine residues. In contrast, other kinases such as ZAP-70 were not capable of phosphorylating CTLA-4. Since all of these studies were carried out in cell lines transfected with CTLA-4 and tyrosine kinases, it is not clear whether CTLA-4 serves as an actual substrate for any of these kinases *in vivo* in primary T cells. In addition, these data do not exclude the possibility that different kinases target different sites in the CTLA-4 tail.

Recent studies [13••] provide evidence for CTLA-4 interaction with the CD3-ζ chain of the TCR complex

intracellularly, both in transfectants and primary T cells — suggesting that CTLA-4 interferes with very early TCR signaling events. The interaction between CD3-ζ and CTLA-4 did not require other T-cell-specific proteins or the phosphorylation of CTLA-4. Overexpression of Lck increased CD3-ζ phosphorylation and the association with CTLA-4 whereas CTLA-4 cross-linking led to a slight reduction of CD3-ζ phosphorylation. Interestingly, earlier work by Kruisbeek and co-workers [12] has shown that phosphorylation of ZAP-70 and the CD3-ζ chain itself are not affected by CTLA-4 engagement. Further studies are needed to examine how these findings relate to B7 engagement of CTLA-4.

Conclusions

CTLA-4 plays a pivotal role in downregulating T cell responses and clearly it is important in modifying the course of autoimmunity and transplantation tolerance in animal models. As a result, CTLA-4 represents an important potential target for therapies of human diseases involving undesired immune responses. Recent studies suggest that CTLA-4 regulates T cells both at the initiation of an immune response and following T cell activation. On resting T cells, CTLA-4 may increase the threshold for T cell activation — thereby preventing undesired activation by low-strength TCR signals that may be needed for survival of naïve and memory cells and protecting against autoimmune responses. In activated T cells, CTLA-4 may limit the extent of effector T cell responses. Recent studies also indicate that CTLA-4 not only serves to counterbalance CD28 signals but also can inhibit immune responses independently of CD28. CTLA-4 also has a critical role in regulating Th2 differentiation; however, much remains unknown about CTLA-4 and its role in different T cell subsets with various activation histories. It is critical to characterize the molecular mechanisms of CTLA-4 signaling. These studies not only will further our understanding of the role of CTLA-4 in T cell activation and tolerance but also should facilitate the design of rational therapeutic approaches to manipulate this key immunoregulatory molecule.

Acknowledgements

This work was supported by grants from the National Institutes of Health (to MFK and DAW), the National Multiple Sclerosis Society (to ABS), Howard Hughes Medical Institute Research Resources Program (to MAC) and Veterans Administration (to RBL). We thank Janet Buhlmann, Gladys Freeman, Alex McAdam and Chris Rudd for helpful comments.

References and recommended reading

Papers of particular interest, published within the annual period of review, have been highlighted as:

- • of special interest
- •• of outstanding interest

1 Lenschow DJ, Walunas TL, Bluestone JA: **CD28/B7 system of T cell costimulation.** *Annu Rev Immunol* 1996, 14:233-258.

2 • McAdam AJ, Schweitzer AN, Sharpe AH: **The role of B7 co-stimulation in activation and differentiation of CD4+ and CD8+ T cells.** *Immunol Rev* 1998, 165:231-247.
This recent review summarizes the role of B7-1 and B7-2 in naive, compared with activated, CD4+ and CD8+ cells.

3 Thompson CB, Allison JP: **The emerging role of CTLA-4 as an immune attenuator.** *Immunity* 1997, 7:445-450.

4 • Scheipers P, Reiser H: **Role of the CTLA-4 receptor in T cell activation and immunity. Physiologic function of the CTLA-4 receptor.** *Immunol Res* 1998, 18:103-115.
This is a recent, thoughtful, comprehensive review of CTLA-4 function.

5 Leach DR, Krummel MF, Allison JP: **Enhancement of antitumor immunity by CTLA-4 blockade.** *Science* 1996, 271:1734-1736.

6 • Karandikar NJ, Vanderlugt CL, Bluestone JA, Miller SD: **Targeting the B7/CD28:CTLA-4 costimulatory system in CNS autoimmune disease.** *J Neuroimmunol* 1998, 89:10-18.
This is a thoughtful review of the B7–CD28/CTLA-4 pathway and its regulatory role in autoimmune responses.

7 • Mandelbrot DA, McAdam AJ, Sharpe AH: **B7-1 or B7-2 is required to produce the lymphoproliferative phenotype in mice lacking cytotoxic T lymphocyte-associated antigen 4 (CTLA-4).** *J Exp Med* 1999, 189:435-440.
Here, B7-1−/− B7-2−/− CTLA-4−/− mice are shown to be phenotypically normal – in contrast to the severe lymphoproliferative disorders observed in the CTLA-4−/−, B7-1−/− CTLA-4−/−, or B7-2−/− CTLA-4−/− mice. When B7-1−/− B7-2−/− CTLA-4−/− mice are given anti-CD28 monoclonal antibodies, the lymphoproliferative phenotype observed in CTLA-4−/− mice develops whereas anti-CD28 has no effect in wild-type mice – demonstrating the potent downregulatory effect of CTLA-4 *in vivo*.

8 •• Hutloff A, Dittrich AM, Beier KC, Eljaschewitsch B, Kraft R, Anagnostopoulos I, Kroczek RA: **ICOS is an inducible T-cell co-stimulator structurally and functionally related to CD28.** *Nature* 1999, 397:263-266.
A novel, human, inducible T cell co-stimulator – ICOS – is identified in this study. ICOS shares homology with CD28; *in vitro* anti-ICOS monoclonal antibodies stimulate T cell proliferation, IL-4 and IL-10 cytokine secretion and immunoglobulin production. Expression of ICOS is demonstrated within the germinal centers of tonsillar T cells.

9 Tivol EA, Borriello F, Schweitzer AN, Lynch WP, Bluestone JA, Sharpe AH: **Loss of CTLA-4 leads to massive lymphoproliferation and fatal multiorgan tissue destruction, revealing a critical negative regulatory role of CTLA-4.** *Immunity* 1995, 3:541-547.

10 Waterhouse P, Penninger JM, Timms E, Wakeham A, Shahinian A, Lee KP, Thompson CB, Griesser H, Mak TW: **Lymphoproliferative disorders with early lethality in mice deficient in Ctla-4.** *Science* 1995, 270:985-988.

11 Hutchcroft JE, Bierer BE: **Signaling through CD28/CTLA-4 family receptors: puzzling participation of phosphatidylinositol-3 kinase.** *J Immunol* 1996, 156:4071-4074.

12 Calvo CR, Amsen D, Kruisbeek AM: **Cytotoxic T lymphocyte antigen 4 (CTLA-4) interferes with extracellular signal-regulated kinase (ERK) and Jun NH2-terminal kinase (JNK) activation, but does not affect phosphorylation of T cell receptor zeta and ZAP70.** *J Exp Med* 1997, 186:1645-1653.

13 •• Lee KM, Chuang E, Griffin M, Khattri R, Hong DK, Zhang W, Straus D, Samelson LE, Thompson CB, Bluestone JA: **Molecular basis of T cell inactivation by CTLA-4.** *Science* 1998, 282:2263-2266.
This study shows an interaction between CTLA-4 and CD3 ζ in transfectants and primary T cells. This suggests that CTLA-4 could directly inhibit early signaling events mediated through the TCR complex.

14 • Lin H, Rathmell JC, Gray GS, Thompson CB, Leiden JM, Alegre ML: **Cytotoxic T lymphocyte antigen 4 (CTLA4) blockade accelerates the acute rejection of cardiac allografts in CD28-deficient mice: CTLA4 can function independently of CD28.** *J Exp Med* 1998, 188:199-204.
In this cardiac allograft model, graft rejection was delayed in CD28−/− mice as compared with wild-type controls. The administration of CTLA-4-Ig or monoclonal antibodies against B7-1 plus B7-2 delayed rejection in wild-type mice. In contrast CTLA-4–Ig or anti-CTLA-4 monoclonal antibodies accelerated graft rejection in CD28−/− mice, suggesting a downregulatory role for CTLA-4 that is independent of CD28.

15 • Fallarino F, Fields PE, Gajewski TF: **B7-1 engagement of cytotoxic T lymphocyte antigen 4 inhibits T cell activation in the absence of CD28.** *J Exp Med* 1998, 188:205-210.
This study shows that CTLA-4 can inhibit T cell activation in the absence of CD28 in 2C, TCR-transgenic CD28−/− T cells. The T cell response to 2C, *Rag*−/− CD28−/− was enhanced by priming with B7-1 co-stimulation; however similar treatment blocked the 2C, *Rag*−/− CD28−/− immune response. Administration of anti-B7-1 or anti-CTLA-4 monoclonal antibodies reversed the inhibition of the 2C, *Rag*−/− CD28−/− T cells.

Case 1:06-cv-00500-SLR-MPT Document 274-3 Filed 09/02/2008 Page 8 of 44

16. Waterhouse P, Bachmann MF, Penninger JM, Ohashi PS, Mak TW:
• **Normal thymic selection, normal viability and decreased lymphoproliferation in T cell receptor-transgenic CTLA-4-deficient mice.** *Eur J Immunol* 1997, 27:1887-1892.
This is the first paper showing the phenotype of CTLA-4$^{-/-}$ mice with a transgenic TCR. Mice with CD8$^+$ TCR-transgenic lymphocytes that are specific for H-Y or LCMV show normal thymic selection and no lymphoproliferation once all endogenous TCR rearrangement is prevented by mutation of *Rag*.

17. Chambers CA, Sullivan TJ, Truong T, Allison JP:
• **Secondary but not primary T cell responses are enhanced in CTLA-4- deficient CD8$^+$ T cells.** *Eur J Immunol* 1998, 28:3137-3143.
This publication describes the phenotype of CTLA-4$^{-/-}$, 2C, TCR-transgenic mice. Naïve CD8$^+$ T cells from CTLA-4$^{-/-}$ and wild-type 2C mice show similar proliferation and cytokine production during priming, but CTLA-4$^{-/-}$ cells proliferate about three-fold more than wild-type cells during re-stimulation.

18. Cilio CM, Daws MR, Malashicheva A, Sentman CL, Holmberg D:
Cytotoxic T lymphocyte antigen 4 is induced in the thymus upon *in vivo* activation and its blockade prevents anti-CD3-mediated depletion of thymocytes. *J Exp Med* 1998, 188:1239-1246.

19. Chambers CA, Cado D, Truong T, Allison JP: **Thymocyte development is normal in CTLA-4-deficient mice.** *Proc Natl Acad Sci USA* 1997, 94:9296-9301.

20. Metz DP, Farber DL, Taylor T, Bottomly K:
• **Differential role of CTLA-4 in regulation of resting memory versus naive CD4 T cell activation.** *J Immunol* 1998, 161:5855-5861.
This paper demonstrates that naïve CD4$^+$ T cells do not contain any CTLA-4 protein, but resting memory T cells have intracellular CTLA-4. This work suggests that CTLA-4 prevents memory T cell activation by regulating the low intensity TCR engagement that is thought to be involved in maintenance of memory cells.

21. Krummel MF, Allison JP: **CTLA-4 engagement inhibits IL-2 accumulation and cell cycle progression upon activation of resting T cells.** *J Exp Med* 1996, 183:2533-2540

22. Walunas TL, Bakker CY, Bluestone JA: **CTLA-4 ligation blocks CD28-dependent T cell activation.** *J Exp Med* 1996, 183:2541-2550.

23. Scheipers P, Reiser H:
• **Fas-independent death of activated CD4(+) T lymphocytes induced by CTLA- 4 crosslinking.** *Proc Natl Acad Sci USA* 1998, 95 10083-10088
This paper points out that cross-linking of CTLA-4 on naive T cells blocks cell cycle progression without induction of apoptosis whereas cross-linking of CTLA-4 on activated CD4$^+$ T cells results in cell death. This cell death of activated CD4$^+$ T cells is not mediated by the Fas pathway, since T cells from Fas mutant lpr mice respond similarly to CTLA-4 cross-linking compared with wild-type cells.

24. Blair PJ, Riley JL, Levine BL, Lee KP, Craighead N, Francomano T, Perfetto SJ, Gray GS, Carreno BM, June CH:
• **CTLA-4 ligation delivers a unique signal to resting human CD4 T cells that inhibits interleukin-2 secretion but allows Bcl-x_L induction.** *J Immunol* 1998, 160:12-15
This study reveals that downregulation of IL-2 and Bcl-x_L can be influenced differentially by anti-CTLA-4 antibodies. It also illustrates that various anti-CTLA-4 antibodies could have different effects on T cell responses.

25. Walunas TL, Bluestone JA:
• **CTLA-4 regulates tolerance induction and T cell differentiation *in vivo*.** *J Immunol* 1998, 160:3855-3860
This study describes the role of CTLA-4 during SEB-induced immune responses. Anti-CTLA-4 treatment resulted in increased numbers of SEB-reactive T cells and blockade of tolerance induction. In addition, anti-CTLA-4 was shown to play a role in cytokine production of both CD4$^+$ and CD8$^+$ T cells and lead to increased levels of IL-4 and IFN-γ production.

26. Khattri R, Auger JA, Griffin M, Sharpe AH, Bluestone JA:
Lymphoproliferative disorder in CTLA-4 knockout mice is characterized by CD28-regulated activation of Th2 responses. *J Immunol* 1998, in press

27. Zhang X, Brunner T, Carter L, Dutton RW, Rogers P, Bradley L, Sato T, Reed JC, Green D, Swain SL: **Unequal death in T helper cell (Th)1 and Th2 effectors: Th1, but not Th2, effectors undergo rapid Fas/FasL-mediated apoptosis.** *J Exp Med* 1997, 185:1837-1849.

28. Schweitzer AN, Sharpe AH:
• **Studies using antigen-presenting cells lacking expression of both B7-1 (CD80) and B7-2 (CD86) show distinct requirements for B7 molecules during priming versus restimulation of Th2 but not Th1 cytokine production.** *J Immunol* 1998, 161:2762-2771
This study examines the role of B7 mediated signals in Th1, compared with Th2, differentiation. Th2 differentiation in naïve CD4$^+$ T cells is dependent on B7-mediated signals whereas IL-4 production in previously activated T cells is B7 independent. During Th1 differentiation, both naïve and primed T cells require B7-mediated signals for IL-2, but not IFN-γ, production.

29. Rulifson IC, Sperling AI, Fields PE, Fitch FW, Bluestone JA:
CD28 costimulation promotes the production of Th2 cytokines. *J Immunol* 1997, 158:658-665.

30. Chen W, Jin W, Wahl SM:
• **Engagement of cytotoxic T lymphocyte associated antigen 4 (CTLA-4) induces transforming growth factor beta (TGF-beta) production by murine CD4(+) T cells.** *J Exp Med* 1998, 188:1849-1857.
In this study the authors demonstrate that anti-CTLA-4 antibody leads to increased TGF-β production by CD4$^+$ T cells. Since TGF-β has a downregulatory effect on immune responses, this could contribute to the inhibitory effect of CTLA-4.

31. Alegre ML, Noel PJ, Eisfelder BJ, Chuang E, Clark MR, Reiner SL, Thompson CB:
Regulation of surface and intracellular expression of CTLA4 on mouse T cells. *J Immunol* 1996, 157:4762-4770.

32. Chambers CA, Sullivan TJ, Allison JP:
•• **Lymphoproliferation in CTLA-4 -deficient mice is mediated by costimulation-dependent activation of CD4$^+$ T cells.** *Immunity* 1997, 7:885-895.
This article focuses on the role of CD4$^+$ cells, compared with CD8$^+$ cells in the lymphoproliferative disease of CTLA-4$^{-/-}$ mice. CD4$^+$ cells are preferentially expanded in CTLA-4$^{-/-}$ mice and are responsible for the initiation of the disease.

33. Bachmann MF, Waterhouse P, Speiser DE, McKall Faienza K, Mak TW, Ohashi PS:
Normal responsiveness of CTLA-4-deficient anti-viral cytotoxic T cells. *J Immunol* 1998, 160:95-100.

34. Vanderlugt CL, Begolka WS, Neville KL, Katz-Levy Y, Howard LM, Eagar TN, Bluestone JA, Miller SD:
The functional significance of epitope spreading and its regulation by co-stimulatory molecules. *Immunol Rev* 1998, 164:63-72.

35. Luhder F, Hoglund P, Allison JP, Benoist C, Mathis D:
•• **Cytotoxic T lymphocyte-associated antigen 4 (CTLA-4) regulates the unfolding of autoimmune diabetes.** *J Exp Med* 1998, 187:427-432.
This study demonstrates that anti-CTLA-4 accelerates the development of disease in a TCR-transgenic model of diabetes. In order to affect the onset of disease anti-CTLA-4 needed to be administered early – before the development of insulitis – suggesting a role for CTLA4 in initiating, rather than modifying, the course of diabetes.

36. Nistico L, Buzzetti R, Pritchard LE, Van der Auwera B, Giovannini C, Bosi E, Larrad MT, Rios MS, Chow CC, Cockram CS *et al*:
The CTLA-4 gene region of chromosome 2q33 is linked to, and associated with, type 1 diabetes. Belgian Diabetes Registry. *Hum Mol Genet* 1996, 5:1075-1080.

37. Marron MP, Raffel LJ, Garchon HJ, Jacob CO, Serrano-Rios M, Martinez Larrad MT, Teng WP, Park Y, Zhang ZX, Goldstein DR *et al*:
Insulin-dependent diabetes mellitus (IDDM) is associated with CTLA4 polymorphisms in multiple ethnic groups. *Hum Mol Genet* 1997, 6:1275-1282

38. Donner H, Braun J, Seidl C, Rau H, Finke R, Ventz M, Wallish PG, Usadel KH, Badenhoop K:
Codon 17 polymorphism of the cytotoxic T lymphocyte antigen 4 gene in Hashimoto's thyroiditis and Addison's disease. *J Clin Endocrinol Metab* 1997, 82:4130-4132.

39. Awata T, Kuzuya S, Iitaka M, Takei S, Inoue I, Ishii C, Negishi K, Izumida T, Yoshida Y, Hagura R *et al*:
Association of CTLA-4 gene A-G polymorphism (IDDM12 locus) with acute- onset and insulin-depleted IDDM as well as autoimmune thyroid disease (Graves' disease and Hashimoto's thyroiditis) in the Japanese population. *Diabetes* 1998, 47:128-129

40. Braun J, Donner H, Siegmund T, Wallish PG, Usadel KH, Badenhoop K:
CTLA-4 promoter variants in patients with Graves' disease and Hashimoto's thyroiditis. *Tissue Antigens* 1998, 51:563-566

41. Judge TA, Wu Z, Zheng XG, Sharpe AH, Sayegh MH, Turka LA:
The role of CD80, CD86, and CTLA4 in alloimmune responses and the induction of long-term allograft survival. *J Immunol* 1999 162:1947-1951

42. Kaufman KA, Bowen JA, Tsai AF, Bluestone JA, Hunt JS, Ober C:
The CTLA-4 gene is expressed in placental fibroblasts. *Mol Hum Reprod* 1998, 5:84-87

43. Tsai AF, Kaufman KA, Walker MA, Kamson TG, Odum RR, Barnes RB, Scott JR, Schreiber JR, Stephenson MD, Ober C:
Transmission disequilibrium of maternally-inherited CTLA-4 microsatellite alleles in idiopathic recurrent miscarriage. *J Reprod Immunol* 1998, 40:147-157

44. Leung HT, Bradshaw J, Cleaveland JS, Linsley PS: **Cytotoxic T lymphocyte-associated molecule-4, a high-avidity receptor for CD80 and CD86, contains an intracellular localization motif in its cytoplasmic tail.** *J Biol Chem* 1995, 270:25107-25114.

45. Bradshaw JD, Lu P, Leytze G, Rodgers J, Schieven GL, Bennett KL, Linsley PS, Kurtz SE: **Interaction of the cytoplasmic tail of CTLA-4 (CD152) with a clathrin- associated protein is negatively regulated by tyrosine phosphorylation.** *Biochemistry* 1997, 36:15975-15982.

46 •• Chuang E, Lee KM, Robbins MD, Duerr JM, Alegre ML, Hambor JE, Neveu MJ, Bluestone JA, Thompson CB: **Regulation of cytotoxic T lymphocyte-associated molecule-4 by Src kinases.** *J Immunol* 1999, 162:1270-1277.

This paper addresses several issues regarding CTLA-4 signaling and translocation. It shows that the tyrosine-phosphatase inhibitor pervanadate can increase CTLA-4 cell surface expression, providing evidence that this process is indeed phosphorylation dependent. The authors also demonstrate (by using CTLA 4 mutants and antibodies that recognize distinct, phosphorylated forms of CTLA-4) that Lck can interact with CTLA-4 and phosphorylate both tyrosine motifs

47. Schneider H, Prasad KVS, Shoelson SE, Rudd CE: **CTLA-4 binding to the lipid kinase phosphatidylinositol 3-kinase in T cells.** *J Exp Med* 1995, 181:351-355.

48. Zhang Y, Allison JP: **Interaction of CTLA-4 with AP50, a clathrin-coated pit adaptor protein.** *Proc Natl Acad Sci USA* 1997, 94:9273-9278.

49. Marengere LE, Waterhouse P, Duncan GS, Mittrucker HW, Feng GS, Mak TW: **Regulation of T cell receptor signaling by tyrosine phosphatase SYP association with CTLA-4.** *Science* 1996, 272:1170-1173.

50 Frearson JA, Alexander DR: **The phosphotyrosine phosphatase SHP-2 participates in a multimeric signaling complex and regulates T cell receptor (TCR) coupling to the Ras/mitogen-activated protein kinase (MAPK) pathway in Jurkat T cells.** *J Exp Med* 1998, 187:1417-1426.

51 Chambers CA, Allison JP: **The role of tyrosine phosphorylation and PTP-1C in CTLA-4 signal transduction.** *Eur J Immunol* 1996, 26:3224-3229

52 Schneider H, Schwartzberg PL, Rudd CE: **Resting lymphocyte kinase (Rlk/Txk) phosphorylates the YVKM motif and regulates PI 3-kinase binding to T-cell antigen CTLA-4.** *Biochem Biophys Res Commun* 1998, 252:14-19.

EXHIBIT 13

neuron responded at the second syllable, and the response was suppressed by deletion of the first or second syllable.
13. D. Margoliash, *J. Neurosci.* **3**, 1039 (1983); D. Margoliash, E. S. Fortune, *J. Neurosci.* **12**, 4309 (1992).
14. We gathered sufficient data from 14 neurons (from three birds) to permit quantitative comparisons between ongoing discharge and singing. Interspike interval histograms of the ongoing discharge of RA neurons during sleep are bimodal; the longer interval peak is related to nonbursting activity. Thus, bursts were defined as continuous sequences of interspike intervals falling outside of the normal (nonbursting) distribution of intervals.
15. Two tests of significance were devised. For each neuron, a distance was computed between each ongoing burst and the exemplar stretch of activity during singing. Each best match (lowest distance) was tested for significance by using a bootstrap procedure that assessed the probability of occurrence of the exact sequence of intervals observed in the burst. In the second test, for the one bird with the greatest number of recordings, we also compared each neuron's ongoing discharges during sleep with the premotor data from other neurons. For seven out of eight neurons, there were more matches with the neuron's own premotor data than with the premotor data from the other neurons. The same neuron failed to achieve significance in both tests.
16. The procedures for identifying bursts in ongoing activity, matching bursts to premotor activity, and assessing the significance of the matches are described in detail on *Science* Online (*24*).
17. M. Konishi, *Z. Tierpsychol.* **22**, 770 (1965).
18. C. E. Carr, W. Heiligenberg, G. J. Rose, *J. Neurosci.* **6**, 107 (1986); *J. Neurosci.* **6**, 1372 (1986); A. Moiseff, M. Konishi, *J. Neurosci.* **1**, 40 (1981); C. E. Carr, M. Konishi, *J. Neurosci.* **10**, 3227 (1990); G. Laurent, M. Wehr, H. Davidowitz, *J. Neurosci.* **16**, 3837 (1996); R. C. deCharms, M. M. Merzenich, *Nature* **381**, 610 (1996); A. K. Engel, P. R. Roelfsema, P. Fries, M. Brecht, W. Singer, *Cereb. Cortex* **7**, 571 (1997); Y. Prut *et al.*, *J. Neurophysiol.* **79**, 2857 (1998).
19. E. T. Vu, M. E. Mazurek, Y.-C. Kuo, *J. Neurosci.* **14**, 6924 (1994).
20. S. W. Bottjer, F. Johnson, *J. Neurobiol.* **33**, 602 (1997).
21. M. Luo, D. J. Perkel, *J. Neurosci.* **19**, 6700 (1999).
22. G. E. Hinton, P. Dayan, B. J. Frey, R. M. Neal, *Science* **268**, 1158 (1995).
23. G. Buzsáki, *Neuroscience* **31**, 551 (1989); M. A. Wilson, B. L. McNaughton, *Science* **265**, 676 (1994); W. E. Skaggs, B. L. McNaughton, *Science* **271**, 1870 (1996); Z. Nádasdy, H. Hirase, A. Czurkó, J. Csicsvari, G. Buzsáki, *J. Neurosci.* **19**, 9497 (1999).
24. Supplemental data are available at www.sciencemag.org/feature/data/1051099.shl.
25. We thank T. Q. Gentner, J.-M. Ramirez, P. S. Ulinski, and especially two anonymous reviewers for valuable comments on the manuscript. This work was supported by grants from the NIH (MH59831 and MH60276) to D.M. and (MH11615) to A.S.D.

6 April 2000; accepted 8 September 2000

Structure of Murine CTLA-4 and Its Role in Modulating T Cell Responsiveness

David A. Ostrov,[1,2] Wuxian Shi,[2] Jean-Claude D. Schwartz,[1] Steven C. Almo,[2]* Stanley G. Nathenson[1,3]*

The effective regulation of T cell responses is dependent on opposing signals transmitted through two related cell-surface receptors, CD28 and cytotoxic T lymphocyte–associated antigen 4 (CTLA-4). Dimerization of CTLA-4 is required for the formation of high-avidity complexes with B7 ligands and for transmission of signals that attenuate T cell activation. We determined the crystal structure of the extracellular portion of CTLA-4 to 2.0 angstrom resolution. CTLA-4 belongs to the immunoglobulin superfamily and displays a strand topology similar to Vα domains, with an unusual mode of dimerization that places the B7 binding sites distal to the dimerization interface. This organization allows each CTLA-4 dimer to bind two bivalent B7 molecules and suggests that a periodic arrangement of these components within the immunological synapse may contribute to the regulation of T cell responsiveness.

T cell–dependent immune processes require cell-surface interactions that mediate the initiation, modulation, and the ultimate course of the response. The specificity of T cell recognition is determined by the engagement of the T cell receptor (TCR) on T cells with cognate peptide–major histocompatibility complex (MHC) complexes presented by antigen-presenting cells (APCs) (*1*, *2*). Additional signals are required to sustain and enhance T cell activity, the most important of which is provided by the engagement of CD28 on T cells with its ligands B7-1 (CD80) and B7-2 (CD86) on APCs (*3*, *4*). In contrast, the interaction of B7 isoforms with CTLA-4, a CD28 homolog (31% identity), provides inhibitory signals required for down-regulation of the response (*5*).

Unlike CD28, which is expressed on resting T cells, CTLA-4 is not detected on the cell surface until 24 hours after activation, peaking at 36 to 48 hours after activation (*6*). In addition, CTLA-4 exhibits an affinity for the B7 isoforms that is 10 to 100 times that for CD28 (*7*). On the basis of these differences in expression patterns and affinities, it is likely that CTLA-4 directly competes with CD28 for binding B7 and also directs the assembly of inhibitory signaling complexes that lead to quiescence or anergy (*8*). Consistent with the inhibitory role of CTLA-4, mice deficient in CTLA-4 die as a consequence of unchecked polyclonal T cell expansion, which results in fatal lymphoproliferative disorders (*9*). Thus, the balance between the opposing signals elicited by CD28 and CTLA-4 is central to the regulation of T cell responsiveness and homeostasis (*10*).

Because of its dominant role in modulating T cell activity, CTLA-4 has received considerable attention as a therapeutic agent (*11*). The soluble CTLA-4–immunoglobulin (CTLA-4–Ig) fusion protein acts as an inhibitor of CD28-B7 costimulation and has specific inhibitory effects in animal models of autoimmunity, transplant rejection, asthma, and allergy (*3*, *12*). The efficacy of CTLA-4–Ig treatment of human disease has been demonstrated in clinical trials on patients with psoriasis vulgaris (*13*). This approach may well extend to a variety of T cell–mediated diseases including autoimmune diabetes, rheumatoid arthritis, systemic lupus erythematosus, and graft-versus-host disease (*13*). In contrast to strategies that interfere with the CD28-B7 association, reagents that interfere with the CTLA-4–B7 interaction intensify specific T cell responses. For example, blocking antibodies directed against CTLA-4 enhance rejection of preestablished tumors and protect against secondary challenge in animal models of prostate cancer and colon carcinoma (*14*).

The structure of the soluble extracellular domain of murine CTLA-4 (*15*) revealed two independent copies of the CTLA-4 dimer in the asymmetric unit of the crystal (Fig. 1, A and B, and Table 1) (*16*). The CTLA-4 monomer is a two-layer β-sandwich that exhibits the chain topology found in the immunoglobulin variable domains (Fig. 1A) (*17*). The front and back sheets, composed of strands A′GFCC′ and ABEDC″, respectively, are connected by two intersheet disulfide bonds. The disulfide bond between the B and F strands is a signature for the immunoglobulin fold; the disulfide bond joining strands C′ and D is unique to the CD28/CTLA-4 family (Fig. 1A) (*17*, *18*).

The nuclear magnetic resonance (NMR) structure of a monomeric form of human CTLA-4 (*18*) shows the same overall topology as the murine homolog, with a root mean square (rms) deviation of 2.4 Å between equivalent Cα atoms. The most significant

[1]Department of Microbiology and Immunology, [2]Department of Biochemistry, [3]Department of Cell Biology, Albert Einstein College of Medicine, Bronx, NY 10461, USA.

*To whom correspondence should be addressed. E-mail: almo@aecom.yu.edu or nathenso@aecom.yu.edu

BMS 002569166

difference involves the C″ strand, which in the crystal structure is hydrogen-bonded to the ABED sheet, as in Vα domains (Fig. 1A); in the NMR structure this region is defined as a loop and does not interact with either sheet (A′GFCC′ or ABED). Structural alignment (*19*) shows that CTLA-4 is most similar to the Vα and V_H domains present in antigen receptors, with rms deviations of 3.0 and 3.1 Å, respectively (*20*).

The CTLA-4 dimer interface is not formed by the A′GFCC′ sheet (front-to-front packing) as observed in variable (v-type) immunoglobulin dimers, such as VαVβ and V_LV_H heterodimers and CD8 homodimers (*21*). Instead, CTLA-4 exhibits a dimer interface similar to that present in the constant (c-type) family members, such as C_H3 homodimers and C_LC_H1 heterodimers, which involves the BED strands (back-to-back packing) (Fig. 1B) (*22*). Several distinct features of the CTLA-4 monomer are consistent with this unusual dimerization mode: (i) The front sheet of CTLA-4 is flatter than other v-type immunoglobulin domains, precluding a number of contacts critical for front-to-front packing; (ii) CTLA-4 lacks one (C′ strand) of the two β bulges (C′ and G) in the front sheet that are characteristic of front-to-front packing; (iii) the front sheet of CTLA-4 is considerably less hydrophobic than v-type dimers, consistent with its exposure to solvent; (iv) the placement of the C″ strand in CTLA-4 augments the back sheet (strands ABEDC″), contributing six van der Waals contacts to the dimerization interface that are not present in other v-type dimers; and (v) modeling studies show that putative front-to-front packing of CTLA-4 monomers is sterically incompatible with the known binding surface for B7 ligands (*18*).

The CTLA-4 dimer interface is stabilized by four hydrogen bonds, 48 van der Waals contacts, and 15 water-mediated hydrogen bonds, involving a number of residues that are largely conserved among CTLA-4 homologs, including His^{14}, Glu^{22}, Arg^{74}, and Gln^{80} (Fig. 1C). These residues are not conserved in CD28 (Fig. 2), suggesting differences in the dimer interface and/or quaternary organization. The total surface area buried at the CTLA-4 dimer interface is 1597 $Å^2$, which is comparable with the C_LC_H1 (1500 to 2100 $Å^2$) and C_H3C_H3 interfaces (2200 $Å^2$) (*23*). Although CTLA-4 and the c-type immunoglobulin dimers both utilize back-to-back packing, the relative orientation of the monomers within the dimers differs considerably. Superposition of a CTLA-4 monomer with C_H1 would require a 10° to 12° rotation and a 9 to 10 Å translation to align the second CTLA-4 monomer on C_L (*24*). The structure of human B7-1 reveals that the membrane distal domain, which binds CTLA-4, displays the v-type immunoglobulin topology and also homodimerizes via the back face (*25*). The structural similarity

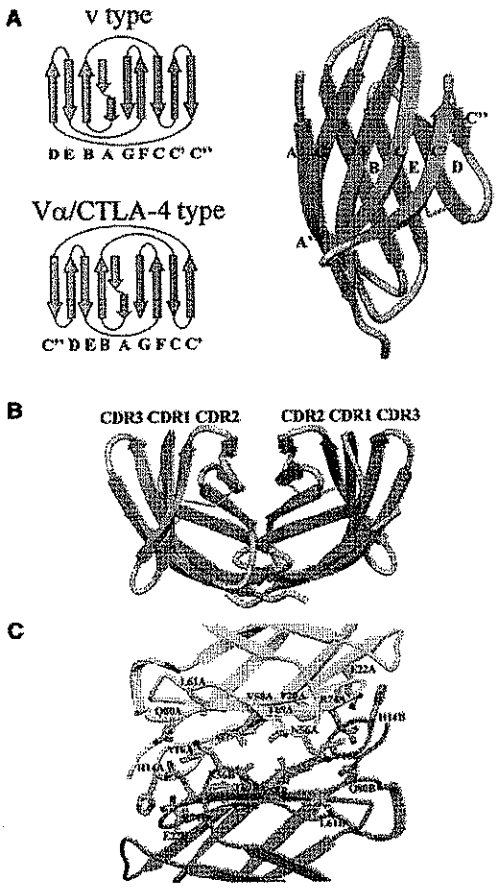

Fig. 1. Structure of CTLA-4. (A) On the right, ribbon diagram of the CTLA-4 monomer. The β strands are labeled: A (3 to 6), A′ (7 to 11), B (16 to 24), C (30 to 39), C′ (43 to 53), C″ (56 to 59), D (65 to 70), E (74 to 80), F (87 to 99), and G (103 to 114). The A′GFCC′ (front) and ABEDC″ (back) sheets are shown in gold and blue, respectively. Intersheet disulfide bonds between the B and F strands and between the C′ and D strands are shown in yellow. Inset on the top left shows the strand topology for typical v-type immunoglobulin domains (e.g., V_H, V_L, Vβ). Inset on the bottom left shows the strand topology for Vα domains and CTLA-4 in which the C″ strand is part of the back sheet. (B) Ribbon diagram of the CTLA-4 dimer. The CTLA-4 homodimer is oriented with the molecular diad axis situated vertically in the plane of the page. In this orientation, the COOH-termini extend from the bottom of the molecule. The dimer interface is formed primarily by the ABEDC″ (back) sheets, shown in blue. The CDR analogous regions, CDR1 (BC loop), CDR2 (C′C″ loop), and CDR3 (FG loop), form the top surface of the molecule. The distance between the CDR3 analogous regions in the dimer is 47 Å. (C) Detailed view of the CTLA-4 dimer interface. The twofold axis of the dimer is perpendicular to the page. The backbones of the CTLA-4 monomers are shown in green and in sky blue. The side chains involved in hydrogen bonding and van der Waals interactions at the dimer interface are displayed (*23*), with C, O, and N atoms depicted in yellow, red, and blue, respectively. Figure 1 was made with the program SETOR (*41*).

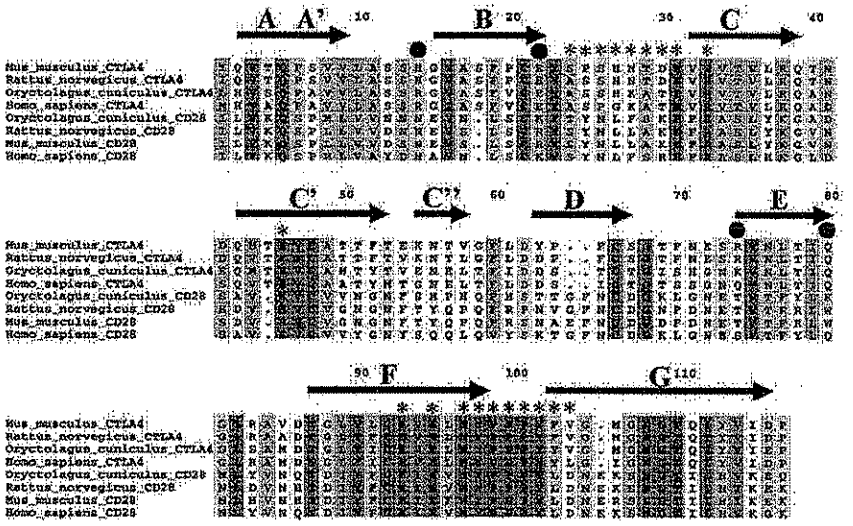

Fig. 2. Sequence alignment of the CTLA-4 and CD28 family (*43*). CTLA-4 and CD28 sequences were aligned with ClustalX (*42*). Positions with 50 to 100% sequence similarity are colored in hues graded from yellow to green. Mutations that affect the binding of CTLA-4 to B7 are labeled "*". Residues contributing to hydrogen bonds at the CTLA-4 dimer interface are indicated with filled circles. The β strands were defined according to the murine CTLA-4 structure. Figure 2 was made with ALSCRIPT (*44*).

BMS 002569167

within this receptor-ligand pair suggests an evolutionary relationship.

Mutagenesis studies have identified a series of residues involved in B7 binding that cluster to a single surface on CTLA-4, including the FG loop, the BC loop, and residues on the A′GFCC′ face (Arg^{33}, Thr^{35}, Leu^{37}, Glu^{46}, Thr^{51}; Fig. 3C) (*18*, *26*). The FG loop, which is analogous to CDR3 present in immunoglobulins and TCRs, contains the $Met^{97}TyrProProProTyr^{102}$ sequence motif, which is highly conserved in CTLA-4 and CD28 sequences from different species (Fig. 2) and is critical in mediating the interaction with B7. The unique *cis-trans-cis* conformations of the three consecutive proline residues and their relatively low B factors suggest that these residues play a direct role in binding B7 and are required to maintain the loop in a productive binding conformation. Residues in the BC loop, the region analogous to CDR1, also appear to be determinants of binding affinity, as grafting the CDR1 region of CTLA-4 onto CD28 dramatically increased the binding strength of the chimeric molecule for B7 (*26*). A prominent feature evident on the B7 binding surface of CTLA-4 is a predominantly hydrophobic pocket, approximately 10 Å in diameter and 9 Å deep, formed by residues contributed by the CDR1- and CDR3-like loops. This pocket may con-

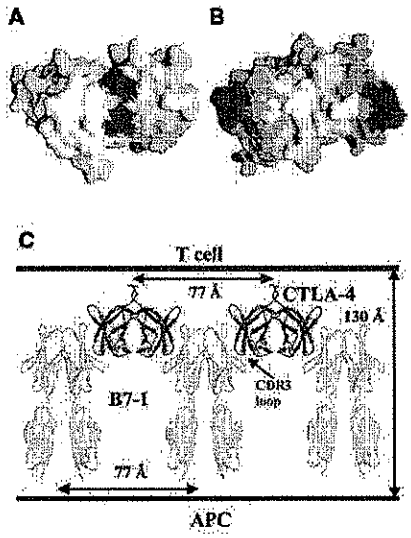

Fig. 3. B7 binding sites on CTLA-4 and placement of CDR3 regions in dimers of immunoglobulin domains. The molecular surfaces of the TCR VαVβ heterodimer (1tcr) and the CTLA-4 homodimer (1dqt) are shown in (**A**) and (**B**), respectively, with the CTLA-4 twofold axis oriented perpendicular to the page. Because of front-to-front packing in the TCR, the CDR3 regions shown in red are juxtaposed at the dimer interface (A), whereas the back-to-back packing present in CTLA-4 positions the CDR3 regions distal to the dimer interface (B). The two B7 binding sites on the CTLA-4 homodimer, as mapped by mutagenesis (*26*), include the FG loop (CDR3) shown in red, the BC loop (CDR1) shown in yellow, and solvent-accessible residues on the A′GFCC′ sheet (Glu^{31}, Arg^{33}, Glu^{46}, Lys^{93}, Glu^{95}, Phe^{103}, and Val^{104}), shown in yellow (*18*). In contrast to VαVβ and Fab, which are monovalent for their respective ligands (i.e., peptide-MHC complex and antigen), the placement of ligand binding sites at the extremes of the CTLA-4 dimer suggests that each CTLA-4 monomer may interact with an individual B7 dimer. (A) and (B) were prepared with GRASP (*45*). (**C**) Model of organized interactions between CTLA-4 and B7 dimers in the immunological synapse. CTLA-4 dimers, shown in red, are depicted with their COOH-termini modeled to include the disulfide bond at Cys^{120} near the T cell plasma membrane. CTLA-4 was manually docked to B7-1 d1, shown in light blue, to maximize the interaction between residues implicated by site-directed mutagenesis, in particular, CDR3 ($Met^{97}TyrProProProTyr^{102}$) of CTLA-4, and a hydrophobic patch on the A′GFCC′C″ face of B7-1 (*25*). Each CTLA-4 dimer is depicted as binding two independent B7 dimers with an intermolecular spacing of approximately 77 Å and an intermembrane distance spanned by the CTLA-4–B7 ligand pair of approximately 100 Å. (C) was made with the program SETOR (*41*).

Table 1. Crystallographic analysis. Native and selenomethionyl-substituted *Mus musculus* CTLA-4 were expressed in *Escherichia coli*. Crystals of CTLA-4 were grown by hanging drop vapor diffusion at 18°C. A portion (2 μl) of a 10 mg/ml protein solution was mixed with 2 μl of crystallization buffer composed of 20% PEG 6000, 2.0 M NaCl, pH 6.5, and equilibrated against a 1-ml reservoir of the same buffer. Diffraction from these crystals is consistent with the space group $P4_32_12$ ($a = b = 112.85$ Å, $c = 102.50$ Å; four monomers in the asymmetric unit, 58% solvent). Crystals were transferred stepwise to cryoprotectant solution containing 20% ethylene glycol in crystallization buffer and flash cooled at 100 K. MAD data were collected at beamline X12C (National Synchrotron Light Source, Brookhaven National Laboratory). Data were recorded at wavelengths of 0.9789, 0.9786, and 0.9500 Å on a Brandeis charge-coupled device detector and reduced with the HKL suite (*34*). The 12 selenium sites were located by direct methods (*35*) and by difference Patterson and cross validation difference Fourier methods implemented in the SOLVE package (*36*). Electron density maps, enhanced with fourfold noncrystallographic averaging and solvent flattening using DM (*37*), allowed 95% of the residues to be traced using the program O (*38*). The model was refined against native data collected on a MAR345 detector at beamline X9B (NSLS, BNL) and subjected to anisotropic and bulk solvent correction, simulated annealing refinement, and individual B-factor refinement using the CNS package (*39*). The final model is of high quality, with 99% of the residues in the most favored and additionally allowed regions (*40*). The rms deviation between related by noncrystallographic symmetry is 0.5 Å.

	Data collection statistics			
Data set	CTLA-4 native	Se edge	Se peak	Se remote
Detector	Mar345	Brandeis CCD	Brandeis CCD	Brandeis CCD
Beamline	X-9B (NSLS)	X-12C (NSLS)	X-12C	X-12C
Resolution (Å)*	2.0 (2.07–2.00)	3.0 (3.05–3.00)	3.0 (3.05–3.00)	3.0 (3.05–3.00)
Wavelength (Å)	0.9789	0.9789	0.9786	0.9500
Reflections:				
Total	301,486	77,098	76,888	74,730
Unique	44,587	13,676	13,669	13,708
$I/\sigma(I)$	36.5 (5.7)	21.0 (9.1)	18.0 (7.3)	23.7 (11.0)
Completeness:	99.4 (95.7)	98.7 (100.0)	98.7 (100.0)	98.5 (100.0)
R_{sym} (%)†	6.2 (36.3)	6.9 (12.7)	8.8 (16.3)	6.8 (11.4)
R_{anom} (%)‡		4.9	6.8	4.3
		Refinement statistics		
Resolution (Å)		20.0–2.0		
R_{cryst} (%)§		20.9		
R_{free} (%)‖		25.4		
Reflections over 2σ:				
For refinement		35,364		
For R_{free}		3,965		
Protein atoms		3,632		
Water molecules		431		
Average B factors (Å²)				
Protein		31.9		
Water		42.4		
rms deviations from ideal				
Bond lengths (Å)		0.009		
Angles (°)		1.55		
		Ramachandran plot		
Most favored (%)		92.0		
Additionally allowed (%)		7.0		
Generously allowed (%)		1.0		
Disallowed (%)		0.0		

*Values in parentheses are for the highest resolution shell. †$R_{sym} = \Sigma_i |I_{hi} - \langle I_{hi}\rangle| / \Sigma_i |I_{hi}|$, where h specifies unique reflection indices, i indicates symmetry equivalent observations of h. ‡$R_{anom} = \Sigma_h |I_h^+ - I_h^-| / \Sigma_h |I_h^+ + I_h^-|$, where h specifies unique reflection indices. §$R_{cryst} = \Sigma |F_o - F_c| / \Sigma |F_o|$ for all reflections, where F_o and F_c are the observed and calculated structure factors, respectively. ‖R_{free} was calculated against 10% of the reflections removed at random from the refinement.

tact a hydrophobic patch on the membrane distal part of B7-1, including Met^{38}, Trp^{50}, and Tyr^{53}, which are essential for binding to CTLA-4 (*25*).

Certain features of the CTLA-4 dimer, in particular the placement of CDR3, appear to be relevant to its interaction with B7 and the regulation of signaling events at the synapse formed by the T cell–APC interface. As a consequence of the unusual dimerization mode used by CTLA-4, the FG loop (CDR3) is located distal to the dimerization interface (Figs. 1B and 3B). This organization contrasts with other v-type immunoglobulin domains where CDR3 is located proximal to the dimer interface (Fig. 3A), and provides CTLA-4 with the potential for novel ligand-binding interactions. A model of the CTLA-4/B7 complex was generated by manual docking, which maximized the interactions of residues contributing to the binding interface as defined by site-directed mutagenesis (Fig. 3C). This model predicts that the CTLA-4–B7 interface is formed primarily by the front sheets (A′GFCC′) of the respective molecules and buries a total surface area of ~1200 Å^2. This packing arrangement is similar to that observed in the structures of the heterophilic CD2/CD58 and homophilic Po-Po complexes that bury 1507 and 984 Å^2, respectively (*27*, *28*).

The dimeric organization of both CTLA-4 and B7-1 at the T cell–APC interface is consistent with the formation of a periodic structure, in which each CTLA-4 dimer bridges two B7 molecules, with an interdimer spacing of ~77 Å (Fig. 3C). Steric considerations appear to preclude a bidentate interaction between individual CTLA-4 and B7 dimers. The dimensions of the CTLA-4 and B7 molecules suggest an intermembrane distance of ~100 Å, which is compatible with the linear dimensions of the TCR–peptide/MHC and the CD2-CD58 complexes that measure approximately 130 Å in their maximum dimension (*2*, *27*).

The putative organization of the CTLA-4–B7 complex suggests that in addition to antagonism of CD28 costimulation through competition for B7 by high-avidity CTLA-4 dimers, more elaborate regulatory mechanisms might operate by the recruitment and ordering of intracellular signaling components to the TCR complex in the immunological synapse (*29*, *30*). Initial engagement between T cell and APC results in phosphorylation of the TCR ζ chain, and directs subsequent cytoskeletal events that lead to clustering of the TCR and peptide-MHC complexes within the synapse. As CTLA-4 coimmunoprecipitates with both TCR ζ and SHP-2 phosphatase, the binding of CTLA-4 to B7 in the central region of the synapse could inhibit TCR signaling by directing the SHP-2–mediated dephosphorylation of TCR ζ (*31*–*33*). This physical linkage between CTLA-4 and the TCR complex also suggests that CTLA-4 might direct short-range ordering of signaling components within the central zone of the immunological synapse. Thus, CTLA-4 might function as both a competitor of CD28 function and as an organizing element required for negative signaling within the synapse.

References and Notes

1. C. A. J. Janeway, K. Bottomly, *Semin. Immunol.* **8**, 108 (1996).
2. K. C. Garcia, L. Teyton, I. A. Wilson, *Annu. Rev. Immunol.* **17**, 369 (1999).
3. E. A. Greenfield, K. A. Nguyen, V. K. Kuchroo, *Crit. Rev. Immunol.* **18**, 389 (1998).
4. C. A. Chambers, J. P. Allison, *Curr. Opin. Cell Biol.* **11**, 203 (1999).
5. M. F. Krummel, J. P. Allison, *J. Exp. Med.* **182**, 459 (1995).
6. C. B. Thompson, J. P. Allison, *Immunity* **7**, 445 (1997).
7. P. A. van der Merwe, D. L. Bodian, S. Daenke, P. Linsley, S. J. Davis, *J. Exp. Med.* **185**, 393 (1997).
8. P. S. Linsley, P. Golstein, *Curr. Biol.* **6**, 398 (1996).
9. E. A. Tivol *et al.*, *Immunity* **3**, 541 (1995).
10. J. A. Bluestone, *J. Immunol.* **158**, 1989 (1997).
11. M. H. Sayegh, *J. Clin. Invest.* **103**, 1223 (1999).
12. D. J. Lenschow *et al.*, *Immunity* **5**, 285 (1996).
13. J. R. Abrams *et al.*, *J. Clin. Invest.* **103**, 1243 (1999).
14. E. D. Kwon *et al.*, *Proc. Natl. Acad. Sci. U.S.A.* **94**, 8099 (1997).
15. The extracellular domain of CTLA-4 encompassing residues 1 to 119 was expressed in BL21(DE3), refolded from inclusion bodies, and purified by anion-exchange chromatography.
16. CTLA-4 expressed on the surface of T cells contains at least one N-linked carbohydrate (*7*). Human CTLA-4 expressed in Chinese hamster ovary (CHO) cells is glycosylated on Asn^{76} and Asn^{108}, the equivalents of Asn^{78} and Asn^{110} in murine CTLA-4. The observed crystal structure is not compatible with glycosylation at Asn^{78}, as this would interfere with the formation of the back-to-back dimer interface. This apparent inconsistency is perhaps attributable to differences in the glycosylation properties of T cells and CHO cells. However, the observed dimer is compatable with glycosylation at the solvent exposed Asn^{110}, which resides in the G strand β bulge on the front sheet of murine CTLA-4.
17. P. Bork, L. Holm, C. Sander, *J. Mol. Biol.* **242**, 309 (1994).
18. W. J. Metzler *et al.*, *Nature Struct. Biol.* **4**, 527 (1997).
19. L. Holm, C. Sander, *J. Mol. Biol.* **233**, 123 (1993).
20. Protein structures: TCR, Protein Data Bank (PDB) code 1tcr (*21*); Fab of monoclonal antibody to gp120, 1gc1 [P. D. Kwong *et al.*, *Nature* **393**, 648 (1998)]; Po, 1neu [L. Shapiro, J. P. Doyle, P. Hensley, D. R. Colman, W. A. Hendrickson, *Neuron* **17**, 435 (1996)]; CD8, 1cd8 [D. J. Leahy, R. Axel, W. A. Hendrickson, *Cell* **68**, 1145 (1992)]; CD2, 1hnf [D. L. Bodian, E. Y. Jones, K. Harlos, D. I. Stuart, S. J. Davis, *Structure* **2**, 755 (1994)]; CD58, 1ccz [S. Ikemizu *et al.*, *Proc. Natl. Acad. Sci. U.S.A.* **96**, 4289 (1999)]; CD2d1/CD58d1 complex, 1qa9 (*27*); and CH3, 1fc1 [J. Deisenhofer, *Biochemistry* **20**, 2361 (1981)].
21. K. C. Garcia *et al.*, *Science* **274**, 209 (1996).
22. R. Huber, J. Deisenhofer, P. M. Colman, M. Matsushima, W. Palm, *Nature* **264**, 415 (1976).
23. The van der Waals contacts, hydrogen bond interactions, and buried molecular surfaces were calculated as in (*27*). Other subunit interfaces that occur in the CTLA-4 crystal lattice are significantly less extensive, with buried surface areas of 807 Å^2 or less.
24. A V_H domain (1gc1) was first superimposed on one CTLA-4 molecule. The same transformation was then applied to the other CTLA-4 domain to superimpose on the corresponding V_L domain. The additional rotation and translation required to optimize the CTLA-4–V_L superposition describes the domain shift. This procedure is similar to that described in (*27*).
25. S. Ikemizu *et al.*, *Immunity* **12**, 51 (2000).
26. R. J. Peach *et al.*, *J. Exp. Med.* **180**, 20498 (1994).
27. J. H. Wang *et al.*, *Cell* **97**, 791 (1999).
28. L. Shapiro, J. P. Doyle, P. Hensley, D. R. Colman, W. A. Hendrickson, *Neuron* **17**, 435 (1996).
29. M. L. Dustin, A. S. Shaw, *Science* **283**, 649 (1999).
30. A. Grakoui *et al.*, *Science* **285**, 221 (1999).
31. K.-M. Lee *et al.*, *Science* **282**, 2263 (1998).
32. C. Olsson, K. Riebeck, M. Dohlsten, E. Michaëlsson, *J. Biol. Chem.* **274**, 14400 (1999).
33. L. E. M. Marengère *et al.*, *Science* **272**, 1170 (1996).
34. Z. Otwinowski, W. Minor, *Methods Enzymol.* **276**, 307 (1997).
35. C. M. Weeks, R. Miller, *J. Appl. Crystallogr.* **32**, 120 (1999).
36. T. C. Terwilliger, J. Berendzen, *Acta Crystallogr.* **D55**, 849–861, (1999).
37. K. Cowtan, P. Main, *Acta Crystallogr.* **D54**, 487 (1998).
38. T. A. Jones, S. Cowan, J. Y. Zou, M. Kjeldgaard, *Acta Crystallogr.* **A47**, 110 (1991).
39. A. T. Brünger *et al.*, *Acta Crystallogr.* **D54**, 905 (1998).
40. R. A. Laskowski, M. W. MacArthur, D. S. Moss, J. M. Thornton, *J. Appl. Crystallogr.* **26**, 283 (1993).
41. S. V. Evans, *J. Mol. Graphics* **11**, 134 (1993).
42. J. D. Thompson, D. G. Higgins, T. J. Gibson, *Nucleic Acids Res.* **22**, 4673 (1994).
43. Single-letter abbreviations for the amino acid residues are as follows: A, Ala; C, Cys; D, Asp; E, Glu; F, Phe; G, Gly; H, His; I, Ile; K, Lys; L, Leu; M, Met; N, Asn; P, Pro; Q, Gln; R, Arg; S, Ser; T, Thr; V, Val; W, Trp; and Y, Tyr.
44. G. J. Barton, *Methods Enzymol.* **183**, 403 (1990).
45. A. Nicholls, K. A. Sharp, B. Honig, *Proteins Struct. Funct. Genet.* **11**, 281 (1991).

46. Supported by NIH research grants AI07289, CA09173, and AI42970 and Cancer Center support (CORE) grant CA34196. Beamline X9B is supported by RR01633. Beamline X12C is supported by DE-AC02-98CH10886 and RR12408. Coordinates have been deposited at the RCSB structural database (1dqt). We thank J. Bajorath, P. Linsley, and P. Concannon for insightful comments; S. Sheriff, R. Stanfield, C. Weeks, and D. Jeruzalmi for programs, discussions, and advice; and Z. Dauter and R. Sweet for help with data collection. We especially thank J. Bonnano for computational expertise.

18 June 2000; accepted 11 September 2000

BMS 002569169

EXHIBIT 14

THE JOURNAL OF BIOLOGICAL CHEMISTRY
Vol. 271, No. 43, Issue of October 25, pp. 26762–26771, 1996
Printed in U.S.A.
© 1996 by The American Society for Biochemistry and Molecular Biology, Inc.

Covalent Dimerization of CD28/CTLA-4 and Oligomerization of CD80/CD86 Regulate T Cell Costimulatory Interactions*

(Received for publication, April 23, 1996, and in revised form, July 23, 1996)

JoAnne L. Greene, Gina M. Leytze, John Emswiler, Robert Peach, Jürgen Bajorath, Wesley Cosand, and Peter S. Linsley‡

From the Bristol-Myers Squibb Pharmaceutical Research Institute, Seattle, Washington 98121

T lymphocyte receptors CD28 and CTLA-4 bind costimulatory molecules CD80 (B7-1) and CD86 (B7-2) on antigen-presenting cells and regulate T cell activation. While distinct functional roles have been ascribed to each of these molecules, little is known about how they interact. To better characterize these interactions, we have used surface plasmon resonance to perform equilibrium and kinetic binding analyses of extracellular fragments of CD28/CTLA-4/CD80/CD86. We show that CTLA-4 and CD28 binding are both characterized by rapid kinetic on-rates and rapid dissociation rates. Native disulfide-linked homodimers of CD28 and CTLA-4 bound with two kinetically distinct binding sites, one of high avidity and slow dissociation and one of low avidity and more rapid dissociation. Monomeric CTLA-4 bound only with low affinity and rapid dissociation. Therefore, covalent dimerization of CTLA-4 is required for its high avidity binding. Oligomerization of CD80/CD86 is also required for high avidity CTLA-4 binding since CTLA-4 bound with low avidity to monomeric CD86. This contrasts with the ability of CD80/CD86 on antigen-presenting cells to bind CTLA4Ig with high avidity and predicts their organization as oligomers or clusters that permit multivalent binding. Thus, covalent receptor dimerization and ligand oligomerization are two key features of the CD28/CTLA-4/CD80/CD86 receptor system that control ligand binding and may regulate signal transduction by controlling the duration of receptor occupancy.

Intercellular interactions between T lymphocytes and antigen-presenting cells (APC)[1] generate T cell costimulatory signals that regulate T cell responses to antigen in an antigen-nonspecific manner (1, 2). A key costimulatory signal(s) is provided by engagement of T cell receptors CD28 and CTLA-4 with B7 molecules on APC (3–6). CD28 and CTLA-4 are both members of the immunoglobulin superfamily, having single variable-like domains in their extracellular regions (7). These molecules share sequence identity, most notably clustered in their CDR3-like regions (8). Both CD28 and CTLA-4 bind the same natural ligands, B7 family members CD80 (B7-1) and CD86 (B7-2 or B7-0) (7, 9–12). CTLA-4 and CD28 are disulfide-linked homodimers, with each monomeric subunit containing a binding site for CD80/CD86 molecules (13).

Despite the structural similarities and common binding partners of CD28/CTLA-4 receptors and CD80/CD86 ligands, different functional properties have been attributed to each of these molecules. Engagement of CD28 by monoclonal antibodies (mAbs) or B7 ligands greatly enhances T cell activation (3–6), whereas engagement of CTLA-4 by specific mAbs may suppress T cell proliferation (14–16). Additional evidence that CTLA-4 negatively regulates the immune system comes from studies of CTLA-4-deficient mice, which have a severe lethal lymphoproliferative phenotype (18, 19). Thus, CD28 and CTLA-4 apparently have different functions during an immune response (17). CD80 and CD86 have also been reported to have different functions, with CD86 preferentially stimulating the production of interleukin-4, but not interleukin-2 (20, 21).

The different biological properties of CD28 and CTLA-4 receptors and CD80 and CD86 ligands may emanate from differing binding properties or from different patterns of expression. Relatively little is known about how these molecules interact. Studies using recombinant soluble immunoglobulin fusion proteins have shown that CTLA-4 binds with higher avidity to CD80 and CD86 than does CD28 (9–12). Amino acid residues responsible for the increased binding activity of recombinant CTLA4Ig were localized to the CDR1 and extended CDR3-like regions of the Ig variable-like domain (8). CD80 and CD86 had similar equilibrium properties for binding to CTLA-4 and CD28, although different kinetic properties were noted for binding of these ligands to CTLA-4 (11).

Despite these studies, many fundamental properties of CD28/CTLA-4/CD80/CD86 interactions remain unknown. For instance, it is not known how the subunit structures of CD28 and CTLA-4 affect their binding properties. While these molecules have two binding sites per homodimer (13), previous studies have shown only single equilibrium constants for CD80/CD86 binding to CD28 and CTLA-4 (9–12). It is also unclear how previous binding determinations were affected by multivalent Ig fusion proteins. Moreover, very little information is available on the binding properties of CD28, as studies on this molecule have been hampered by its weak avidity.

It was therefore of interest to better characterize the binding interactions of CD28/CTLA-4/CD80/CD86. In this study, we have used surface plasmon resonance (SPR) to measure the precise equilibrium and kinetics of binding of defined fragments of CD28/CTLA-4 and CD80/CD86. SPR provides a sensitive means to measure, in real time, binding interactions between biological molecules without problems associated with other techniques (22). Binding of soluble proteins to immobilized ligands is measured by the accumulation of mass on the surface of a sensor chip. SPR can be used to directly measure equilibrium binding constants and also to estimate kinetic association (k_{on}) and dissociation (k_{off}) rate constants, which can then be used to calculate equilibrium binding constants.

* The costs of publication of this article were defrayed in part by the payment of page charges. This article must therefore be hereby marked "*advertisement*" in accordance with 18 U.S.C. Section 1734 solely to indicate this fact.

‡ To whom correspondence should be addressed: Bristol-Myers Squibb Pharmaceutical Research Inst., 3005 First Ave., Seattle, WA 98121. Tel.: 206-727-3675; Fax: 206-727-3501; E-mail: linsley@bms.com.

[1] The abbreviations used are: APC, antigen-presenting cell(s); mAb, monoclonal antibody; SPR, surface plasmon resonance; PAGE, polyacrylamide gel electrophoresis; RU, resonance unit(s).

The Journal of Biological Chemistry

Downloaded from www.jbc.org by on August 14, 2008

Case 1:06-cv-00500-SLR-MPT Document 274-3 Filed 09/02/2008 Page 17 of 44

The results of our analysis demonstrate previously unknown roles for CD28/CTLA-4 dimerization and CD80/CD86 oligomerization in regulating binding interactions between these molecules.

MATERIALS AND METHODS

Ig Fusion Proteins and Thrombin Fragments—Chimeric mAb L6 was obtained from Bristol-Myers Squibb Pharmaceutical Research Institute (Seattle, WA). Anti-CTLA-4 mAbs 10A8 and 11D4; anti-CD28 mAb 9.3; and Ig fusion constructs CTLA4Ig, CD28Ig, CD80Ig, and CD86Ig have also been described (11, 23). For preparation of recombinant forms of the extracellular domains of CD28 and CTLA-4, Ig fusion proteins were prepared that contained a synthetic thrombin cleavage site between the extracellular domains and the Fc regions. Polymerase chain reaction products encoding the extracellular domains of CD28 and CTLA4Ig (9, 10) were digested with *Hin*dIII and *Bcl*I restriction enzymes and ligated into a *Hin*dIII/*Bam*HI-digested Ig expression vector encoding a synthetic thrombin cleavage site 5′ to the hinge region of a human IgG1 Fc domain (24). The resulting thrombin cleavage site-containing fusion constructs were designated CTLA4tIg and CD28tIg, respectively. Ig fusion proteins were produced by transiently transfected COS cells or stably transfected Chinese hamster ovary cells and purified by affinity chromatography on immobilized protein A-Sepharose (Repligen, Cambridge, MA) (9). The purified recombinant Ig fusion proteins had properties indistinguishable from those of CD28Ig and CTLA4Ig (9, 10). For preparation of the dimeric extracellular domains of these proteins, the fusion proteins were digested with purified bovine thrombin (Armour Pharmaceutical Corp., Kankakee, IL) at a final concentration of 5 units/mg of protein at 37 °C for 40–60 min. The cleaved extracellular domains were purified from other digestion products (13) and are designated CTLA-4tp, and CD28tp, respectively. The predicted amino acid sequence of CTLA-4tp contains residues 1–127 (numbered as in Ref. 8) of CTLA-4 fused to a thrombin-cleaved linker peptide (-PDSD-pgggggrlv-, where lower-case letters denote linker sequences). CD28tp contains residues 1–134 of CD28 fused to a thrombin-cleaved linker (-PSKPdpgggggrlv-). Concentrations of CTLA-4tp and CD28tp were estimated using extinction coefficients of 2.2 and 1.7 ml/mg, respectively; these were experimentally determined by measuring the A_{280} of solutions whose protein concentration was determined by amino acid analysis. Molecular weights were calculated using monomeric molecular weights. CTLA-4tp and CD28tp preparations were analyzed by gel permeation chromatography to ensure their homogeneity; all preparations used in this paper contained <2% of high molecular weight aggregate(s). Some preparations of CTLA-4tp contained excessive amounts of high molecular weight aggregate(s), so these were subjected to further purification by size fractionation of the main dimeric species by gel permeation chromatography. CTLA-4tp and the previously described thrombin fragment, CTLA-4t (13), were used interchangeably in these experiments since they had identical binding properties. Preparation of $CTLA4X_{C120S}$ (a monomeric form of CTLA-4 with a cysteine to serine mutation in the position of the intercham disulfide of CTLA-4) and CD86t (a monomeric form of the extracellular domain of CD86) was described previously (13).

Analytical Techniques—Two columns were used for gel permeation chromatography. In most experiments, protein fragments were analyzed on a TSK-GEL G3000 SWXL column (Tosohaas, Montgomeryville, PA) equilibrated in phosphate-buffered saline containing 0.02% NaN_3 at a flow rate of 1 ml/min. In some experiments, protein fragments were analyzed on a Waters SW 991 column equilibrated with phosphate-buffered saline containing 10 mM Tris-HCl, pH 7.4, and 0.01% NaN_3 at a flow rate of 0.35 ml/min. Equivalent results were obtained with both columns. SDS-PAGE was performed on Tris/glycine gels (Nuvex, San Diego, CA). Gels were stained with Coomassie Blue, and images of wet gels were obtained by digital scanning.

BIAcore Analysis—All experiments were run in BIAcore™ or BIAcore 2000 biosensors (Pharmacia Biotech AB, Uppsala) at 25 °C. Ligands were immobilized on research-grade CM5 sensor chips (Pharmacia) using standard *N*-ethyl-*N*′-(dimethylaminopropyl)carbodiimid/*N*-hydroxysuccinimide coupling (22, 25). Proteins were diluted in 10 mM sodium formate buffer, pH 4.0, and incubated with activated sensor chips for times varied to optimize the degree of derivatization needed for particular experiments. After coupling, excess *N*-hydroxysuccinimide groups were inactivated with ethanolamine HCl (22, 25). Control chips were either derivatized with chimeric mAb L6 or mock-derivatized by activating and then inactivating with ethanolamine without the addition of protein. Identical results were obtained with both types of control chips. After binding of CTLA-4 or CD28, CD80Ig- and CD86Ig-coated chips were regenerated with a 60-s pulse of 50 mM sodium citrate and 500 mM NaCl, pH 4.0 or 5.0, respectively. Control experiments showed that CD80Ig- and CD86Ig-derivatized surfaces were able to withstand >30 rounds of regeneration without losing binding capacity. Before use, all sensor surfaces were subjected to several rounds of analyte binding, followed by regeneration to ensure a stable level of derivatization. Mobile phase buffer for immobilization was phosphate-buffered saline, pH 7.4, containing 0.005% P20 surfactant (Pharmacia). For binding assays, 200 μg/ml bovine serum albumin was added to the mobile phase buffer.

BIAcore Data Analysis—Sensorgram base lines were normalized to zero response units (RU) prior to analysis. Samples were run over mock-derivatized flow cells to determine background RU values due to bulk refractive index differences between solutions. Equilibrium dissociation constants (K_d) were calculated from plots of R_{eq} *versus* C, where R_{eq} is the steady-state response minus the response on a mock-derivatized chip, and C is the molar concentration of analyte. Binding curves were analyzed using commercial nonlinear curve-fitting software (Prism, GraphPAD Software, San Diego, CA). Experimental data were first fit to a model for a single ligand binding to a single receptor one-site model, i.e. a simple Langmuir system, $A + B \leftrightarrow AB$), and equilibrium dissociation constants ($K_d = [A]\cdot[B]/[AB]$) were calculated from the equation $R = R_{max}\cdot C/(K_d + C)$. Subsequently, data were fit to the simplest two-site model of ligand binding (i.e. to a receptor having two non-interacting independent binding sites), as described by the equation $R = R_{max1}\cdot C/(K_{d1} + C) + R_{max2}\cdot C/(K_{d2} + C)$. The goodness-of-fits of these two models were analyzed visually by comparison with the experimental data and statistically by an F test of the sums-of-squares. The simpler one-site model was chosen as the best fit unless the two-site model fit significantly better ($p < 0.1$).

Association and dissociation analyses were performed using BIAevaluation 2.1 software (Pharmacia). Association rate constants (k_{on}) were calculated in two ways, assuming both homogeneous single-site interactions and parallel two-site interactions. For single-site interactions, k_{on} values were calculated according to the equation $R_t = R_{eq}(1 - \exp^{-k_{off}\cdot(t_t - t_0)})$, where R_t is the response at a given time, t; R_{eq} is the steady-state response; t_0 is the time at the start of the injection; and $k_s = dR/dt = k_{on}C + k_{off}$ where C is the concentration of analyte, calculated in terms of monomeric binding sites. For two-site interactions, k_{on} values were calculated according to the equation $R_t = R_{eq1}(1 - \exp^{-k_{on1}(t_t - t_0)}) + R_{eq2}(1 - \exp^{-k_{on2}(t_t - t_0)})$. For each model, the values of k_{on} were determined from the calculated slopes (to ~70% maximal association) of plots of k_s *versus* C.

Dissociation data were analyzed according to one-site ($AB = A + B$) or two-site ($AiBj = Ai + Bj$) models, and rate constants (k_{off}) were calculated from best fit curves. The one-binding site model was used except when the residuals were greater than machine background (2–10 RU, according to machine), in which case the two-binding site model was employed. Half-times of receptor occupancy were calculated using the relationship $t_{1/2} = 0.693/k_{off}$.

RESULTS

Preparation of Defined Fragments of the Extracellular Domains of CTLA-4 and CD28—Accurate measurement of CD28/CTLA-4/CD80/CD86 interactions required preparation of fragments of these molecules with defined valencies. In a previous study (13), we described the preparation and characterization of dimeric and monomeric forms of the extracellular domain of CTLA-4 and a monomeric form of CD86 (CD86t). Preparation of these fragments was accomplished by thrombin cleavage of (presumed) dimeric CTLA4Ig and CD86Ig at a nonclassical cleavage site in the Fc hinge region of these molecules (13). While these fragments were useful, they were difficult to produce in sufficient yield because of inefficient thrombin cleavage. To improve the yield of these extracellular fragments, we re-engineered the CTLA4Ig and CD28Ig fusion proteins such that a synthetic thrombin recognition site was introduced between the extracellular domains of CTLA-4 or CD28 and the Fc domain (see "Materials and Methods"). The resulting CTLA4tIg and CD28tIg fusion proteins had binding properties indistinguishable from those of our original fusion proteins, but

The Journal of Biological Chemistry

Downloaded from www.jbc.org by on August 14, 2008

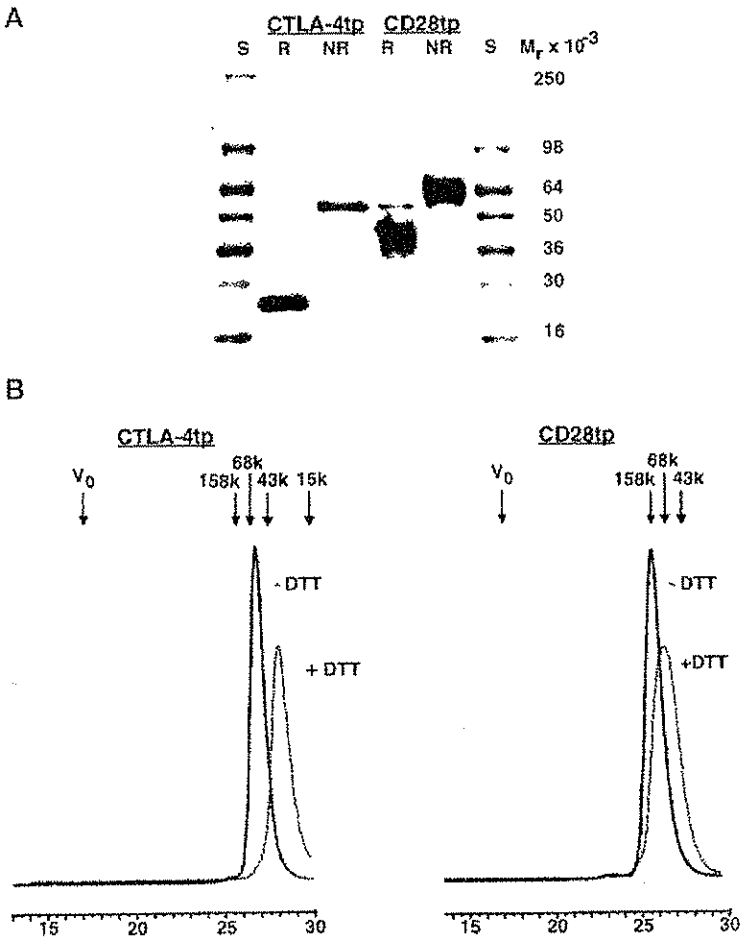

FIG. 1. **Characterization of thrombin-cleaved Ig fusion proteins.** Purified thrombin-cleaved recombinant fragments of CTLA-4 and CD28 were analyzed by SDS-PAGE (*A*) or by gel permeation chromatography (*B*). *A*, samples (~1 μg) of the indicated proteins were analyzed by SDS-PAGE on a 4–20% acrylamide gel under reducing (*R*; plus 2-mercaptoethanol) and nonreducing (*NR*) conditions. Positions of standard proteins (*S*) are indicated. The minor band migrating at M_r ~ 55,000 was present in medium from nontransfected cells and represents a copurifying contaminant, probably bovine Ig. *B*, samples (~3 μg) of the indicated proteins were analyzed on a Waters SW 991 column. Prior to analysis, samples were treated without or with dithiothreitol (*DTT*; 10 mM) for 30 min at 23 °C. *Arrows* indicate elution positions of standards. V_0, void volume.

could be more efficiently cleaved by thrombin.[2] From these new fusion proteins, we prepared fragments of the extracellular domains of CTLA-4 and CD28, termed CTLA-4tp and CD28tp, as described under "Materials and Methods." CTLA-4tp and CD28tp retained binding activities essentially equivalent to those of the corresponding Ig fusion proteins as indicated by monitoring binding activities during purification. These proteins also retained the ability to bind anti-CTLA-4 and anti-CD28 mAbs (data not shown), indicating that they had native conformations. These fragments were characterized by SDS-PAGE and gel permeation chromatography in the experiments shown in Fig. 1. Under nonreducing conditions, CTLA-4tp migrated at M_r = 55,000–60,000 when analyzed by either technique; upon reduction, it migrated at M_r = 25,000–35,000. CTLA-4tp therefore was a disulfide-linked dimer. CD28tp migrated at M_r ~ 65,000 and 45,000 by SDS-PAGE under nonreducing and reducing conditions, respectively. In contrast, during gel permeation chromatography, CD28tp eluted at M_r ~ 180,000 and 65,000 under nonreducing and reducing conditions. The elution volume of CD28tp during gel permeation chromatography was therefore greater than would be predicted by SDS-PAGE. This difference may be due to the predicted extensive glycosylation of CD28tp, or it may indicate that CD28tp in solution existed as a tetramer. At present, we cannot distinguish between these possibilities, but to simplify subsequent calculations, we have assumed that CD28tp was dimeric. Neither CTLA-4tp nor CD28tp preparations used for binding measurements had significant amounts of aggregated material present. Monomeric CD86 (CD86t) and monomeric CTLA-4 ($CTLA4X_{C120S}$, prepared by site-directed mutagenesis of the cysteine residue that mediates the intrachain disulfide bond) were prepared as described (13).

Equilibrium Binding Analysis of CTLA-4 and CD28—We initially used SPR to measure equilibrium binding of CTLA4Ig, CD28Ig, CD80Ig, and CD86Ig fusion proteins using the methods of van der Merwe *et al.* (26). This procedure was devised for determining the equilibrium binding properties of lymphocyte surface receptors with low binding avidity and rapid kinetic off-rates. CD80Ig and CD86Ig were coupled to sensor chips, and solutions of CTLA4Ig and/or CD28Ig were added in the mobile phase. The levels of derivatization of the chips were adjusted to ensure that steady-state (equilibrium) binding was achieved at low concentrations of analyte. Similar results were obtained at different levels of chip derivatization. Equilibrium binding of CTLA4Ig at a given concentration was determined by comparing the steady-state RU on CD80Ig- or CD86Ig-coated chips with the value obtained on control chimeric mAb L6 or mock-derivatized chips. From this comparison, levels of specific binding were determined at different concentrations. Equilibrium dissociation constants (K_d) could then be determined from binding isotherms by curve fitting. Similar results were obtained whether we measured binding of CTLA4Ig to immobilized CD80Ig or CD86Ig or binding of CD80Ig or

[2] J. L. Greene, G. M. Leytze, J. Emswiler, R. Peach, J. Bajorath, W. Cosand, and P. S. Linsley, unpublished data.

The Journal of Biological Chemistry

Downloaded from www.jbc.org by on August 14, 2008

TABLE I
Summary of equilibrium constants

Equilibrium binding constants were measured directly in experiments performed as described for Figs. 2–4. Shown are means ± S.D. of equilibrium dissociation constants (K_d) from two to five independent experiments. K_d values were obtained by curve fitting experimental data to one- and two-site models as described under "Materials and Methods." p values for the statistical improvement in choosing a particular two-site model over a one-site model are given. When a two-site model was chosen ($p < 0.1$), both high avidity (K_{d1}) and low avidity (K_{d2}) dissociation constants were calculated. The proportion of total binding attributable to the high avidity site is indicated as percent K_{d1}. Calculated K_d values were derived from experimentally determined kinetic rate constants (see Table II) using the equation $K_d = k_{off}/k_{on}$. Where two k_{off} values were determined (see Table II), two values for K_d are given; the calculated percent K_{d1} was determined from the percentage of total binding attributable to the more slowly dissociating (higher avidity binding) component (see Table II).

Immobilized protein	Analyte	p	Observed			Calculated		
			K_{d1}	K_{d2}	K_{d1}	K_{d1}	K_{d2}	K_{d1}
			nM	*nM*	%	*nM*	*nM*	%
CD80Ig	$CTLA4X_{C120S}$	0.786	211 ± 34	NA[a]	NA	208	NA	NA
CD80Ig	CTLA-4tp	<0.00001	1 ± 1	150 ± 91	78 ± 2	4	100	86 ± 3
CD80Ig	CD28tp	0.091	2500 ± 2100	41,000 ± 19,000	15 ± 12	4900	90,000	31 ± 8
CD86Ig	$CTLA4X_{C120S}$	1.0	2200 ± 970	NA	NA	2000	NA	NA
CD86Ig	CTLA-4tp	<0.001	4 ± 3	510 ± 230	58 ± 10	4	70	62 ± 11
CD86Ig	CD28tp	<0.001	2300 ± 1500	37,000 ± 13,000	23 ± 6	5600	34,000	38 ± 4

[a] NA, not applicable (i.e. a one-binding site model fit the data adequately).

CD86Ig to immobilized CTLA4Ig (data not shown). Thus, the equilibrium constants obtained were not greatly influenced by which protein was immobilized, indicating that protein immobilization to the sensor chip did not significantly affect binding activity (data not shown; also see results presented in Tables I and II, below). For most subsequent experiments, we chose to measure binding of CTLA-4 and CD28 fragments with defined valency to immobilized CD80Ig and/or CD86Ig.

We measured equilibrium binding of monomeric CTLA-4 ($CTLA4X_{C120S}$), dimeric CTLA-4 (CTLA-4tp), and dimeric CD28 (CD28tp). Representative experiments demonstrating equilibrium binding of these fragments to CD80Ig are shown in Figs. 2–4, respectively. A summary of all equilibrium binding experiments is given in Table I. The binding isotherm for $CTLA4X_{C120S}$ was adequately fit by a one-site model as judged by visual examination of the fitted curves (Fig. 2); the more complicated two-site model also did not statistically improve the goodness-of-fit significantly ($p > 0.1$). Therefore, single equilibrium dissociation constants (K_d) were chosen for binding of $CTLA4X_{C120S}$ to CD80Ig and CD86Ig (Table I).

In contrast, the binding isotherm for dimeric CTLA-4tp (Fig. 3) showed more complicated equilibria. Binding saturation was achieved over a wider concentration range than for $CTLA4X_{C120S}$, and although binding of CTLA-4tp was measurable at much lower analyte concentrations than for $CTLA4X_{C120S}$, binding equilibrium for CTLA-4tp was not achieved at lower concentrations, even over relatively long periods of time (compare Figs. 2 and 3). For binding of CTLA-4tp, the two-site model clearly increased the goodness-of-fit, both visually (Fig. 3) and statistically ($p < 0.1$). Both high and low avidity equilibrium dissociation constants (K_d) were estimated for CTLA-4tp (Table I), with the high avidity sites accounting for ~80 and ~60% of the total binding to CD80Ig and CD86Ig, respectively. The low avidity K_d values of CTLA-4tp binding to CD80Ig or CD86Ig were similar to the K_d values for $CTLA4X_{C120S}$ (Table I). The high avidity K_{d1} values for CTLA-4tp binding to CD80Ig and CD86Ig were ~200- and ~500-fold less, respectively (indicating stronger binding), than the K_d values for $CTLA4X_{C120S}$. Thus, CTLA-4tp bound more strongly (avidly) than did $CTLA4X_{C120S}$.

The binding isotherm for dimeric CD28tp also showed complicated equilibria (Fig. 4). Binding of CD28tp was measurable only at very high analyte concentrations. This dictated that large quantities of purified CD28tp were required for binding measurements, and with the amounts of material available, it was not possible to achieve saturation binding. Despite the limited concentration range of analyte used, the CD28tp binding isotherm was better fit by a two-site model, although visually the difference between one- and two-site models was less compelling than with CTLA-4tp (compare Figs. 3 and 4). The two-site model also gave statistically better fits of the data ($p < 0.1$). That support for the two-site model was weaker for CD28tp than for CTLA-4tp may reflect experimental limitations of the weak binding interactions of CD28tp or the limited concentration range of analyte used; alternatively, it may indicate that CD28tp binding is better explained by even more complicated models. However, since the kinetic binding analysis presented below also supports a two-site rather than a one-site model for CD28tp binding, we have chosen to use the simple two-site model to estimate both high and low avidity equilibrium dissociation constants (K_d) for CD28tp (Table I). The percentage of high avidity binding sites (K_{d1}) for CD28tp was less than for CTLA-4tp (~15 and ~23% for binding to CD80Ig and CD86Ig, respectively). The reason for this is presently unknown.

Kinetic Binding Analysis of CTLA-4 and CD28—We also determined binding kinetics for CD28/CTLA-4/CD80/CD86 interactions since these are likely to be critical determinants of the biological effects of dynamic receptor/ligand interactions. We analyzed the kinetics of CTLA-4 and CD28 binding to CD80Ig- and CD86Ig-coated sensor chips. Representative determinations of the association and dissociation kinetics for $CTLA4X_{C120S}$, CTLA-4tp, and CD28tp binding to CD80Ig are shown in Figs. 5 and 6, respectively. A summary of the association (k_{on}) and dissociation (k_{off}) rate constants is presented in Table II.

For determination of association rate constants, sensor chips were derivatized with relatively low amounts of CD80Ig or CD86Ig so that association was not limited by mass transport of analyte to the chip surface. The binding responses over time were determined at several concentrations of analyte for $CTLA4X_{C120S}$, CTLA-4tp, and CD28tp. Curves were fitted to one- and two-site models, and the slopes ($dR/dt = k_s$) were calculated as described under "Materials and Methods."

When k_s values were plotted *versus* analyte concentration, linear relationships were reliably and reproducibly obtained when k_s values were obtained with one-site models. Values of k_{on} could then be calculated from the slopes of plots of k_s *versus* analyte concentration. When association data were analyzed using two-site models, less reliable k_{on} values were obtained for all combinations. In some experiments, it was not possible to calculate two meaningful k_{on} values. In other experiments, when two k_s values could be calculated, the difference between the resulting k_{on} values was always relatively small (less than

THE JOURNAL OF BIOLOGICAL CHEMISTRY VOL. 272 • NO. 42 • OCTOBER 17, 1997

The Journal of Biological Chemistry

Downloaded from www.jbc.org by on August 14, 2008

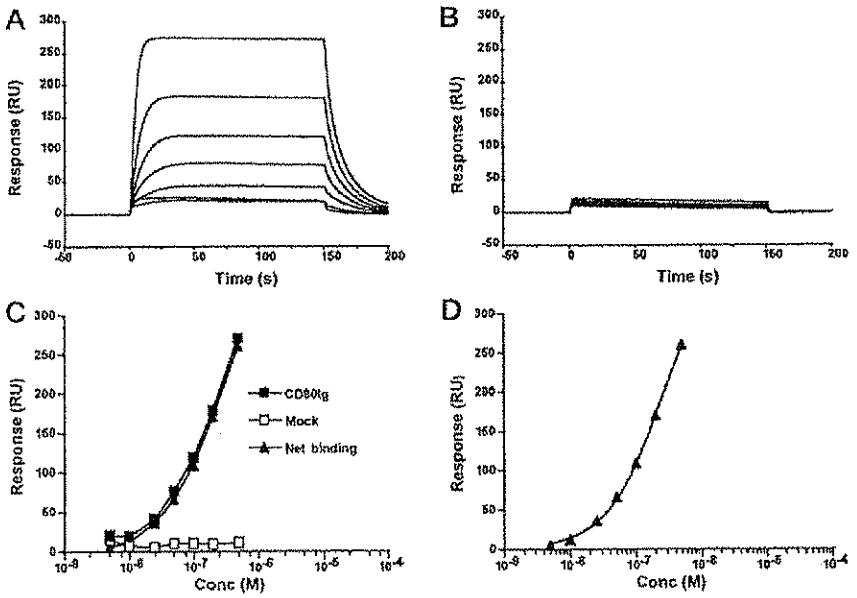

FIG. 2. **Equilibrium binding of monomeric CTLA-4.** *A* and *B*, solutions of increasing concentrations of $CTLA4X_{C120S}$ (5, 10, 25, 50, 100, 200, and 500 nM) were run over a CD80Ig-derivatized (4390 RU) (*A*) or a mock-derivatized sensor chip (*B*), respectively, at a flow rate of 10 μl/min. *C*, presented are binding isotherms showing the RU measured on the CD80Ig-derivatized chip as a function of $CTLA4X_{C120S}$ concentration (*closed squares*), the RU measured on the mock-derivatized chip (*open squares*), and net binding (RU measured on the CD80Ig-derivatized chip minus RU measured on the mock-derivatized chip) (*closed triangles*). *D*, shown is the nonlinear curve-fitting analysis of net binding data from *C* using the one-site (*solid line*) and two-site (*dashed line*) binding equations. These coincide in this figure but not in Figs. 3 and 4. Data shown are representative of five independent experiments.

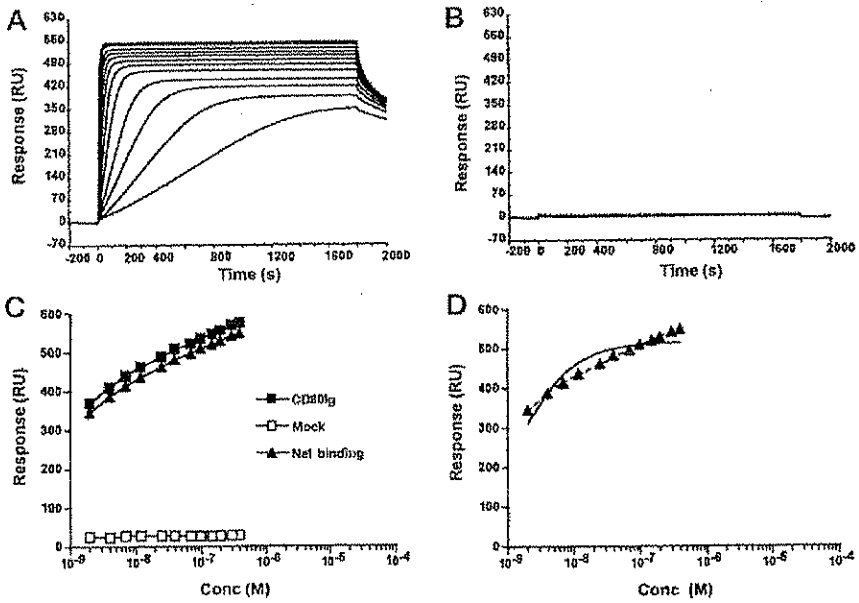

FIG. 3. **Equilibrium binding of dimeric CTLA-4.** *A* and *B*, solutions of increasing concentrations of CTLA-4Ig (2, 4, 7, 12, 25, 40, 70, 100, 150, 200, 300, and 400 nM) were run over a CD80Ig-derivatized (5580 RU) (*A*) or a mock-derivatized sensor chip (*B*), respectively, at a flow rate of 5 μl/min. *C* and *D*, shown is the analysis of binding data, as described in the legend to Fig. 2. Data shown are representative of five independent experiments.

~10-fold). Finally, in no case did use of the more complex two-site model improve the linear relationship (as judged by correlation coefficient (r) and the standard error of measurement) between the k_s values and concentration. For these reasons, we therefore concluded that use of two-site models of association was not justified. We determined a single association rate constant (k_{on}) for each combination of proteins (Table II). Monomeric CTLA-4 bound with k_{on} values within ~2–6-fold those for dimeric CTLA-4 (for CD80Ig and CD86Ig, respectively). The similarity in these k_{on} values argues that the native conformation of monomeric CTLA-4 was maintained. The rapid k_{on} values determined for CTLA-4 were near the limits of instrument detection.

The apparent dissociation rate constants (k_{off}) can be influenced by the rebinding of dissociated analyte. For these determinations, therefore, it was desirable to minimize rebinding by

Downloaded from www.jbc.org by on August 14, 2008

The Journal of Biological Chemistry

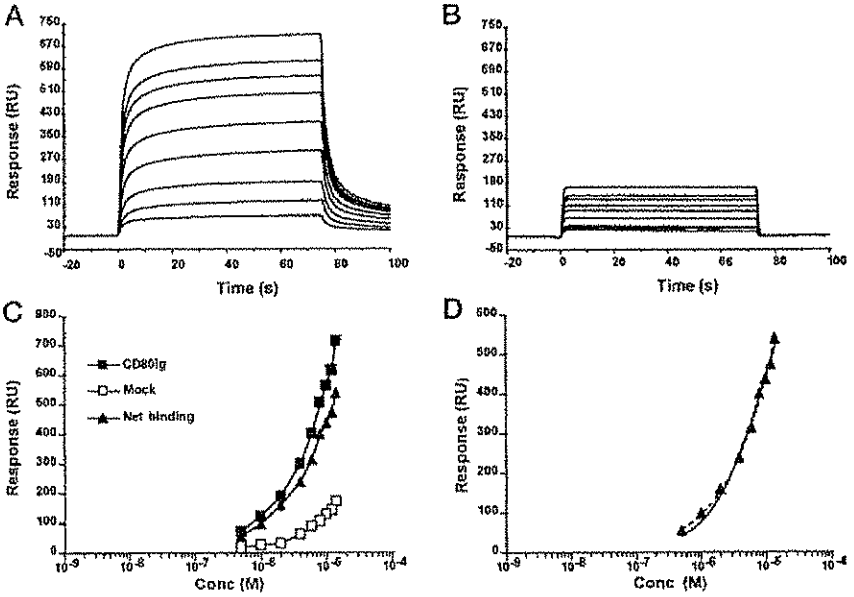

FIG. 4. **Equilibrium binding of dimeric CD28.** *A* and *B*, solutions of increasing concentrations of CD28tp (500, 1000, 2000, 4000, 6000, 8000, 10,000, 12,000, and 14,000 nM) were run over a CD80Ig-derivatized (13,400 RU) (*A*) or a mock-derivatized sensor chip (*B*), respectively, at a flow rate of 20 μl/min. *C* and *D*, shown is the analysis of binding data, as described in the legend to Fig. 2. Data shown are representative of two independent experiments.

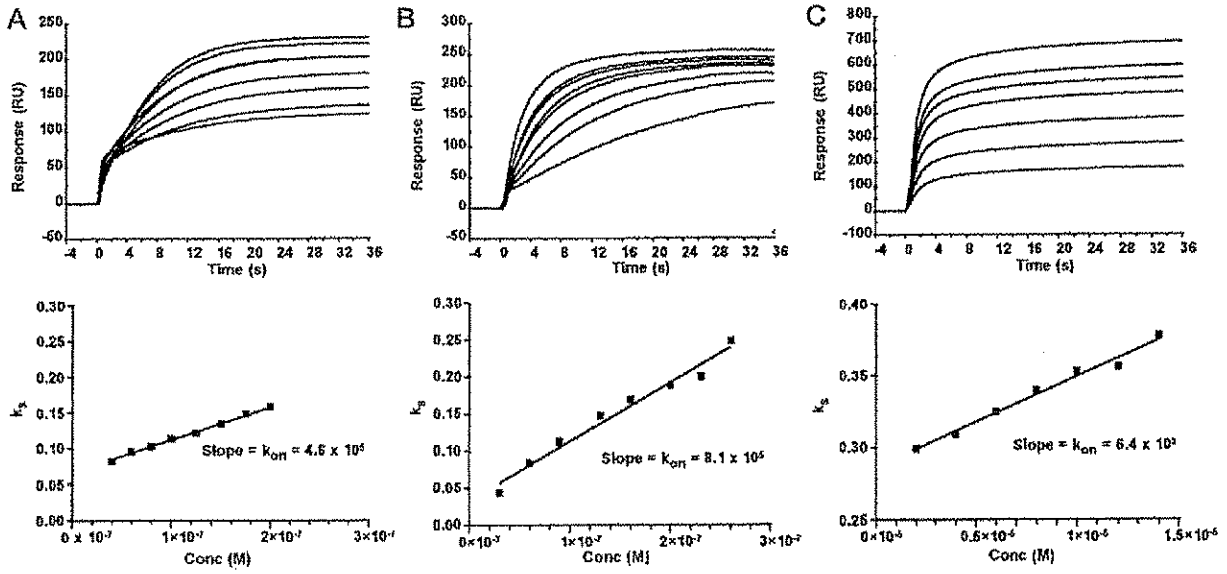

FIG. 5. **Association kinetics of monomeric CTLA4, dimeric CTLA4, and dimeric CD28 binding to immobilized CD80Ig.** *A*, association kinetics of monomeric CTLA-4 binding. Solutions of increasing concentrations of CTLA4X$_{G226S}$ (40, 60, 80, 100, 125, 150, 175, and 200 nM) were run over a sensor chip containing 6250 RU of immobilized CD80Ig at a flow rate of 40 μl/min. *B*, association kinetics of dimeric CTLA-4 binding. Solutions of increasing concentrations of CTLA-4tp (30, 60, 90, 130, 160, 200, 230, and 260 nM) were run over a sensor chip containing 3860 RU of immobilized CD80Ig at a flow rate of 40 μl/min. *C*, association kinetics of dimeric CD28 binding. Solutions of increasing concentrations of CD28tp (500, 1000, 2000, 4000, 6000, 8000, 10,000, 12,000, and 14,000 nM) were run over a sensor chip containing 13,400 RU of immobilized CD80Ig at a flow rate of 20 μl/min. The *upper panels* show *y*-transformed sensorgrams. The *lower panels* show plots of k_s *versus* concentration used to determine the association constants as described under "Materials and Methods."

derivatizing sensor chips with moderately low levels of CD80Ig or CD86Ig and by maximizing analyte concentrations. Dissociation of monomeric and dimeric CTLA-4 and dimeric CD28 was measured from CD80Ig-derivatized (Fig. 6) or CD86Ig-derivatized (data not shown) sensor chips. Dissociation curves were fit with one- and two-binding site models (Fig. 6). Dissociation of monomeric CTLA-4 from CD80Ig (Fig. 6, *A* and *B*) and CD86Ig (data not shown) was approximated by a one-binding site model such that the residuals between the observed and calculated curves were within experimental variation of BIAcore measurements. Analysis of these dissociation curves gave very rapid k_{off} values (Table II), corresponding to half-times of receptor occupancy of ~8 and ~2 s for CD80Ig and CD86Ig, respectively. The k_{off} values calculated in this way were in good agreement with those estimated from the *y* intercept of the k_s *versus* concentration plots used to calculate k_{on} values (Fig. 5). From

Downloaded from www.jbc.org by on August 14, 2008

TABLE II
Summary of apparent kinetic constants

Association and apparent dissociation rate constants were determined from experiments performed as described for Figs. 5 and 6, respectively. Shown are means ± S.D. of association (k_{on}) and dissociation (k_{off}) rate values from multiple experiments; association rate determinations were performed two to four times, and dissociation rate determinations, four to eight times. Where a two-site model best fitted the data, two values for k_{off} are given. Percent k_{off1} is the percentage of total binding accounted for by the slower dissociating (higher avidity binding) component. k_{off} values >400 × 10^{-3} s^{-1} are less reliable since they approach the limits of the BIAcore.

Immobilized protein	Analyte	k_{on} (×10^{-3})	k_{off1} (×10^{-3})	k_{off2} (×10^{-1})	k_{off1}
		M^{-1} s^{-1}	s^{-1}	s^{-1}	%
CD80Ig	CTLA4X$_{C120S}$	440 ± 40	91 ± 39	NA*	NA
CD80Ig	CTLA-4tp	890 ± 220	4 ± 2	90 ± 77	86 ± 3
CD80Ig	CD28tp	? ± 0.1	32 ± 34	580 ± 290	31 ± 8
CD86Ig	CTLA4X$_{C120S}$	210 ± 33	420 ± 130	NA	NA
CD86Ig	CTLA-4tp	1300 ± 96	5 ± 4	93 ± 65	62 ± 11
CD86Ig	CD28tp	24 ± 6	140 ± 84	830 ± 540	38 ± 4

* NA, not applicable (i.e. a one-binding site model fitted the data adequately).

the determined k_{off} and k_{on} values for monomeric CTLA-4 binding to CD80Ig and CD86Ig, equilibrium binding constants (K_d) could be calculated (Table I), which were in good agreement with the experimentally determined K_d values.

Analysis of dissociation curves for dimeric CTLA-4 and CD28 was more complicated (Fig. 6, *C* and *D*, and *E* and *F*, respectively). In neither case did a one-binding site model provide a satisfactory fit to the experimental data (Fig. 6, *C* and *E*); residuals were greater than the experimental variation, especially in the early phases of the dissociation curves. However, for both dimeric CTLA-4 and CD28, two-binding site models gave reasonable agreement between the observed and expected binding (Fig. 6, *D* and *F*), and residuals were within experimental variation. From these models, two k_{off} values could be calculated (Table II), consistent with the calculation of two equilibrium binding constants (K_d) (Table I). From the kinetic constants (k_{on} and k_{off}) (Table II), equilibrium binding constants (K_d) for CTLA-4tp and CD28tp binding could be calculated (Table I). These, for the most part, agreed well with the experimentally determined values, both in magnitude and in percentage of total binding.

High Avidity Binding of CTLA-4 Is Due to Rebinding—Binding of dimeric CTLA-4tp was characterized by two K_d values and two k_{off} values (Tables I and II). The more rapidly dissociating (weaker binding) k_{off2} values for dimeric CTLA-4tp approximated the k_{off} value for monomeric CTLA4X$_{C120S}$. Slower dissociation (stronger binding) could indicate rebinding of dimeric CTLA-4 during the dissociation measurements (11). To test this possibility, we measured k_{off} rates of CTLA-4tp from immobilized CD80Ig and CD86Ig in the presence of increasing amounts of soluble CD80Ig (Fig. 7). This would be expected to occupy free CTLA-4tp binding sites and prevent their rebinding to immobilized CD80Ig or CD86Ig.

As shown in Fig. 7, the rate of dissociation of CTLA-4tp increased in the presence of increasing concentrations of soluble CD80Ig. Very high concentrations (>1 mg/ml) of CD80Ig were required to produce these effects, probably because of the high density of CD80Ig and CD86Ig immobilized on the sensor chips. The apparent dissociation constants (k_{off}) values determined using a one-binding site model) for CTLA-4tp measured in the presence of increasing competitor increased asymptotically and approached values determined for monomeric CTLA4X$_{C120S}$ (Table II). The more slowly dissociating, higher avidity component of dimeric CTLA-4tp binding was therefore reduced when rebinding was blocked. In other experiments, we measured the effects of increasing concentrations of CD80Ig on the dissociation of CTLA4X$_{C120S}$ and CD28tp from immobilized CD80Ig and CD86Ig. In contrast to its effects on dissociation from CTLA-4tp, soluble CD80Ig did not greatly affect dissociation of these other molecules (<2-fold effect). Thus, rebinding of monomeric CTLA-4 or dimeric CD28 affected dissociation measurements less than it did for dimeric CTLA-4. It should be emphasized that the k_{off} values determined for these molecules in the absence of competition were near the limit of detection, so further increases may not have been possible to measure.

Effects of CD86 Valency on High Avidity Binding of CTLA-4—It was also important to determine the effects of valency of CD80/CD86 molecules on CTLA-4 binding avidity. We therefore measured binding of monomeric CD86 to immobilized CTLA4Ig. The use of immobilized CTLA4Ig was justified by other experiments (data not shown) showing that CTLA4Ig gave similar equilibrium and kinetic constants as CTLA-4tp for binding to immobilized CD80Ig and CD86Ig.

We compared equilibrium binding of monomeric CD86t and multimeric CD86Ig to immobilized CTLA4Ig (Table III). For monomeric CD86t, the data were adequately fit by a one-binding site model, yielding a low affinity K_d of ~1400 nM. This was similar to the K_d measured for binding of monomeric CTLA4X$_{C120S}$ to immobilized CD86Ig (~2200 nM) (Table II). The association constants (k_{on} and k_{off}) for CD86t binding to CTLA4Ig were estimated as 3.7 × 10^5 M^{-1} s^{-1} and 0.5 s^{-1}, which were also very similar to those measured for binding of monomeric CTLA4X$_{C120S}$ to immobilized CD86Ig (Table II). Thus, both equilibrium and kinetic binding constants for binding of monomeric CD86t to CTLA4Ig reflect low avidity binding. In contrast, binding of multimeric CD86Ig gave both high and low avidity equilibrium binding constants (K_d = 7 and 110 nM), which were very similar to those determined for dimeric CTLA-4tp binding to immobilized CD86Ig (Table II). Thus, valency of both CTLA-4 and CD86 affects binding avidity.

DISCUSSION

Previous studies showed that a covalent CTLA-4 homodimer contained two binding sites for CD80/CD86 molecules, but how these two sites affected binding avidity was not examined (13). Indeed, studies on the binding properties of CTLA-4 and CD28 identified only single avidity classes of binding sites on these molecules (7, 9–12). Here, using the more sensitive techniques of SPR, we show that dimeric CD28 and CTLA-4 show both high and low avidity binding, consistent with their 2:2 binding stoichiometries.

Binding of both monomeric and dimeric CTLA-4 to CD80Ig or CD86Ig was characterized by very rapid apparent k_{on} values (~0.2–1 × 10^6 M^{-1} s^{-1}). It should be mentioned that determination of kinetic on-rates to ligands immobilized in a polymer matrix can lead to underestimation of the true kinetic on-rates (28). The kinetic on-rates for CTLA-4 binding are comparable to those for other T lymphocyte receptor/ligand pairs, such as CD2/CD58 (≥4 × 10^5 M^{-1} s^{-1}) (26) and T cell receptor-major histocompatibility class I peptide complexes (2.1 × 10^5 M^{-1} s^{-1})

The Journal of Biological Chemistry

Downloaded from www.jbc.org by on August 14, 2008

Case 1:06-cv-00500-SLR-MPT Document 274-3 Filed 09/02/2008 Page 23 of 44

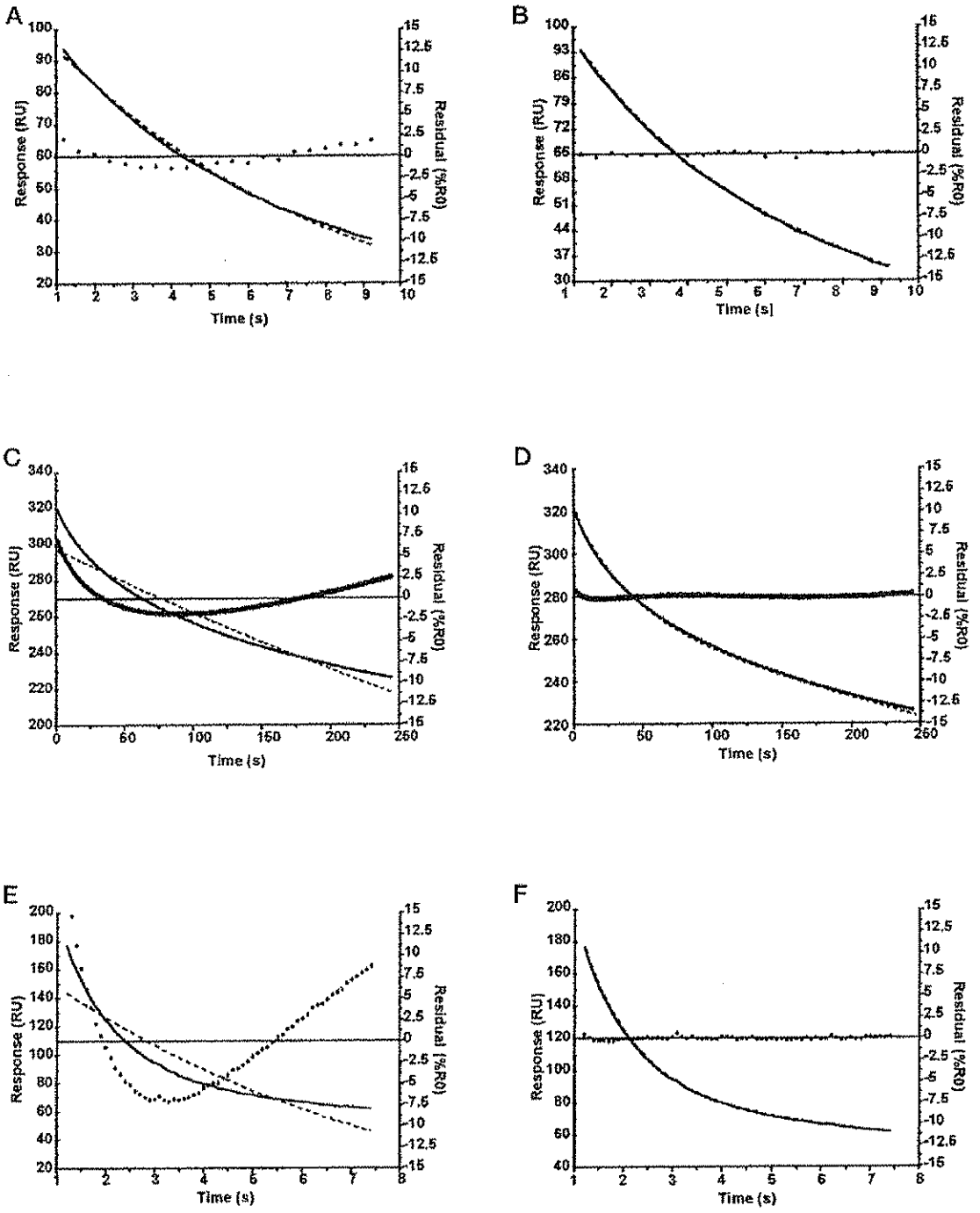

FIG. 6. **Apparent dissociation kinetics of monomeric CTLA-4, dimeric CTLA-4, and dimeric CD28 binding to immobilized CD80Ig.** Shown is a comparison of dissociation models for binding of monomeric CTLA-4 (*A* and *B*), dimeric CTLA-4 (*C* and *D*), and dimeric CD28 (*E* and *F*). Representative dissociation sensorgrams (*solid lines*) are compared with models (*dashed lines*) for one-site (*left panels*) and two-site (*right panels*) dissociation. Residuals between observed and expected values are expressed as a percentage of the analyte bound at the start of the dissociation (*dotted lines*). Dissociation of $CTLA4X_{C120S}$, CTLA-4tp, and CD28tp was measured at concentrations of 200, 200, and 10,000 nM, respectively; in each case, the amount of CD80Ig immobilized was 2290, 3640, and 4300 RU, respectively. Analyses were run at 60 μl/min, and the resulting sensorgrams were normalized to $t = 0$ at the start of the dissociation period.

(27). The k_{off} values for CD28 binding to CD80Ig and CD86Ig were also very rapid, but were similar to other lymphocyte surface receptors (26, 27). This would predict a short time of receptor occupancy for CD28/CD80/CD86 interactions (half-times of less than ~1 s for CD28/CD80/CD86, compared with less than or equal to ~6 s for CD2/CD58 (26) and ~17 s for T cell receptor/major histocompatibility complex class I peptide interactions (27)). These values for CD28 were calculated from

Downloaded from www.jbc.org by on August 14, 2008

Case 1:06-cv-00500-SLR-MPT Document 274-3 Filed 09/02/2008 Page 24 of 44

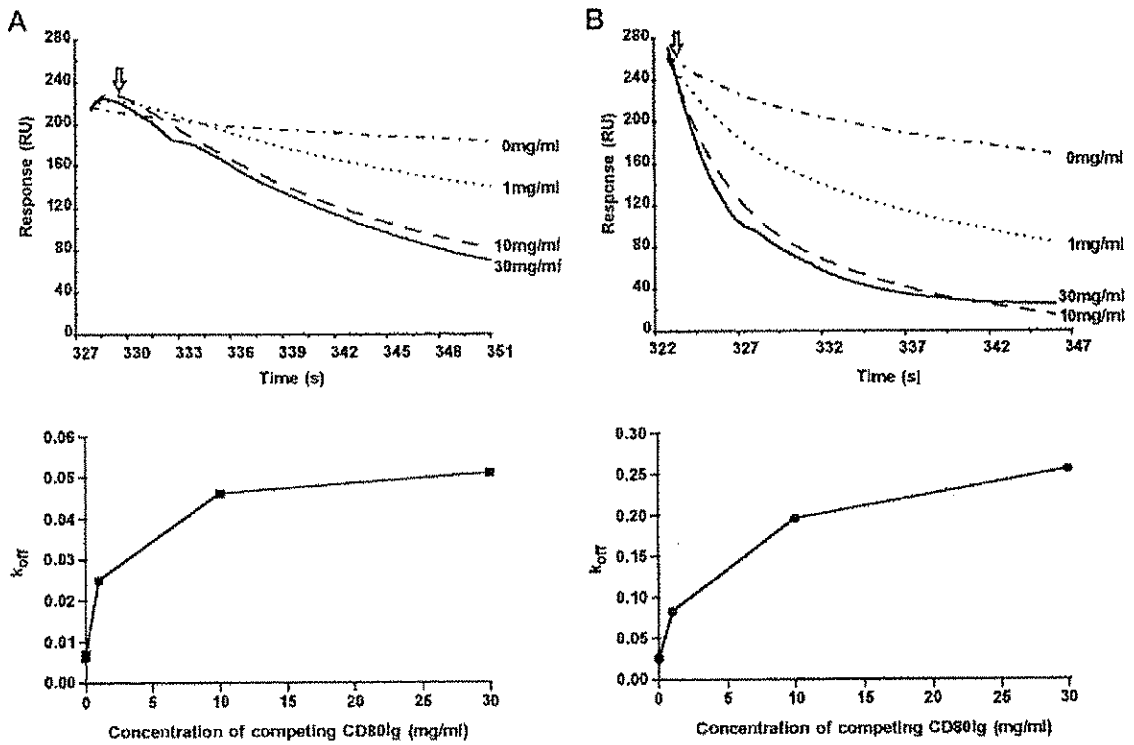

FIG. 7. **Slow apparent dissociation of dimeric CTLA-4 is due to rebinding.** Shown are the effects of increasing concentrations of soluble CD80Ig on the dissociation of CTLA-4tp from immobilized CD80Ig (*A*) or CD86Ig (*B*). For CD80Ig and CD86Ig, 2200 and 2280 RU were immobilized, respectively. Dissociation measurements were run at 60 μl/min. The *upper panels* show raw sensorgrams transformed to remove bulk refractive index changes due to the high concentrations of competing CD80Ig. The *lower panels* show the dissociation rate constant (k_{off}) as a function of competitor concentration. The k_{off} values were determined for the dissociation of 20% of bound CTLA-4tp, beginning after bulk refractive index changes (*arrows*).

TABLE III
High avidity binding of CTLA-4 requires multivalent CD86

Equilibrium binding of the indicated pairs of proteins was measured as described in the legend to Fig. 2. High avidity (K_{d1}) and low avidity (K_{d2}) equilibrium dissociation constants were calculated from best fit curves calculated from a two-site model as described under "Materials and Methods." Values presented are the average of two experiments.

Immobilized protein	Analyte	K_{d1}	K_{d2}
		nM	nM
CTLA4Ig	CD86t	1400	NA[a]
CTLA4Ig	CD86Ig	7	110

[a] NA, not applicable (*i.e.* data were adequately fit by a one-site model).

bivalent (higher avidity) binding constants; monovalent (lower avidity) binding would lead to much shorter occupancy times. Comparison of occupancy times for dimeric CTLA-4 is more difficult because of the effects of receptor valency on apparent dissociation rate. Dimeric CTLA-4 has slower kinetic off-rates compared with CD28, but its time of receptor occupancy is still relatively short (half-time of less than ~180 s). Monomeric CTLA-4 binding would also lead to a short period of receptor occupancy (less than ~8 and ~2 s for binding to CD80Ig and CD86Ig, respectively), but the physiological relevance of this is unclear since CTLA-4 primarily exists as a disulfide-linked homodimer.

CD80 and CD86 have very similar equilibrium binding properties, despite sharing very little amino acid sequence homology (11). Nevertheless, CD80 and CD86 were reported to deliver qualitatively different costimulatory signals during T cell activation (20, 21). It is therefore of interest to examine the binding properties of these molecules in detail. Certain of the measurements made here confirm measurements made in previous studies (11). For example, the K_d values for dimeric CTLA-4 binding to CD80Ig and CD86Ig were similar to those reported previously for CTLA4Ig binding. Also, binding of dimeric CTLA-4 to CD80Ig was 3–4-fold higher than to CD86Ig (11). The difference in the kinetic off-rates of monomeric CTLA-4 binding to CD80Ig and CD86Ig (Table II) was similar to a previous estimate made using transfected cells (11). In other instances, however, SPR has permitted comparisons which were not possible in previous studies. Here we provide the first estimates of affinity constants (as opposed to avidity constants) for monomeric CTLA-4 binding to CD80Ig and CD86Ig (~200 and ~2200 nM), which differ by ~10-fold. It remains to be determined how different CD80 and CD86 binding properties affect signaling properties of these molecules.

A comparison of the binding properties of CTLA-4 and CD28 is important in light of the apparently different biological functions of these molecules (17). Binding of dimeric CTLA-4 to CD80Ig was 2500- and 270-fold stronger (for K_{d1} and K_{d2}, respectively) compared with dimeric CD28. This difference is greater than that previously determined (9, 10) because of the more than ~10-fold larger (indicating weaker binding) K_d values for high avidity binding of dimeric CD28 measured in the present study. This difference probably arises from aggregation and uncertain valencies of the Ig fusion proteins used previously. Despite the weak binding of dimeric CD28 measured in this study, our analysis predicts that monomeric CD28 would bind even weaker. Binding of dimeric CTLA-4 to CD86Ig was

THE JOURNAL OF BIOLOGICAL CHEMISTRY
The Journal of Biological Chemistry

Downloaded from www.jbc.org by on August 14, 2008

570- and 70-fold stronger (for K_{d1} and K_{d2}, respectively) compared with CD28.

Rapid kinetic off-rates facilitate the transitory intercellular interactions characteristic of lymphocytes, but present the problem of how to maintain CD80/CD86 ligand occupancy long enough to generate productive signals. We have demonstrated here two characteristics of the CD28/CTLA-4/CD80/CD86 receptor system that would tend to counteract the effect of fast kinetic off-rates and thereby increase the duration of receptor occupancy. The first of these is the influence of the two CD80/CD86-binding sites per pre-existing CD28/CTLA-4 covalent dimer; the second, oligomerization of CD80/CD86 molecules on APC.

We have shown that bivalent CTLA-4 and probably CD28 have different kinetic and equilibrium binding characteristics compared with the monomeric molecules. Bivalently bound CD28/CTLA-4 receptors have a decreased likelihood of dissociating from CD80/CD86 ligands. This decreased dissociation due to bivalent binding would prolong the effective receptor occupancy time.

Oligomerization of CD80 and/or CD86 molecules would also tend to prolong CD28/CTLA-4 receptor occupancy. CD80/CD86 molecules are not known to dimerize (7). However, while (dimeric) CTLA4Ig binds with high avidity to APC, CTLA-4 dimers do not bind with high avidity to monomeric CD86. High avidity binding of CTLA4Ig to APC may be accounted for by oligomerization or clustering of CD80/CD86 molecules on the cell surface. Clusters of CD80/CD86 could either pre-exist or may be ligand (CTLA4Ig)-induced. Available data support the existence of pre-existing clusters of CD80/CD86 molecules since high avidity binding of CTLA4Ig is observed under conditions that discourage ligand-induced clustering (*i.e.* at low temperature, in the presence of metabolic inhibitors, or on fixed cells). The existence of pre-existing oligomers of CTLA4Ig-binding molecules on human Langerhans cells was also suggested by earlier immunofluorescence microscopy studies (29). Pre-existing oligomers of CD80/CD86 molecules would favor multiple engagements with CD28 and/or CTLA-4 receptors.

Engagement of CD28 and/or CTLA-4 receptors by clustered CD80/CD86 ligands would increase the local receptor concentration and provide for greater receptor occupancy. Despite the concentration-driven increase in receptor occupancy, the rapid dissociation kinetics of CD28/CTLA-4/CD80/CD86 complexes would still result in transiently unoccupied CD80/CD86 molecules. These could then rebind other CD28/CTLA-4 receptors, perhaps allowing engagement of many CD28/CTLA-4 receptors by relatively few CD80/CD86 molecules. A similar process has been suggested for T cell receptor-major histocompatibility class I peptide complexes (30).

Clustering of CD80/CD86 molecules on the APC surface may explain earlier findings that CD28 aggregation by mAbs enhances signaling through this receptor and alters the biochemical nature of signals generated (reviewed in Ref. 31). Clusters of CD80/CD86 molecules could cross-link different CD28/CTLA-4 receptors because of their bivalent binding. Cross-linking would also be favored by the rapid kinetic on- and off-rates of binding. Clustering of CD80/CD86 molecules on APC may therefore be an important control point for the activity of this receptor/ligand system.

Acknowledgments—We thank Steve Nadler and Mark Stebbins for performing high pressure liquid chromatography analysis and Julie Rodgers and Joe Naemura for excellent technical help.

REFERENCES

1. Schwartz, R. H. (1990) *Science* **248**, 1349–1355
2. Mueller, D. L., Jenkins, M. K., and Schwartz, R. H. (1989) *Annu. Rev. Immunol.* **7**, 445–489
3. Schwartz, R. H. (1992) *Cell* **71**, 1065–1068
4. Linsley, P. S., and Ledbetter, J. A. (1993) *Annu. Rev. Immunol.* **11**, 191–212
5. Allison, J. P. (1994) *Curr. Opin. Immunol.* **6**, 414–419
6. Guinan, E. C., Gribben, J. G., Boussiotis, V. A., Freeman, G. J., and Nadler, L. M. (1994) *Blood* **10**, 3261–3282
7. June, C. H., Bluestone, J. A., Nadler, L. M., and Thompson, C. B. (1994) *Immunol. Today* **15**, 321–332
8. Peach, R. J., Bajorath, J., Brady, W., Leytze, G., Greene, J., Naemura, J., and Linsley, P. S. (1994) *J. Exp. Med.* **180**, 2049–2058
9. Linsley, P. S., Brady, W., Grosmaire, L., Aruffo, A., Damle, N. K., and Ledbetter, J. A. (1991) *J. Exp. Med.* **173**, 721–730
10. Linsley, P. S., Brady, W., Urnes, M., Grosmaire, L. S., Damle, N. K., and Ledbetter, J. A. (1991) *J. Exp. Med.* **174**, 561–569
11. Linsley, P. S., Greene, J. L., Brady, W., Bajorath, J., Ledbetter, J. A., and Peach, R. (1994) *Immunity* **1**, 793–801
12. Morton, P. A., Fu, X.-T., Stewart, J. A., Giacoletto, K. S., White, S. L., Leysath, C. E., Evans, R. J., Shieh, J.-J., and Karr, R. W. (1996) *J. Immunol.* **156**, 1047–1054
13. Linsley, P. S., Nadler, S. G., Bajorath, J., Peach, R., Leung, H. T., Rogers, J., Bradshaw, J., Stebbins, M., Leytze, G., Brady, W., Malacko, A. R., Marquardt, H., and Shaw, S.-Y. (1995) *J. Biol. Chem.* **270**, 15417–15424
14. Walunas, T. L., Lenschow, D. J., Bakker, C. Y., Linsley, P. S., Freeman, G. J., Green, J. M., Thompson, C. B., and Bluestone, J. A. (1994) *Immunity* **1**, 405–413
15. Krummel, M. F., and Allison, J. P. (1995) *J. Exp. Med.* **182**, 459–465
16. Gribben, J. G., Freeman, G. J., Boussiotis, V. A., Rennert, P., Jellis, C. L., Greenfield, E., Barber, M., Restivo, V. A., Jr., Ke, X., Gray, G. S., and Nadler, L. M. (1995) *Proc. Natl. Acad. Sci. U. S. A.* **92**, 811–815
17. Linsley, P. S. (1995) *J. Exp. Med.* **182**, 289–292
18. Tivol, E. A., Borriello, F., Schweitzer, A. N., Lynch, W. P., Bluestone, J. A., and Sharpe, A. H. (1995) *Immunity* **3**, 541–547
19. Waterhouse, P., Penninger, J. M., Timms, E., Wakeham, A., Shahinian, A., Lee, K. P., Thompson, C. B., Griesser, H., and Mak, T. W. (1995) *Science* **270**, 985–988
20. Freeman, G., Boussiotis, V. A., Anumanthan, A., Bernstein, G. M., Ke, X. Y., Rennert, P. D., Gray, G. S., Gribben, J. G., and Nadler, L. M. (1995) *Immunity* **2**, 523–532
21. Kuchroo, V. K., Das, M. P., Brown, J. A., Ranger, A. M., Zamvil, S. S., Sobel, R. A., Weiner, H. L., Nabavi, N., and Glimcher, L. H. (1995) *Cell* **80**, 1–20
22. Johnsson, B., Lofas, S., and Lindquist, G. (1991) *Anal. Biochem.* **198**, 268–277
23. Linsley, P. S., Greene, J. L., Tan, P., Bradshaw, J., Ledbetter, J. A., Anasetti, C., and Damle, N. K. (1992) *J. Exp. Med.* **176**, 1595–1604
24. Hollenbaugh, D., Douthwright, J., McDonald, V., and Aruffo, A. (1995) *J. Immunol. Methods* **188**, 1–7
25. Khilko, S. N., Corr, M., Boyd, L. F., Lees, A., Inman, J. K., and Margulies, D. H. (1993) *J. Biol. Chem.* **268**, 15425–15434
26. van der Merwe, P. A., Barclay, A. N., Mason, D. W., Davies, E. A., Morgan, B. P., Tone, M., Krishnam, A. K. C., Ianelli, C., and Davis, S. J. (1994) *Biochemistry* **33**, 10149–10160
27. Corr, M., Slanetz, A. E., Boyd, L. F., Jelonek, M. T., Khilko, S., Al-Ramadi, B. K., Kim, Y. S., Maher, S. E., Bothwell, A. L. M., and Margulies, D. H. (1994) *Science* **265**, 946–949
28. Schuck, P. (1996) *Biophys. J.* **70**, 1230–1249
29. Symington, F. W., Brady, W., and Linsley, P. S. (1993) *J. Immunol.* **150**, 1286–1295
30. Vallitutti, S., Muller, S., Cella, M., Padovan, E., and Lanzavecchia, A. (1995) *Nature* **375**, 148–151
31. Linsley, P. S., Ledbetter, J., Peach, R., and Bajorath, J. (1995) *Res. Immunol.* **146**, 130–140

Downloaded from www.jbc.org by on August 14, 2008

EXHIBIT 15

This is an EDGAR HTML document rendered as filed. [Alternative Formats]

SECURITIES AND EXCHANGE COMMISSION

Washington, D.C. 20549

FORM 8-K

CURRENT REPORT

PURSUANT TO SECTION 13 OR 15(D) OF THE SECURITIES EXCHANGE ACT OF 1934

July 15, 2002
Date of Report (Date of earliest event reported)

AMGEN INC.

(Exact Name of Registrant as Specified in Its Charter)

Delaware	000-12477	95-3540776
(State or other Jurisdiction of Incorporation)	(Commission File Number)	(IRS Employer Identification Number)

Amgen Inc.
One Amgen Center Drive
Thousand Oaks, CA
(Address of principal executive offices)

91320-1799
(Zip Code)

805-447-1000
(Registrant's telephone number, including area code)

N/A
(Former Name or Former Address, if Changed Since Last Report)

Item 2. ***Acquisition or Disposition of Assets***

On July 15, 2002, Amgen Inc. (*"Amgen"*) announced the closing of its acquisition of Immunex Corporation (*"Immunex"*) pursuant to the Amended and Restated Agreement and Plan of Merger dated as of December 16, 2001 among Amgen, AMS Acquisition Inc., a wholly owned subsidiary of Amgen (*"Merger Sub"*), and Immunex, as amended by the First Amendment to Amended and Restated Agreement and Plan of Merger dated as of July 15, 2002 (the *"Merger Agreement"*). Pursuant to the Merger Agreement, Immunex was merged with and into Merger Sub, with Merger Sub continuing as the surviving corporation and a wholly-owned subsidiary of Amgen, and each share of Immunex common stock outstanding at the effective time of the merger was converted into the right to receive 0.44 of a share of Amgen common stock and $4.50 in cash.

A copy of Amgen's press release dated July 16, 2002 announcing the closing of the acquisition is attached hereto as Exhibits 99.1 and is incorporated herein by reference.

A description of certain factors that may affect Amgen's business, after giving effect to the acquisition, is attached to this Current Report as Exhibits 99.5 and is incorporated herein by reference.

Item 5. ***Other Events.***

Set forth below is an update to the description of the business of Amgen Inc. and its consolidated subsidiaries (including Immunex Corporation, unless the context requires otherwise, *"Amgen"* or the *"Company"*) set forth in Amgen's Annual Report on Form 10-K for the year ended December 31, 2001 to reflect Amgen's acquisition of Immunex on July 15, 2002. The updated business description is primarily based on filings made by Immunex with the Securities and Exchange Commission prior to Amgen's acquisition of Immunex. While we have no reason to believe this description is inaccurate, we can give you no assurance that this current description will conform with our operation of Immunex following the acquisition.

BUSINESS

Products Acquired in Connection with Immunex Acquisition

Enbrel® (etanercept)

Enbrel® (proper name - etanercept) is Immunex's trademark for its soluble tumor necrosis factor (*"TNF"*) receptor. Enbrel® blocks the biologic activity of TNF by competitively inhibiting TNF binding to the TNF cell surface receptors, which is expressed in a wide variety of tissues. TNF production is induced in response to inflammatory stimuli and mediates various physiologic responses including inflammatory and immunological responses.

In November 1998, Immunex received FDA approval and began marketing Enbrel® in the U.S. for the reduction of the signs and symptoms in patients with moderately to severely active rheumatoid arthritis (*"RA"*). In May 1999, Immunex received FDA approval of Enbrel® for treating moderately to severely active polyarticular-course juvenile RA (*"JRA"*), in patients who have had an inadequate response to one or more disease-modifying, anti-rheumatic drugs (*"DMARDs"*). In June 2000, the FDA approved Enbrel® for inhibiting the progression of structural damage in patients with moderately to severely active RA. In December 2000, the Canadian Health Protection Bureau approved Enbrel® in adults for reduction in signs and symptoms of moderately to severely active RA in patients who have had an inadequate response to one or more DMARDs. In January 2002, the FDA approved Enbrel® for reducing the signs and symptoms of active arthritis in patients with psoriatic arthritis (*"PsA"*). Because Enbrel® has been marketed only since 1998, its long-term effects are largely unknown. See "Factors that May

Affect Amgen—We may be required to perform additional clinical trials or change the labeling of our products if we or others identify side effects after our products are on the market."

Because demand for Enbrel® was projected to temporarily exceed supply, Immunex began an Enbrel® enrollment program in November 2000 to help ensure uninterrupted therapy for U.S. patients prescribed Enbrel® before January 1, 2001. The Enbrel® enrollment program called for these patients to register with Immunex and receive an enrollment number. As of January 1, 2001, patients considering therapy with Enbrel®, but not yet receiving treatment, were invited to enroll in the program and were placed on a waiting list. These patients receive Enbrel® on a first come, first served basis once additional supply of Enbrel® becomes available. In the second quarter of 2002, Immunex experienced a brief period where no Enbrel® was available to fill patient prescriptions, primarily due to variation in the production yield from BI Pharma. Once supply of Enbrel became available, Immunex resumed filling orders on a first come, first served basis. See *"Factors that May Affect Amgen—Limits on our current source of supply for Enbrel® will constrain Enbrel® sales growth"* and *"—Our sources of supply for Enbrel® are limited."*

Amgen owns the rights to Enbrel® in the U.S. and Canada, and Wyeth, formerly American Home Products Corporation, owns rights to Enbrel® in all other countries. Accordingly, Amgen does not receive royalties or a share of gross profits from sales of Enbrel® outside the U.S. and Canada. Amgen and Wyeth are marketing Enbrel® in the U.S. and Canada under a promotion agreement. See *"—Joint Ventures and Business Relationships—Wyeth."*

Enbrel® sales for the years ended December 31, 2001, December 31, 2000 and December 31, 1999 were $761.9 million, $652.4 million, and $366.9 million, respectively.

Novantrone® (mitoxantrone)

Novantrone® (proper name - mitoxantrone for injection concentrate) is Immunex's trademark for its compound similar to doxorubicin and idarubicin, two chemotherapeutic agents frequently used to treat some cancers, but with a molecular change that results in less damage to the heart. In December 1987, the FDA approved Novantrone® for initial therapy of acute nonlymphocytic leukemia in combination with other drug(s). In November 1996, Novantrone® was approved by the FDA for use in combination with corticosteroids for the treatment of pain in advanced hormone refractory prostate cancer. In October 2000, the FDA approved Novantrone® for reducing neurologic disability and/or the frequency of clinical relapses in patients with secondary progressive, progressive relapsing or worsening relapsing-remitting Multiple Sclerosis (*"MS"*). Novantrone® is not indicated for primary progressive MS.

Novantrone® sales for the years ended December 31, 2001, December 31, 2000 and December 31, 1999 were $71.2 million, $59.9 million and $44.5 million, respectively.

Leukine®

In May 2002, Immunex announced that it had agreed to sell its Leukine® (proper name-sargramostim) business to Schering AG Germany for approximately $380 million in cash plus the payment of additional cash consideration upon achievement of certain milestones. Immunex has agreed to sell its Leukine® business as a condition to obtaining regulatory approval of Amgen's acquisition of Immunex.

Thioplex

Thioplex® (proper name - thiotepa for injection) is Immunex's trademark for a powder formulation of thiotepa for injection. Thioplex® is approved for the palliative treatment of a wide variety of tumor types, which means that it alleviates symptoms without curing the underlying disease. The FDA has approved Thioplex® for a number of oncology indications. In 2001, Thioplex® began to face generic competition.

Acquired Product Candidates

Inflammation

Poor regulation of TNF occurs in conditions such as psoriasis and ankylosing spondylitis. Psoriasis is a skin disorder that most commonly appears as inflamed swollen skin lesions, which can be extremely painful and disfiguring. Ankylosing spondylitis is a unique form of chronic inflammatory arthritis characterized by joint stiffness, pain and extra bone growth that can result in partial or complete fusion of the spine.

In August 2001, Immunex announced the results of a six-month randomized, placebo-controlled, double-blind Phase 2 clinical trial indicating that psoriasis patients treated with Enbrel® experienced significant improvement compared to patients who were treated with placebo. In the fourth quarter of 2001, Immunex commenced Phase 2/3 dose ranging clinical trial in psoriasis. In the second quarter of 2002, a second large, controlled trial was initiated. Immunex also collected data in its Phase 2 and 3 clinical trials in psoriatic arthritis that will assist Amgen in evaluating the safety and efficacy of Enbrel® in treating patients with psoriasis. Enbrel® is being studied in a large Phase 3 clinical trial in ankylosing spondylitis. Enbrel® is also being studied in a Phase 3 clinical trial for Wegner's Granulomatosis.

Amgen is developing IL-1 Receptor Type 2, a natural regulator of IL-1. IL-1 Receptor Type 2 is believed to work by competitively binding IL-1, which prevents IL-1 from binding to cell surface receptors, potentially preventing a signal to the cell that can lead to inflammatory disease. IL-1 Receptor Type 2 is in a Phase 1 clinical trial in RA to assess tolerability.

In May 1999, Immunex entered into an agreement with Genmab A/S, or Genmab, for HuMax-IL-15, a fully human antibody against interleukin-15, or IL-15. IL-15 is a cytokine that plays a role in the cascade of reactions that cause the inflammatory process involved in diseases such as RA, psoriasis and Crohn's disease. Under the terms of the agreement, Genmab is responsible for developing, at its cost, HuMax-IL-15 through Phase 2 clinical trials, but Amgen has an exclusive option to assume development responsibility of Phase 3 clinical trials, and then to market and sell HuMax-IL-15 should it receive FDA approval. In October 2001, Genmab announced the initiation of a Phase 1/2 clinical trial of HuMax-IL-15 in patients with RA.

Cancer

Certain tissue growth factors are believed to play a role in the development and growth of tumors. Immunex had entered into, and Amgen is continuing, a joint development and commercialization agreement with Abgenix, Inc. (*"Abgenix"*) for both parties to develop and commercialize human antibody ABX-EGF. See *"—Joint Ventures and Business Relationships-Abgenix."* It is believed that ABX-EGF targets the receptor for human epidermal growth factor, or EGFr, which is over expressed in some of the most prevalent human tumor types, including lung, prostate, pancreatic, colorectal, renal cell and esophageal. ABX-EGF is in a series of Phase 2 clinical trials to evaluate its tolerability and efficacy for the treatment of several types of cancers. These include clinical trials in patients with kidney, colorectal, prostate and non-small cell lung cancer.

Joint Ventures and Business Relationships

Wyeth

Background. Prior to the acquisition of Immunex, Wyeth and Immunex were parties to several agreements relating to business and corporate governance matters. As a result of the closing of the acquisition of Immunex, some of these agreements were terminated, however, some agreements have survived the acquisition. In connection with the acquisition, Amgen entered into several agreements with Wyeth relating to these agreements to establish the framework for the ongoing relationship between Wyeth, Immunex and Amgen. In the following discussion, Wyeth refers to Wyeth, or its various divisions or affiliates.

Amended and Restated Promotion Agreement. In connection with the acquisition of Immunex, Amgen entered into an agreement with Wyeth to amend

and restate an existing long-term Enbrel® promotion agreement between Wyeth and Immunex. The principal operative terms of the amendment and restatement of the Enbrel® promotion agreement became effective at the closing of the acquisition of Immunex.

In 1997, Immunex entered into an Enbrel® promotion agreement with Wyeth. Under the terms of the Enbrel® promotion agreement, Enbrel® was promoted in the U.S. and Canada by the sales and marketing organization of Wyeth.

Under the amended and restated promotion agreement, Wyeth and Amgen will jointly market and sell Enbrel® to all appropriate customer segments in the U.S. and Canada for all approved indications other than oncology. The rights to promote Enbrel® in the U.S. and Canada for oncology indications are reserved to Amgen.

Under the amended and restated promotion agreement, an Enbrel® management committee comprised of an equal number of representatives from Wyeth and from Amgen will be responsible for overseeing the marketing and sales of Enbrel® including strategic planning, approval of an annual marketing plan, product pricing and establishing an Enbrel® brand team. The Enbrel® brand team, with equal representation from each party, will prepare and implement the annual marketing plan and will be responsible for all sales activities. The agreement provides that each of Wyeth and Amgen will:

- have primary tactical execution responsibility for specific activities identified within the agreement or as directed by the management committee;
- be required to maintain a minimum level of financial commitment to promotion and marketing and a minimum number of sales personnel for Enbrel® as established from time to time by the management committee; and
- pay a defined percentage of all marketing and sales expenses approved by the management committee.

The amended and restated promotion agreement further provides that Amgen will:

- pay Wyeth a percentage of the annual gross profits of Enbrel® in the U.S. and Canada attributable to all indications for Enbrel®, other than oncology indications, on a scale that increases as gross profits increase;
- be entitled to keep all of the gross profits attributable to any future U.S. or Canadian oncology indications for Enbrel®; and
- pay Wyeth specified residual royalties on a declining scale based on net sales of Enbrel® in the U.S. and Canada in the three years following the expiration or termination of Wyeth's detailing and promotion of Enbrel®.

If Wyeth sells or distributes a biologic product in the U.S. and Canada that is directly competitive with Enbrel®, as defined in this agreement, and subject to several exclusions, Wyeth will give Amgen prior written notice and, upon Amgen's request, the parties will attempt in good faith to either establish mutually acceptable terms under which Amgen will co-promote this competitive biologic product or establish other terms for a commercial relationship with Wyeth, or negotiate an adjustment to the gross profits allocated to Wyeth under this agreement. If Amgen is unable to establish acceptable terms with Wyeth within 90 days of its request, Amgen will have the option to reacquire from Wyeth all marketing rights to Enbrel® in the U.S. and Canada and terminate this agreement, subject to the payment by Amgen of a substantial amount to Wyeth over a defined period. If Wyeth obtains a biologic product that is directly competitive with Enbrel® through the acquisition of another company and Amgen reacquires the marketing rights to Enbrel® in the U.S. and Canada, Wyeth's primary field sales force that had detailed Enbrel® in the relevant territory within the U.S. and Canada for a specified period will not sell, detail or otherwise distribute the competitive biologic product for a specified period in the U.S. and Canada.

Wyeth has agreed to reimburse Amgen for a defined percentage of the clinical and regulatory expenses Amgen incurs in connection with the filing and approval of any new indications for Enbrel® in the U.S. and Canada, excluding oncology and rheumatoid arthritis indications. Wyeth's reimbursement of these clinical and

regulatory expenses is in addition to another existing cost-sharing arrangement between Amgen and Wyeth for development costs related to Enbrel®. The additional Wyeth reimbursement for clinical and regulatory expenses under this agreement, a portion of which is payable upon regulatory filing of any new indication and the remainder of which will be payable upon regulatory approval of any new indication, if any, applies for that part of the U.S. and Canadian clinical and regulatory expenses for Enbrel® for which Amgen would otherwise be financially responsible under the cost-sharing provisions in the other cost-sharing agreement. Wyeth will also provide reimbursement under this agreement for a defined percentage of specified patent expenses related to Enbrel®, including any up-front license fees and milestones, as well as patent litigation and interference expenses.

Subject to specified limitations, Wyeth will also be responsible for a defined percentage of the liabilities, costs and expenses associated with the manufacture, use or sale of Enbrel® in the U.S. or Canada.

Agreement Regarding Governance and Commercial Matters. In connection with the acquisition of Immunex, Amgen also entered into an agreement regarding governance and commercial matters with Wyeth. This agreement relates to, among other things:

- the rights of Wyeth to complete the development of and sell identified products under development by Immunex and the rights to market and promote those products developed by Immunex under an existing products rights agreement (described below);
- amending the product rights agreement as of the closing of the acquisition of Immunex to terminate the rights described above in exchange for a specified payment to Wyeth;
- Amgen's agreement not to sue Wyeth under any of Amgen's patents or any patents that come under Amgen's control for infringement for developing, making, using, marketing, distributing, importing or selling Enbrel® anywhere in the world outside of the U.S. and Canada; and
- Amgen's grant to Wyeth of an exclusive option to acquire, subject to the approval of a third party, an exclusive sublicense under a license agreement between a third party and Amgen. Wyeth may exercise this option at any time on or before December 31, 2002. If exercised, in addition to all upfront payments, milestone payments, and royalties payable under the sublicense agreement, Wyeth will reimburse Amgen in an amount not to exceed a defined cap for amounts paid to the third party in 2002 to maintain the license agreement.

TNFR License and Development Agreement. In July 1996, Immunex entered into a TNFR license and development agreement with Wyeth under which Immunex retained marketing rights to Enbrel® in the U.S. and Canada, and Wyeth retained marketing rights to Enbrel® outside of the U.S. and Canada. The TNFR agreement also addresses joint project management, cost sharing for development activities related to Enbrel®, manufacturing responsibilities, intellectual property protection and disposition of rights upon relinquishment or termination of product development.

Agreements Related to the Manufacturing of Enbrel®. Under the TNFR agreement, Immunex agreed with Wyeth to negotiate the terms of a supply agreement for

the commercial supply of Enbrel® to Wyeth outside the U.S. and Canada. In November 1998, Immunex and Wyeth entered into an Enbrel® Supply Agreement with Boehringer Ingelheim Pharma KG (*"BI Pharma"*), for the commercial supply of Enbrel® to Immunex in the U.S. and Canada, and to Wyeth outside of the U.S. and Canada. The Enbrel® Supply Agreement was amended in June 2000 to offer BI Pharma financial incentives to provide additional near-term production capacity for Enbrel®, to facilitate process improvements for Enbrel® and to extend the term of the agreement. The parties have agreed to further amend the Enbrel® Supply Agreement, to be effective June 2002, to reflect the transfer of production to a new BI Pharma manufacturing facility, to provide for the use of an improved manufacturing process, to extend the term of the agreement, and to offer BI Pharma additional financial incentives to provide additional near-term production capacity for Enbrel®.

On January 1, 2002, Immunex purchased from Wyeth a large-scale biopharmaceutical manufacturing facility in West Greenwich, Rhode Island. Immunex collaborated with Wyeth to retrofit this facility and it is intended for the production of Enbrel®. In connection with the signing of the purchase agreement for the Rhode Island manufacturing facility, Immunex and Wyeth entered into a collaboration and global supply agreement related to the manufacture, supply, inventory, and allocation of defined supplies of Enbrel® produced at the Rhode Island manufacturing facility, and a new Rhode Island manufacturing facility under construction as well as particular supplies of Enbrel® produced by either BI Pharma in Germany or Wyeth at a manufacturing facility Wyeth is constructing in Ireland. However, until the Rhode Island manufacturing facility receives regulatory approval, a preliminary August 2000 agreement among Immunex and Wyeth will continue to govern the allocation of supplies of Enbrel®. See *"—Manufacturing and Raw Materials."*

Stockholders' Rights Agreement. In connection with Amgen's acquisition of Immunex, Amgen entered into a stockholders' rights agreement with Wyeth.

Standstill Provisions. Under the stockholders' rights agreement, Wyeth agreed that until December 16, 2006, it may not:

- acquire or propose to acquire any Amgen securities or securities of Amgen subsidiaries or any assets of Amgen or its subsidiaries or make any public announcement with respect to any of the foregoing;
- participate in any way in any solicitation of proxies to vote, or seek to advise or influence any person with respect to the voting of, any of Amgen securities or make any public announcement with respect to any of the foregoing;
- form or in any way participate in a group in connection with any of the foregoing;
- otherwise act to seek to control or influence Amgen management, board of directors or policies;
- request Amgen to amend or waive the standstill provisions of the stockholders' rights agreement or take any action which would reasonably be expected to require Amgen to make a public announcement regarding the possibility of a business combination or merger or make any public announcement with respect to any of the restrictions in this clause; or
- advise, assist or encourage, or direct any person to advise, assist or encourage any other persons, in connection with any of the foregoing.

The above restrictions do not apply to:

- purchases by Wyeth of Amgen common stock for employee benefit or other plans not to exceed 1% of the outstanding shares of Amgen common stock; or
- securities held by a company that Wyeth acquires in the future, if the fair market value of the securities represents less than 20% of the assets of that company; however, Wyeth must use commercially reasonable efforts to divest those securities within 18 months of the consummation of the acquisition.

Voting of Amgen Common Stock. Under the stockholders' rights agreement, Wyeth agreed that, until

Wyeth beneficially owns in the aggregate less than 2% of the outstanding shares of Amgen common stock, Wyeth must cause all shares of Amgen common stock beneficially owned by it to be voted:

- with respect to the election of directors, in favor of those individuals nominated by Amgen's board of directors or a nominating committee of Amgen's board of directors;
- on all proposals of Amgen's other stockholders, in accordance with the recommendation of Amgen's board of directors; and
- on all other matters that come before Amgen's stockholders for a vote, in proportion to the votes cast by the other Amgen stockholders.

Lock-Up of Shares of Common Stock Acquired in the Acquisition. Under the stockholders' rights agreement, Wyeth and Amgen agreed that, for 90 days following the closing of Amgen's acquisition of Immunex, Wyeth may not transfer any shares of Amgen's common stock other than transfers:

- to a wholly-owned subsidiary of Wyeth;
- pursuant to a third party tender offer or exchange offer which was not induced by Wyeth and (a) which is approved by Amgen's board of directors or (b) in circumstances in which it is reasonably likely that Wyeth would be, as a result of not tendering or exchanging, forced to receive consideration that is different than the consideration available to those stockholders who did tender or exchange;
- arising as a result of a merger or similar transaction involving Amgen; or
- in the form of a pledge in connection with bona fide financings (other than derivative transactions) with a financial institution, provided the pledgee agrees to the applicable restrictions set forth in stockholders' rights agreement.

Volume Limitations on Sales of Common Stock. Wyeth may not transfer more than 20 million shares of Amgen common stock (including common stock underlying derivative transactions) in any calendar quarter, excluding shares of Amgen common stock transferred pursuant to underwritten syndicated offerings.

In addition, the aggregate number of shares of Amgen common stock underlying derivative transactions effected in any calendar week by Wyeth may not exceed 20% of the aggregate trading volume of Amgen common stock on the Nasdaq National Market in the immediately preceding calendar week.

Registration Rights.

Shelf Registration. Under the stockholders' rights agreement, Amgen agreed that Amgen would prepare and file with the SEC immediately after the closing of the acquisition of Immunex a registration statement registering the resale of Amgen common stock from time to time by Wyeth or any other permitted holders of Amgen common stock received by Wyeth in the acquisition. Amgen further agreed to use commercially reasonable efforts to:

- cause the shelf registration statement to be declared effective within 90 days after the closing of the acquisition of Immunex; and
- keep the shelf registration statement continuously effective until the earlier of (a) the first anniversary of the closing of the acquisition of Immunex and (b) the sale of all of the securities included in the shelf registration statement.

Wyeth, or any other permitted holders of Amgen common stock received by Wyeth in the acquisition, may request Amgen to effect an underwritten syndicated offering by supplement or amendment to the shelf registration

statement. In this case, the requesting party or parties and Amgen will enter into an underwriting agreement in customary form with the underwriters for the offering which will be underwritten by two co-managing underwriters with the requesting holders selecting one co-managing underwriter and with Amgen selecting the second co-managing underwriter. In some circumstances, Amgen may delay an offering for a limited period of time.

Amgen is only obligated to effect two offerings under the shelf registration statement and each of these offerings must include at least 5 million shares of common stock. In addition, these underwritten offerings will be subject to cutback if either of the co-managing underwriters reasonably advises Amgen that the number of shares of Amgen common stock requested to be included in the offering exceeds the number that can be sold in the offering at a price reasonably related to the then current market value of Amgen common stock.

Demand Registration Rights. Beginning on the first anniversary of the closing of the acquisition of Immunex, and until the fourth anniversary of the closing of the acquisition of Immunex, Wyeth, or any other permitted holders of Amgen common stock received by Wyeth in the acquisition, may request that Amgen file a registration statement covering the registration of a minimum of 5 million shares of Amgen common stock held by these holders in an underwritten offering. Amgen has agreed to use its commercially reasonable efforts to cause to be registered all the shares that the requesting party or parties have requested to be registered.

Amgen is obligated to effect up to four demand registrations, less the number of underwritten offerings effected under the shelf registration statement. In certain circumstances, Amgen may delay an offering for a limited period of time. Furthermore, Amgen's board of directors may delay the filing of a demand registration statement if the filing would likely materially interfere with a potential contemplated material financing, acquisition, corporation reorganization, corporate development or merger or other transaction involving Amgen. Other terms of the demand registration are comparable to those provided with respect to the shelf registration described above.

If Amgen files a demand registration statement registering an underwritten offering of Amgen common stock on behalf of Wyeth, or any other permitted holders of Amgen common stock received by Wyeth in the acquisition, Amgen may include in the registration statement shares of Amgen common stock for Amgen's own account. Amgen's right is subject to cutback if either of the co-managing underwriters reasonably advises Wyeth that the number of shares of common stock requested to be included in the offering exceeds the number that can be sold in the offering at a price reasonably related to the then current market value of Amgen common stock.

Piggy Back Registration Rights. If Amgen files a registration statement registering an underwritten offering of Amgen common stock on Amgen's behalf or on behalf of other holders of Amgen common stock, Wyeth, or any other permitted holders of common stock received by Wyeth in the acquisition, have the right to request that Amgen include their shares in the registration statement. Their right to include shares is subject to customary cutbacks if the managing underwriter, to be selected by Amgen, advises Amgen that the number of shares of common stock requested to be included in the offering exceeds the number that can be sold in the offering at a price reasonably related to the then current market value of Amgen common stock. Furthermore, Amgen may decide for any reason not to proceed with the proposed registration and may, at Amgen's election, give written notice of the determination to the parties requesting inclusion in the registration, and, thereupon, Amgen will be relieved of its obligation to register any shares of Amgen common stock in connection with that registration statement.

Termination. Except with respect to the standstill provisions and the voting provisions, which will terminate as described above, the stockholders' rights agreement and the obligations of the parties under it will terminate on the first date on which Wyeth beneficially owns less than 5 million shares of Amgen common stock.

Terminated Agreements. Wyeth also entered into the following agreements with Immunex that were terminated upon the closing of the acquisition of Immunex.

Product Rights Agreement. In July 1998, Immunex entered into a product rights agreement with Wyeth, under which Immunex granted Wyeth, among other things, an option to obtain royalty-bearing worldwide exclusive licenses to a limited number of Immunex products for all clinical indications. This option is referred to as a "product

call." The product rights agreement also granted Wyeth a right of first refusal to Immunex covered products and technologies that may only be exercised if the Immunex board of directors decides that Immunex will not market a covered product or technology by itself in any part of the world where it has or acquires marketing rights. In accordance with the agreement regarding governance and commercial matters, the product rights agreement was amended at the closing of the acquisition of Immunex to terminate Wyeth's product call right and right of first refusal in exchange for a specified payment to Wyeth by Amgen. Under the terms of the agreement, termination of these rights also terminated the agreement.

Governance Agreement. Prior to the acquisition of Immunex, Immunex and Wyeth were parties to a governance agreement which related to, among other things:

- corporate governance, including the composition of the Immunex board of directors (immediately prior to the closing of the acquisition of Immunex, Wyeth had the right to designate for election two directors of Immunex);
- Wyeth's right to purchase additional shares of Immunex common stock from Immunex if specified events occur;
- future purchases and sales of Immunex common stock by Wyeth;
- the requirement that members of the Immunex board of directors designated by Wyeth approve specified corporate actions; and
- the requirement that a supermajority of the members of the Immunex board of directors approve specified corporate actions.

Pursuant to the terms of the governance agreement and the agreement regarding governance and commercial matters, the governance agreement terminated as of the closing of the acquisition of Immunex.

Abgenix

Amgen and Abgenix have an agreement providing for the joint development and commercialization of ABX-EGF. Under the agreement, development and commercialization costs will be shared equally, as would any potential profits from sales of ABX-EGF. Abgenix has responsibility for completing the ongoing Phase 1 clinical trial, Amgen and Abgenix are responsible for the ongoing and future Phase 2 clinical trials and Amgen has primary responsibility for future Phase 3 clinical trials. If the clinical trials for ABX-EGF are successful and regulatory approval is received, Amgen would play the primary role in marketing ABX-EGF, while Abgenix would retain co-promotion rights.

Marketing

Amgen and Wyeth share commercialization responsibilities for Enbrel® under a co-promotion agreement. Under the Enbrel promotion agreement, Amgen and Wyeth jointly promote Enbrel in the U.S. and Wyeth promotes Enbrel in Canada to healthcare providers such as doctors and hospitals, pharmacy benefit managers and managed care organizations. In February 2002, Immunex began detailing Enbrel® in the U.S. through its own dedicated sales force. Immunex has focused its sales force on double covering certain key rheumatologists currently visited by Wyeth sales representatives and on promoting the new PsA indication for Enbrel to dermatologists. See *"—Joint Ventures and Business Relationships—Wyeth."* Enbrel® is reimbursed by private payors, and changes in coverage and reimbursement policies of these payors could have a material adverse effect on sales of Enbrel®.

Amgen uses pharmaceutical wholesalers and specialty distributors for Enbrel® and Novantrone®. For Enbrel®, rather than stocking inventory of product at wholesalers, wholesaler orders for Enbrel® are primarily drop-shipped directly to pharmacies for end-users. Amgen receives and processes product orders through a centralized

customer service and sales support group. A third party provides Amgen with shipping, warehousing and data processing services on a fee basis.

Because demand for Enbrel® was projected to temporarily exceed supply, Immunex began an Enbrel® enrollment program in November 2000 to help ensure uninterrupted therapy for U.S. patients prescribed Enbrel® before January 1, 2001. The Enbrel® enrollment program called for these patients to register with Immunex and receive an enrollment number. As of January 1, 2001, patients considering therapy with Enbrel®, but not yet receiving treatment, were invited to enroll in the program and were placed on a waiting list. These patients receive Enbrel® on a first come, first served basis once additional supply of Enbrel® becomes available. In the second quarter of 2002, Immunex experienced a brief period where no Enbrel® was available to fill patient prescriptions, primarily due to variation in the production yield from BI Pharma. Once supply of Enbrel became available, Immunex resumed filling orders on a first come, first served basis. See *"Factors that May Affect Amgen—Limits on our current source of supply for Enbrel® will constrain Enbrel® sales growth"* and *"—Our sources of supply for Enbrel® are limited."*

Competition

Any products or technologies that are directly or indirectly successful in addressing RA could negatively impact the market for Enbrel®. A number of companies are marketing or developing biological or other products that compete or are expected to compete with Enbrel®. Companies marketing treatments include: Centocor/Johnson & Johnson, which currently markets Remicade® for use with methotrexate to treat RA; Aventis, which markets Arava®; Pharmacia Corporation, which markets Celebrex®; Merck, which markets Vioxx®; and other generic competitors which market methotrexate, gold, sulphazine and Plaquinil. The Company also markets Kineret for the reduction of the signs and symptoms of moderately to severely active RA in patients 18 years of age or older who have failed one or more DMARD. Companies developing treatments include: Abbott Laboratories/Knoll, which is developing D2E7; Pharmacia/Celltech Group plc, which is developing CDP870; Genentech/Hoffman-LaRoche Inc., which is studying Rituxan for use in treating RA; Ares-Serono, which is studying Rebif and TBP-1 in RA; Regeneron Pharmaceuticals Incorporated, which is developing IL-1 TRAP; various other companies, including Vertex and Scios, are developing programs against the P38 MAP target; Vertex Pharmaceuticals Incorporated/Aventis Pharmaceuticals, which is developing pralnacasan; Alexion Pharmaceuticals Inc., which is developing an antibody that inhibits the complement cascade; Immune Response Corporation, which is developing a proprietary immune-based vaccine therapy; and various other competitors, such as Celgene, working with Selective Cytokine Inhibitory Drugs, Glaxo SmithKline, Altana and ICOS Corporation, with respect to PDE-4. Because demand for Enbrel® was projected to temporarily exceed supply, Immunex began an Enbrel® enrollment program in November 2000 to help ensure uninterrupted therapy for U.S. patients prescribed Enbrel® before January 1, 2001. In the second quarter of 2002, Immunex experienced a brief period where no Enbrel® was available to fill patient prescriptions, primarily due to variation in the production yield from BI Pharma. Once supply of Enbrel® became available, Immunex resumed filling orders on a first come, first served basis. See *"Factors that May Affect Amgen—Limits on our current source of supply for Enbrel® will constrain Enbrel® sales growth"* and *"—Our sources of supply for Enbrel® are limited."* Amgen believes that supply constraints being experienced by Amgen may make competitive products more attractive to patients and physicians.

A number of companies are marketing products that compete with Novantrone® for its oncology indications or may compete with Novantrone® for its new MS indication. The companies include Biogen, Berlex Laboratories (a subsidiary of Schering AG), Serone, Teva Pharmaceuticals Industries Limited, Pharmacia and Bedford Laboratories (a division of Ben Venue Laboratories, Inc.)

Manufacturing and Raw Materials

Substantially all the raw materials used to manufacture Enbrel® are available from multiple sources. However, two of the raw materials used in the production of Enbrel are manufactured by single suppliers. A material shortage, contamination or recall could adversely impact or disrupt commercial manufacturing of Enbrel®.

Amgen is dependent on a third party contract manufacturer for commercial production of Enbrel®. Failure by these third parties to supply the quantities of Enbrel® for which Amgen has contracted could adversely affect Enbrel® sales. All finished dosage forms of Enbrel are currently manufactured by BI Pharma and packaged by a

third-party contract packager. All finished dosage forms for Novantrone® are manufactured by Wyeth subsidiaries or sourced by Wyeth from third-party manufacturers.

In November 1998, Immunex and Wyeth entered into a long-term supply agreement with BI Pharma to manufacture commercial quantities of Enbrel®. Until the retrofitted Rhode Island manufacturing facility receives FDA approval, Amgen's sales of Enbrel® are entirely dependent on BI Pharma manufacturing the product. Amgen has made significant purchase commitments to BI Pharma under the BI Pharma supply agreement to manufacture commercial inventory of Enbrel®. Under the BI Pharma supply agreement, BI Pharma has reserved a specified level of production capacity for Enbrel®, and Amgen's purchase commitments for Enbrel® are manufactured from that reserved production capacity. Amgen is required to submit a rolling three-year forecast for manufacturing the bulk drug for Enbrel®, and a rolling forecast for a shorter period for the number of finished vials of Enbrel® to be manufactured from the bulk drug. Amgen has submitted firm orders for the maximum production capacity that BI Pharma currently has reserved for Enbrel®. Amgen and Wyeth will be responsible for substantial payments to BI Pharma if Amgen and Wyeth fail to use a specified percentage of the production capacity that BI Pharma has reserved for Enbrel® each calendar year, or if the BI Pharma supply agreement is terminated prematurely under specified conditions. In June 2000, Immunex, Wyeth and BI Pharma amended the BI Pharma supply agreement to offer BI Pharma financial incentives to provide additional near-term production capacity for Enbrel®, to facilitate process improvements for Enbrel, and to extend the term of the agreement. The parties have agreed to further amend the Enbrel® Supply Agreement, to be effective June 2002, to reflect the transfer of production to a new BI Pharma manufacturing facility, to provide for the use of an improved manufacturing process, to extend the term of the agreement, and to offer BI Pharma additional financial incentives to provide additional near-term production capacity for Enbrel®.

On January 1, 2002, Immunex purchased from Wyeth a large-scale biopharmaceutical manufacturing facility in West Greenwich, Rhode Island (the *"RI Facility"*). Immunex and Wyeth have invested substantial sums and worked closely together to retrofit the Rhode Island manufacturing facility to accommodate the commercial production of Enbrel bulk drug. FDA approval is required for commercial production of Enbrel at this facility.

In November 2001, Immunex broke ground on the BioNext Project™, a new manufacturing plant to be built adjacent to the RI Facility. When the facility is completed and approved by the FDA, it is scheduled to produce Enbrel® and possibly other products that may be developed.

In April 2002, Immunex announced that it had entered into a manufacturing agreement with Genentech, Inc. to produce Enbrel® at Genentech's manufacturing facility in South San Francisco, California. The manufacturing facility is subject to FDA approval, which the parties hope to obtain in 2004. Upon approval, the Genentech facility will become a licensed manufacturing site for commercial supply of Enbrel®. Under the terms of the agreement, Genentech will produce Enbrel® through 2005, with an extension through 2006 by mutual agreement.

Amgen is currently unable to supply enough Enbrel® to meet patient demand. BI Pharma's ability to provide additional production runs depends in part on factors beyond its control, including contractual commitments to other customers. There can be no assurances that Amgen will be able to supply sufficient quantities of Enbrel® in the future. Additionally, there can be no assurances that Amgen will be able to accurately anticipate future demand and have or retain adequate manufacturing capacity for either Enbrel® or Novantrone®. In the second quarter of 2002, Immunex experienced a brief period where no Enbrel® was available to fill patient prescriptions, primarily due to variation in the production yield from BI Pharma. Once supply of Enbrel became available, Immunex resumed filling orders on a first come, first served basis. See "Factors that May Affect Amgen—We depend on third party manufacturers for our supply of Enbrel®", *"—Our sources of supply for Enbrel® are limited"* and *"—Limits on our current source of supply for Enbrel® will constrain Enbrel® sales growth."*

Patents and Trademarks

Enbrel® is a fusion protein consisting of a dimer of two subunits, each comprising a TNF receptor domain derived from a TNF receptor known as *"p80,"* fused to a segment derived from a human antibody molecule known as an *"Fc domain."* Immunex believes that it was the first to isolate a recombinant DNA encoding p80 TNFR and also the first to express the protein using recombinant DNA technology. Immunex has been issued U.S. patents

covering p80 TNFR, DNAs encoding p80 TNFR, and methods of using TNFR:Fc, including for the treatment of arthritis. Immunex was granted a European patent in December 1995 covering p80 TNFR DNAs, proteins and related technology.

Two other companies, BASF and Yeda Research & Development Company, Ltd., filed patent applications disclosing partial amino acid sequence information of specified TNF-binding proteins, or TBPs, shortly prior to the time Immunex filed its patent applications claiming the full-length p80 TNFR DNAs and proteins corresponding in part to the TBPs disclosed by BASF and Yeda Research. BASF was issued a U.S. patent based on its TBP disclosure. Due to limitations in the claims of the BASF U.S. patent, Immunex has not entered into a license with BASF for its U.S. patent. This BASF U.S. patent lost an interference proceeding, which BASF is currently appealing through a U.S. district court action. In June 2000, Immunex entered into a royalty-bearing license agreement with respect to the BASF TBP patent family excepting the U.S. patent. If BASF were able to validly assert its U.S. TBP patent to cover TNFR:Fc in the U.S., Amgen's commercialization of Enbrel made in the U.S. could be impeded.

The Yeda Research TBP patents and patent applications are controlled by Ares-Serono International S.A. and its affiliate Inter-Lab Ltd. (collectively Serono). In January 1999, Immunex entered into a settlement agreement with Serono under which Immunex and Serono agreed to settle potential disputes concerning the patents and patent applications controlled by Serono that relate to TBPs. Under the settlement, Serono has agreed not to assert any of the foregoing patent rights against the manufacture, use or sale of Enbrel in any territory in consideration of the payment of fees and royalties by us to Serono for a specified term in respect of the net sales of Enbrel sold or manufactured in designated countries, including Germany and the U.S., where Yeda Research's patent rights have been filed.

After the effective dates on which Immunex filed its patent applications, Hoffmann-La Roche, or Roche, and Amgen, through Synergen Inc., also filed patent applications directed to p80 TNFR DNAs. No patents covering full-length TNFR or the intact extracellular domain of TNFR have been issued to Roche.

Immunex has also been granted a royalty-bearing worldwide exclusive license under patent rights jointly owned by Aventis SA (through its predecessor Hoechst AG) and Massachusetts General Hospital claiming cytokine receptor-Fc fusion proteins, including TNFR:Fc. Roche has filed patent applications with claims covering TNFR:Fc fusions, which were filed after the Aventis and Massachusetts General Hospital patent applications licensed to us. Roche has been granted a patent containing these claims in Japan. In September 1999, Immunex entered into a royalty-bearing worldwide co-exclusive license agreement with Roche under these Roche patents and patent applications.

ZymoGenetics, Inc. and Genentech have separately been issued U.S. patents having claims directed to specified fusion proteins comprising immunoglobulin constant region domains and specified processes for making these proteins, and have also filed corresponding European applications that have not yet been granted. On March 7, 2002, ZymoGenetics filed a patent infringement lawsuit against us in the U.S. District Court for the Western District of Washington. ZymoGenetics seeks a declaration of infringement and available remedies under the patent laws, including monetary damages and injunctive relief. In May 1999, Immunex entered into a royalty-bearing worldwide co-exclusive license agreement under the Genentech patents under which Immunex made an up-front payment to Genentech, a portion of which was reimbursed to us by Wyeth under the Enbrel® promotion agreement.

The Kennedy Institute of Rheumatology has been issued a patent having some claims directed to a method of treating arthritis by co-administering methotrexate and a soluble TNF receptor or a functional portion thereof. Immunex does not believe that the Kennedy Institute of Rheumatology patent would be successfully asserted against Enbrel®.

Immunex has been issued or obtained rights to U.S. patents relating to mitoxantrone that cover aspects of methods of using mitoxantrone are to treat leukemia and solid tumors (expiring in 2006) and to treat neuroimmunologic diseases (expiring in 2005).

Immunex has obtained U.S. registration of its Enbrel® and Novantrone® trademarks.

Properties

Amgen leases space in approximately 10 buildings in downtown Seattle and in two buildings in Bothell, Washington housing laboratory and office facilities. Amgen owns a manufacturing and development center in Bothell, Washington that includes a process development facility. Immunex has acquired approximately 20 acres of undeveloped land adjacent to the manufacturing and development center in Bothell, Washington.

On January 1, 2002, Immunex purchased from Wyeth a large-scale biopharmaceutical manufacturing facility in West Greenwich, Rhode Island. Amgen is in the process of preparing the Rhode Island manufacturing facility to accommodate the commercial production of Enbrel® bulk drug. FDA approval is required for commercial production of Enbrel® at this facility.

In November 2001, Immunex broke ground on the BioNext Project™, a new manufacturing plant to be built adjacent to the RI Facility. When the facility is completed and approved by the FDA, it is scheduled to produce Enbrel® and possibly other products that may be developed.

Immunex also owns 29 acres of land in Seattle, Washington that is under construction as a research and technology center and that may allow Amgen to consolidate its non-manufacturing operations at this one site. The initial phase of the project is known as the Helix Project. Immunex also has additional acreage adjacent to this construction site for potential future expansion of this project.

In March 2001, Immunex entered into a seven and one-half year lease to finance construction of the Helix Project. The total amount committed by the lessor to fund the costs of the project, including financing costs, was $750 million. Under the terms of the Helix Project lease, Immunex was permitted to acquire the lessor's interest in the Helix Project for the sum of the lessor's equity in the Helix Project improvements and the outstanding balance of the lease financing funded with commercial paper. As of July 1, 2002, the purchase option price of the Helix Project improvements based on such amounts was approximately $250 million. The Helix Project lease financing was subject to acceleration upon a change of control of Immunex. In connection with the acquisition of Immunex by Amgen on July 15, 2002, Immunex exercised its purchase option to acquire the Helix Project improvements from the lessor. As part of the lease transaction, Immunex was required to restrict as collateral cash or investment securities worth $765 million during the construction of the Helix Project. Immunex has elected to apply a portion of the liquidated collateral to the payment of the purchase option price, which payment and the resulting termination of the lease financing occurred immediately prior to the closing of Amgen's acquisition of Immunex. As a result, the Helix Project improvements were demised to Immunex, as the fee owner of the land associated with such improvements.

Legal Proceedings

ZymoGenetics litigation

On March 7, 2002, ZymoGenetics filed a patent infringement lawsuit against Immunex in the U.S. District Court for the Western District of Washington, relating to U.S. patents having claims directed to specified fusion proteins comprising immunoglobulin constant region domains and specified processes for making these proteins. ZymoGenetics seeks a declaration of infringement and available remedies under the patent laws, including monetary damages and injunctive relief.

Average Wholesale Price Litigation

Immunex is also named in several putative class action, also naming Amgen, broadly alleging that it, together with a large number of other pharmaceutical manufacturers, reported prices for certain products that overstated the Average Wholesale Price (*"AWP"*), allegedly inflating reimbursements, including co-payments paid to providers who prescribe and administer the products. The complaints assert claims under the federal RICO statute and its state law corollaries, as well as state law claims for deceptive trade practices and common law fraud and seek

an undetermined amount of damages, as well as other relief, including declaratory and injunctive relief. The cases include: Citizens for Consumer Justice et. al. v. Abbott Laboratories, Inc. et. al. (United States District Court, District of Massachusetts); State of Nevada v. American Home Products Corporation et. al. (Second Judicial District Court, Washoe County, Nevada); and State of Montana ex rel. Mike McGrath, Attorney General v. Abbott Laboratories, Inc. et. al. (First Judicial District Court, Lewis and Clark County, Montana).

Forward Looking Information

Except for the historical information contained in this Current Report, the matters discussed herein are by their nature forward-looking. Investors are cautioned that forward-looking statements or projections made by Amgen, including those made in this Current Report, are subject to risks and uncertainties that may cause actual results to differ materially from those projected. Amgen operates in a rapidly changing environment that involves a number of risks, some of which are beyond its control. Future operating results and Amgen's stock price may be affected by a number of factors, including, without limitation: (i) the results of preclinical and clinical trials; (ii) regulatory approvals of product candidates, new indications and manufacturing facilities; (iii) health care guidelines and policies relating to Amgen's products; (iv) reimbursement for Amgen's products by governments and private payors; (v) intellectual property matters (patents) and the results of litigation; (vi) competition; (vii) fluctuations in operating results; and (viii) rapid growth of Amgen. In addition, Amgen may not realize all of the anticipated benefits of its acquisition of Immunex, including the anticipated synergies, cost savings and growth opportunities from integrating the businesses of Immunex with the businesses of Amgen. These factors and others are discussed herein and in the sections appearing under the heading *"Factors That May Affect Amgen"* contained in Exhibit 99.5 attached hereto and in Amgen's other filings with the Securities and Exchange Commission, which sections are incorporated herein by reference.

Item 7. ***Financial Statements and Exhibits***

(a) Financial statements of business acquired.

(1) Immunex's audited consolidated balance sheets at December 31, 2001 and 2000 and audited consolidated statements of income, cash flows, and shareholders' equity for each of the three years in the period ended December 31, 2001 and notes thereto and report of Independent Auditors.

(2) Immunex's unaudited consolidated condensed balance sheets at March 31, 2002 and December 31, 2001 and unaudited consolidated condensed statements of income and cash flows for the three month period ended March 31, 2002 and 2001 and notes thereto.

(b) Pro forma financial information:

(1) Amgen's unaudited pro forma condensed combining balance sheet as of March 31, 2002 and unaudited pro forma condensed combining statements of operations for the year ended December 31, 2001 and the three months ended March 31, 2002.

(c) Exhibits—see Exhibit Index

SIGNATURES

Pursuant to the requirements of the Securities Exchange Act of 1934, as amended, the Registrant has duly caused this report to be signed on its behalf by the undersigned hereunto duly authorized.

AMGEN INC.

Date: July 16, 2002

By: */s/ Steven M. Odre*
Name: Steven M. Odre
Title: Senior Vice President, General Counsel and Secretary

EXHIBIT INDEX

Exhibit Number	Document Description
2.1	First Amendment to Amended and Restated Agreement and Plan of Merger dated as of July 15, 2002, by and among Amgen Inc., AMS Acquisition Inc. and Immunex Corporation (filed as Exhibit 2.2 to Post-Effective Amendment No. 1 to Form S-4 Registration Statement (File No. 333-81832) on July 15, 2002 and incorporated herein by reference)
21	Subsidiaries
23.1	Consent of Ernst & Young LLP, Independent Auditors
99.1	Press release dated July 16, 2002
99.2	Immunex's audited consolidated balance sheets at December 31, 2001 and 2000 and audited consolidated statements of income, cash flows, and shareholders' equity for each of the three years in the period ended December 31, 2001 and notes thereto and report of Independent Auditors (filed as Exhibit 99.3 to Current Report on Form 8-K filed on May 22, 2002 and incorporated herein by reference)
99.3	Immunex's unaudited consolidated condensed balance sheets at March 31, 2002 and December 31, 2001 and unaudited consolidated condensed statements of income and cash flows for the three month period ended March 31, 2002 and 2001 and notes thereto (filed as Exhibit 99.3 to Current Report on Form 8-K filed on May 22, 2002 and incorporated herein by reference)
99.4	Amgen's unaudited pro forma condensed combining balance sheet as of March 31, 2002 and unaudited pro forma condensed combining statements of operations for the year ended December 31, 2001 and the three months ended March 31, 2002 (filed as Exhibit 99.1 to Current Report on Form 8-K filed on May 22, 2002 and incorporated herein by reference)
99.5	*"Factors That May Affect Amgen"*

Dates Referenced Herein *and* Documents Incorporated By Reference

This 8-K Filing	*Date*	*Other Filings*
	12/31/99	10-K405, 11-K
	12/31/00	11-K, 10-K
	1/1/01	
	3/31/01	10-Q
	12/16/01	8-K
	12/31/01	10-K, 11-K
	1/1/02	
	3/7/02	
	3/31/02	10-Q
	5/22/02	8-K, S-3
	7/1/02	
For The Period Ended	7/15/02	POS AM
Filed On / Filed As Of	7/16/02	S-8, S-3
	12/31/02	10-K, 4, 11-K
	12/16/06	

Top List All Filings

Filing Submission - Alternative Formats (Word / Rich Text, HTML, Plain Text, SGML, XML, et al.)

*Copyright © 2008 **Fran Finnegan & Company** All Rights Reserved.*
www.secinfo.com - Mon, 25 Aug 2008 20:28:06.2 GMT - Privacy - Help